Die Bedeutung von TACC3, eines Proteins der mitotischen Spindel, für die zelluläre Proliferation und Viabilität

(Role of the mitotic spindle associated protein TACC3 in cell proliferation and survival)

Inaugural-Dissertation

zur

Erlangung des Doktorgrades der
Mathematisch-Naturwissenschaftlichen Fakultät
der Heinrich-Heine-Universität Düsseldorf

vorgelegt von

Leonid Schneider

aus Zhitomir (Ukraine)

April 2008

Aus dem Institut für Biochemie und Molekularbiologie II
der Heinrich-Heine Universität Düsseldorf

Gedruckt mit der Genehmigung der
Mathematisch-Naturwissenschaftlichen Fakultät der
Heinrich-Heine-Universität Düsseldorf
Referent: Prof. Dr. Dr. B. Nürnberg
Koreferent: Prof. Dr. P. Westhoff
Tag der mündlichen Prüfung: 18.06.2008

„Dankbar“

Ein Lied von: “Die Toten Hosen“

Contents

Figure index

Abbreviations

APC/C	anaphase promoting complex / cyclosome
ATP	adenosine-5’-triphosphate
β-Gal	β-Galactosidase
BBS	BES buffered saline
BES	N,N-Bis (2-hydroxyethyl)-2-aminoethansulfon acid
BrdU	bromodeoxyuridine
BSA	bovine serum albumin
Cdk	cyclin dependent kinase
CHAPS	3-[(3-Cholamidopropyl)dimethylammonio]-1-propanesulfonate
cLSM	confocal laser scanning microscopy
DAPI	4,6 diamidino-2-phenylindole
DMSO	dimethysulfoxide
DNA	deoxyribonucleic acid
DOX	doxycyclin
D-PBS	Dulbecco’s phosphate buffered saline
DTT	dithiothreitol
E. coli	Escherichia coli
ECL	enhanced chemiluminescence
EDTA	ethylendiamine-N,N,N’,N’-tetra-acetate
EGTA	bis(aminoethyl)-glycolether-N,N,N’,N’-tetra-acetate
ERK1/2	extracellular signal-regulated kinase 1/2
FACS	fluorescent-activated cell sorting
FITC	fluorescein isothiocyanate
GFP	green fluorescent protein
GTP	guanosine-5’-triphosphate
HEPES	N-(2-Hydroxyethyl)piperazine-N′-(2-ethanesulfonic acid)
HRP	horseradish peroxidase
KRAB	kruppel-associated box domain
LB-medium	Luria-Bertani medium
LCI	life cell imaging
LTR	long terminal repeat
MEF	mouse embryonic fibroblasts

MT	microtubules
NBD	nuclear breakdown
NP-40	Nonidet™ P-40 (Octylphenyl-polyethylene glycol)
PAGE	polyacryamid gel electrophoresis
PARP	poly (ADP-ribose) polymerase
PBS	phosphate buffered saline
pBS	pBluescript vector
PCM	pericentriolar material
PCR	polymerase chain reaction
PEG	polyethylene glycol
pH	logarithmic measure of hydrogen ion concentration
PI3K	phosphatidylinoside-3-kinase
Q-VD (Q-VD-OPH)	N-(2-quinolyl)valyl-aspartyl-(2,6-difluorophenoxy)methylketone
RNA	ribonucleic acid
SAC	spindle assembly checkpoint
SA-β-gal	senescence-associated-β-galactosidase
SD	standard deviation
SDS	sodium dodecyl sulfate
shRNA	short hairpin RNA
siRNA	short interfering RNA
TACC	transforming acidic coiled-coil
TBS	tris buffered saline
TRIS	tris(hydroxymethyl)-aminomethane
Triton X-100	*t*-Octylphenoxypolyethoxyethanol
tTR (tetR)	tetracycline transrepressor
Tween-20	polyoxyethylen-(20)-monolaurate
UV	ultra violet light
v/v	volume per volume
w/v	weight per volume
x g	gravitation (g)-force, 9.81 m/s^2
X-Gal	5-bromo-4-chloro-3-indolyl α-D-galactopyranoside
YFP	yellow fluorescent protein

1 Introduction

1.1 The mitotically expressed protein TACC3

All living cells proliferate by replicating their genome and subsequent cell division, where the chromosomes are equally distributed among the arising cells. In prokaryotic organisms, genome replication and cell division occur almost continuously and are only restricted by nutrient supply. In eukaryotes, however, the progress of the cell cycle presents a more complex challenge (e.g. due to chromosomal arrangement and nuclear compartmentation of DNA) and is also tightly controlled (Lodish et al., 1999). In particular, in multicellular organisms the initiation and the progression of the cell cycle are governed by the superimposed interests of the organism, e.g. tissue differentiation, organ morphogenesis, immune defence and last but not least tumour prevention. Each phase of the cell cycle is influenced by extrinsic and intrinsic control mechanisms, e.g. growth factors stimuli respectively DNA damage response and is characterised by the presence and/or activity of its own unique regulatory proteins (Lodish et al., 1999). Progression through a specific phase of the cell cycle is ensured by its respective cyclins, which are expressed and degraded in a cell cycle dependent fashion (Lodish et al., 1999). They perform their duty by regulating typical cyclin-dependent kinases (Cdk), when assembling into the cell cycle phase specific, active cyclin-Cdk complexes. A enzymatically competent cyclin-Cdk complex consists of a regulatory subunit (cyclin) and a catalytic subunit (Cdk) and function biochemically by phosphorylating various target proteins involved in the cell cycle (Sanchez & Dynlacht, 2005). For instance, the process of genome segregation and cell division during the mitotic phase of the cell cycle is tightly controlled by a mitosis-dependent expression and a timely degradation of cyclin B1 and numerous other regulatory and structural proteins (Pines, 2006).

Another cyclically expressed mitotic protein is the mammalian protein TACC3. Members of the evolutionary conserved family of centrosomal TACC (transforming acidic coiled-coil) proteins share a 200 amino acid coiled coil motif at their C-terminus, but have only limited homology outside this so called TACC domain (Still et al., 2004). Unlike other mammalian TACC isoforms, i.e. TACC1 and TACC2, TACC3 is highly expressed prior and during the mitotic phase and is degraded afterwards (Gergely et al., 2000). Furthermore, TACC3 is found exclusively in proliferating

tissues, i.e. during embryogenesis, and in adult proliferating tissues like haematopoietic and reproductive organs (Sadek et al., 2003). However, the role of TACC3 in mitosis and the cell cycle in general is poorly understood.

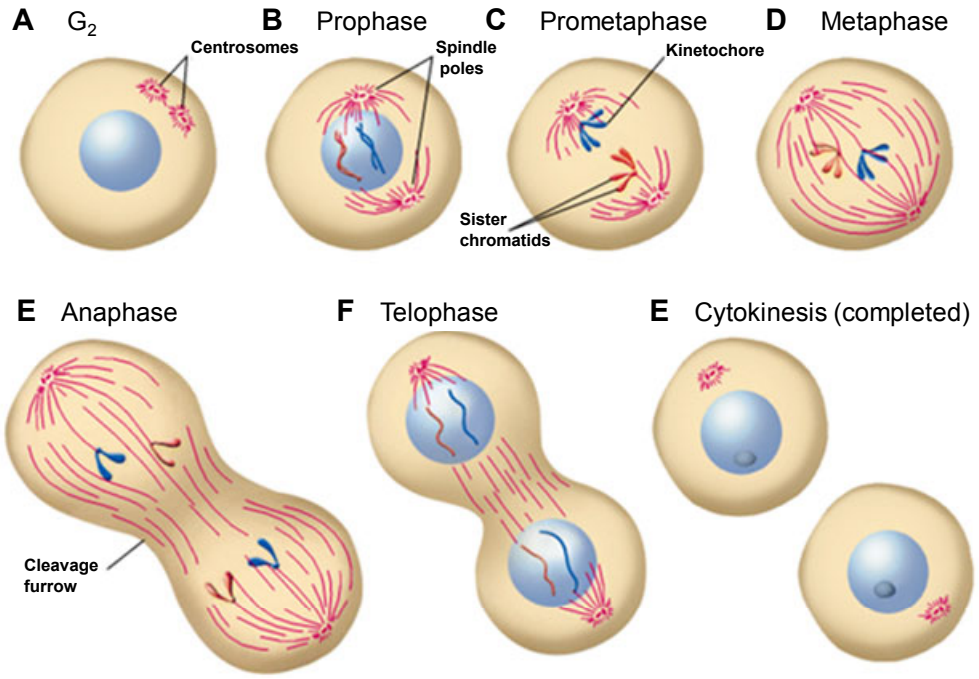

Fig. 1: Mitotic phases.

The centrosome is duplicated during the S-G_2 phase (**A**), the spindle poles then position themselves on the opposite sides of the nucleus (**B**). NBD (nuclear envelope breakdown) takes place at the prophase (**B**) and the mitotic spindle is assembled at the (pro)metaphase (**C-D**). Anaphase is initiated by cyclin B1 degradation so the chromosome segregation can start (**E**). Nuclear envelopes of the two dividing cells are re-assembled during the telophase (**F**) and cell division is completed at cytokinesis (**G**). Diagram adapted from Lodish et al., 1999.

During mitosis, TACC3 localises to the mitotic spindle apparatus (Gergely et al., 2000). The assembly of this microtubule-comprised structure is initiated during the first mitotic sub-phase, the prophase (Fig. 1). Also during this stage, the cell rounds up and the chromosomes condense inside the nucleus. The duplicated centrosomes move apart from each other and position themselves at the opposite poles in order to produce a mitotic spindle. In the prometaphase, the nuclear envelope breakdown (NBD) happens, which is required for spatial separation of the duplicated chromosome sets (Lodish et al., 1999). The assembly of the mitotic spindle is progressing. The microtubule (MT) strands of the mitotic spindle consist of α- and β-tubulin dimers which are nucleated at the centrosome (minus-end) and depolymerised at their tips (plus-end). This dynamic interplay is crucial in order to

achieve the proper bipolar attachment of the microtubule arms to the chromosomes (Compton, 2000).

The MT contact with the condensed DNA occurs at the kinetochores, protein enriched centromere areas of the chromosomes. Eventually, at the metaphase, all chromosomes are attached to the spindle microtubules in a bipolar fashion and congress at the midzone. A proper arrangement is followed by the detachment of the sister chromatids from each other and they start to tract towards the opposite spindle poles (Fig. 1). This hallmarks the onset of the anaphase, which is followed by the telophase, where the chromatids reach their respective spindle poles and begin to decondense. A new nuclear envelope forms around the DNA, while the beginning of cytokinesis is recognised by the progressing cell division with the building of a constriction (cleavage furrow) around the midzone. Finally, the arising daughter cells pull apart from each other with the cleavage furrow ingressing onto a mitotic bridge. After separation, both cells spread onto the surface and move away from each other (Lodish et al., 1999).

1.2 Centrosome, mitotic spindle and TACC proteins

The centrosome is an important cellular organelle, which was first discribed by Theodor Boveri more than 100 years ago (Boveri, 1895). Its most prominent function is the nucleation of the microtubules in order to produce the interphase MT-cytoskeleton or the mitotic spindle (Fig. 1). Its positioning also determines the polarity of the interphase cell and in mitosis the poles of the arising spindle. Analysis by electron microscopy revealed that the centrosome contains two cylinder-like centrioles, which are imbedded into a so called filamentous pericentriolar material (PCM; Rieder et al., 2001). Within the PCM, the ring-shaped complex containing γ-tubulin and pericentrin is responsible for microtubule nucleation and anchoring (Rieder et al., 2001). In addition to structural proteins, PCM contains a substantial number of various regulatory proteins, which are required for the control of the cell cycle (Doxsey et al., 2005). Important examples in this context are centrosome-associated kinases of the Plk (polo-like kinase) and Aurora family, but also the small GTPase Ran and the tumour suppressor and transcription factor p53. Interestingly, numerous centrosomal proteins contain a C-terminal coiled-coil domain, which is also typical for TACC family proteins (Andersen et al., 2003). Most centrosomal proteins

are not static and were reported to relocate from the centrosome towards other regions of the mitotic spindle during the mitotic progression (Doxsey et al., 2005).
The nucleation of the microtubules usually initiates inside the PCM, however if the centrosome and the PCM is removed this process can be performed by yet unknown back-up mechanisms (Basto et al., 2006; Rieder et al., 2001). In fact, plants and fungi lack centrosomes, but still assemble functional mitotic spindles. Alternatively, non-centrosomal γ-TuRC (γ-tubulin ring complexes) were suggested as sources of the MT nucleation (Luders & Stearns, 2007).

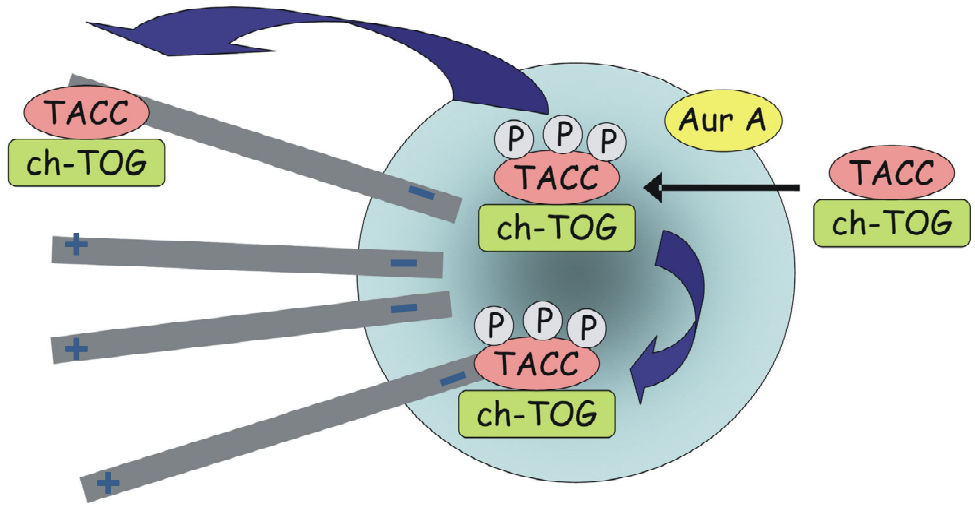

Fig. 2: TACC proteins at the centrosome.

Aurora A phosphorylates TACC, thus targeting it and its interacting partner ch-TOG to the centrosome. There phospho-TACC/ch-TOG is retained at the centrosome and stabilises the attachment of the minus ends of microtubules to the centrosome. In contrast, unphosphorylated TACC/ch-TOG complexes presumably stabilise the mitotic spindle at the plus ends of microtubules. Adapted from Brittle and Ohkura, 2005.

TACC proteins are thought to function as important structural components of the centrosome/spindle apparatus (Gergely et al., 2000a). Their relevance for the mitotic spindle is indicated by the fact that TACC proteins are found throughout the metazoan kingdom in vertebrates, insects and nematodes (Still et al., 2004). Also, the fungal TACC homologue Alp7 has been recently discovered in *Schizosaccharomyces pombe* (Sato et al., 2003). Using CD (conserved domain) search software (Marchler-Bauer & Bryant, 2004), the occurrence of TACC proteins can be predicted *in silico* in MT-associated protein complexes in plants like *Arabidopsis thaliana* and *Vitis vinifera* (http://www.ncbi.nlm.nih.gov/Structure/cdd/cdd.shtml).

TACC proteins contain a unique C-terminal, highly homologous coiled-coil (CC) domain of approximately 200 amino acids, but lack significant homology outside of this domain (Gergely et al., 2002). The CC-domain is essential for the localisation of TACC proteins to the centrosome-spindle apparatus (Gergely et al., 2002), however, the role of the N-terminal parts of mammalian TACC isoforms in protein-protein interaction and function is currently unclear. It has been shown that centrosomal localization of TACC3 relies also on its regulatory phosphorylation by the mitotic kinase Aurora A. In particular, as indicated in Fig. 2, phosphorylation of TACC3 homologues occurs at Serin-33, Serin-620 and Serin-626 in *Xenopus laevis,* and at Serin-34, Serin-552 and Serin-558 in humans ((Barros et al., 2005; Giet et al., 2002; Kinoshita et al., 2005; Peset et al., 2005)., as indicated in Fig. 2. At the mitotic spindle, TACCs interact through its CC-domain with the microtubule-stabilizing and evolutionary highly conserved protein ch-TOG/Msps/XMAP215 (Lee et al., 2001; Cullen and Ohkura, 2001). ch-TOG/Msps/XMAP215 plays an important role in centrosome integrity, centrosome-dependent assembly of microtubules during mitosis and spindle stability (Cassimeris & Morabito, 2004; Gergely et al., 2003; Kinoshita et al., 2002; O'Brien et al., 2005; Peset et al., 2005). Additionally, the *Xenopus laevis* TACC3 homologue, named Maskin, is involved in the translational regulation of the cyclin B1 mRNA in the oocyte (Groisman et al., 2000; Meijer et al., 2007). However, it is currently unclear whether TACC proteins are engaged in a comparable translational regulation in mammalian cells.

The isoformspecific roles of TACC proteins at the centrosome and at the mitotic spindle are still unclear. In mammals, TACC1 and TACC2 proteins are expressed rather ubiquitously and found predominantly in postmitotic tissues (Schuendeln et al., 2004). In contrast, TACC3 mRNA and protein are restricted to proliferating tissues (Sadek et al., 2003)Piekorz et al., 2002). A possible functional redundancy of mammalian TACC isoforms is suggested by a lack of any detectable phenotype in TACC2-deficient mice (Schuendeln et al., 2004). In contrast, TACC3 deficiency in mice leads to severe developmental defects and embryonic lethality indicating an isoformspecific role of TACC3 in highly proliferating cells (Piekorz et al., 2002).

Certain evidence points towards the involvement of TACC3 in spindle stability and chromosomal alignment (Gergely et al., 2003). In fact, during mitosis, TACC3 is not only present at the centrosome but also to a lower extent at MT binding to chromosomes (Fig. 2). These MT reach their targets, the chromosomal kinetochores,

through a highly dynamic process of “searching and capturing”. An attachment of one kinetochore of a duplicated chromatid pair to a MT results in the movement of the chromosome towards the minus end of the MT, i.e. towards the centrosome. The subsequent capture of the other, unattached, kinetochore by MT accomplishes the biorientation and positioning of the chromosome at the future metaphase midzone (Cleveland et al., 2003). Correct chromosome capture and alignment are therefore crucial, since alterations in centrosome and mitotic spindle architecture have profound consequences for cell cycle progression and lead to chromosomal instability and aneuploidy (Doxsey, 2002; Nigg, 2002; Nigg, 2006; Sluder, 2005). The possibile role of TACC3 in the process of chromosomal alignment and segregation was one important research focus of this work.

1.3 Pharmacological and toxicological inhibition of spindle assembly

Spindle assembly, capturing of kinetochores by MT and chromosomal segregation can be efficiently inhibited by various pharmacological compounds (Jablonski et al., 2003). They allow not only the study of these biological processes, but also a clinical targeting of highly proliferative cancer cells by inducing mitotic stress. This mitotic stress is counteracted by several sequentially activated checkpoints, which can in turn culminate in cell death, a desired event in cancer therapy (Blagosklonny, 2007). Several natural and synthetic inhibitors of the spindle dynamics interfere with the MT-assembly (Jablonski et al., 2003). The carbamic acid nocodazole and vinca alkaloids, for instance, reversibly bind to the MT component β-tubulin, thus preventing its association with α-tubulin and suppressing the assembly of microtubules required for formation of the mitotic spindle (Hung et al., 1996). Especially nocodazole is widely applied in cell biological studies for synchronization of cells at prometaphase; its removal allows cells to re-assemble a spindle and finish their mitotic progression.

Several microtubule-interfering substances are used as chemotherapeutic agents in cancer therapy. One particularly important pharmacological inhibitor of mitotic spindle dynamics is the taxane paclitaxel (Taxol®), which is a natural compound from the bark of the pacific yew *Taxus brevifolia* (Abal et al., 2003). Paclitaxel is among the most effective chemotherapeutic agents for treatment of patients with prostate,

breast and non-small cell lung cancer (Crown & O'Leary, 2000; Jordan & Wilson, 2004). In contrast to MT-destabilizing agents such as nocodazole, paclitaxel promotes the stabilization of microtubules by binding to β-tubulin and preventing its dissociation (Hung et al., 1996). This leads to the suppression of MT-dynamics during the process of spindle assembly. Relatively low nanomolar paclitaxel concentrations exert subtle effects on MT-dynamics and therefore delay mitotic progression and result in aneuploidy. In contrast, high nanomolar and micromolar concentrations of paclitaxel prevent a spindle assembly altogether and induce mitotic arrest and cell death (Abal et al., 2003).

1.4 Regulation of mitosis by the spindle assembly checkpoint

Mitotic arrest is characterized by the activation of the spindle assembly checkpoint (SAC). A successful (amphitelic) attachment of chromosomes to the microtubules (bi-orientation) creates a tension, which is not provided if one of the chromatids is unattached (monotelic) or both chromatids are connected to the same spindle pole (syntelic; Fig. 3). These misattachments result in SAC activation and mitotic arrest until the attachment of MT to chromatids is corrected and re-established probably (Nasmyth, 2002). Lack of tension and chromosomal attachment as caused by paclitaxel impedes this correction process and thus prevents the SAC from being satisfied and switched off. Cells are therefore unable to transgress into anaphase and to separate their sister-chromatids (Millband et al., 2002).

Entry into the anaphase requires the activity of the anaphase promoting complex (APC/C), a multiprotein-comprised ubiquitine ligase (Nasmyth, 2002). A correct chromosome alignment in the metaphase enables APC/C mediated degradation of various inhibitors of anaphase entry. One such important substrate for APC/C ubiquitination is cyclin B1, its degradation is a reliable marker for the onset of anaphase (Pines, 2006). The anaphase-promoting activity of APC/C is initiated by its activation through the Cdc20 protein (Bharadwaj & Yu, 2004; Pines, 2006; Weaver & Cleveland, 2005). Until the proper bi-orientation of the chromosomes is insured, Cdc20 is engaged by the inhibitory mitotic checkpoint complex of SAC proteins. SAC complex proteins localise to the unattached kinetochores. They belong to the Mad and Bub protein family, most important members are Mad2 and BubR1 (Bharadwaj & Yu, 2004; Kadura & Sazer, 2005). Their initial localization to kinetochores is

dependent on the chromosomal passenger complex (CPC) protein Aurora B (Ditchfield et al., 2003; Vigneron et al., 2004). BubR1 is hyper-phosphorylated during mitosis by Cdc5 and Aurora B kinases and remains in this state when SAC is activated (Rancati et al., 2005).

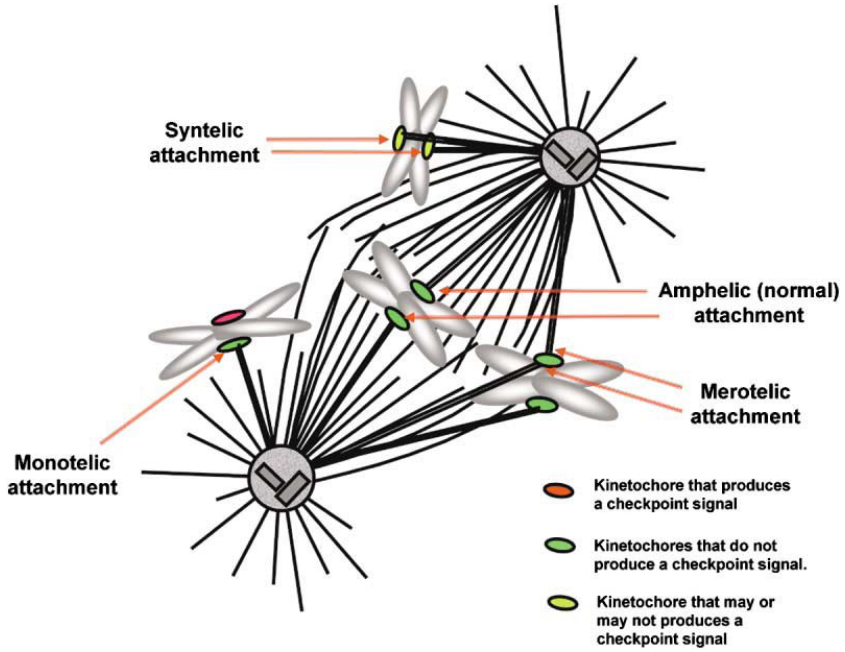

Fig. 3: Normal and aberrant kinetochore attachment

Incorrect binding of MT to kinetochores results in the activation of the SAC. This checkpoint is activated until a proper chromosome capture of all MT can be established. Figure adapted from Rieder & Maiato, 2004.

Sustained SAC activation can result in mitotic catastrophe, where the affected mitotic cells commit caspase-dependent apoptosis through p53-independent mechanisms (Castedo et al., 2004; Mansilla et al., 2006). For instance, treatment with high concentrations of paclitaxel leads to a permanent mitotic arrest and cell death (Giannakakou et al., 2001). An attenuation of SAC by pharmacological inhibitors or removal of checkpoint proteins like BubR1 and Mad2 compromises the ability of the cell to arrest in mitosis and consequently results in chromosomal instability (Weaver & Cleveland, 2005). However, like all checkpoints, SAC is also subject to adaptation. Here, cells gradually degrade cyclin B1 and escape from the mitotic block block by mitotic slippage (Brito & Rieder, 2006; Weaver & Cleveland, 2005). Cells exiting mitosis without proper segregation of sister chromatids and/or cytokinesis give rise to genetically unstable/aneuploid cells, a process associated with tumourigenesis (Bharadwaj & Yu, 2004; Doxsey, 2002).

1.5 Post-mitotic p53-dependent checkpoint

After completion of mitosis, cells return to the physiological condition of a somatic cell which is the diploid state, with two of each chromosomes being present inside the nucleus. This phase of the cell cycle is termed G_1 (gap phase 1, Lodish et al., 1999). Also, following an aberrant mitosis, cells will normally arrest in a polyploid G_1-like state through a post-mitotic checkpoint. This prevents the entry of the cell into the next round of DNA replication (S-phase). Unlike the mitotic SAC, the G_1 checkpoint is p53- and $p21^{WAF}$-dependent (Blagosklonny, 2006; Margolis et al., 2003). For instance, low concentrations of paclitaxel (>50 nM) cause aneuploidy following mitotic delay (Ikui et al., 2005). Consequently, the delay in mitosis is responded to by the stabilization and hence increased activity of the tumour suppressor p53 (Fig. 4).

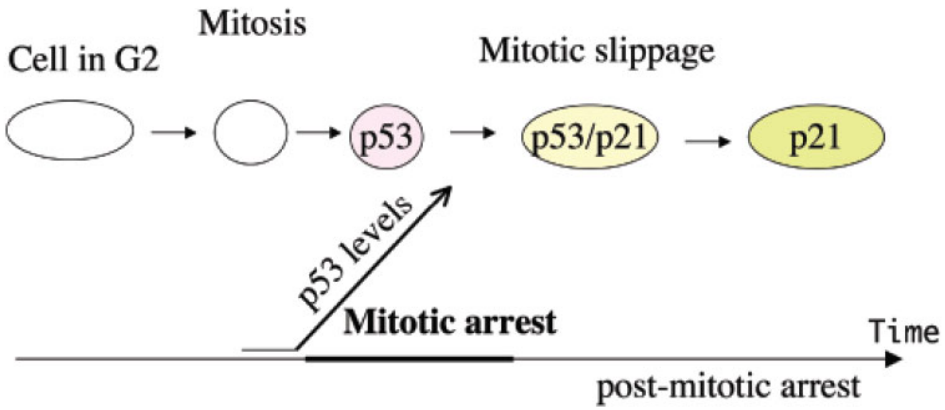

Fig. 4: Model for p53-$p21^{WAF}$ induction through prolonged mitosis (p53 as "mitotic clock").

Normal mitotic progression does not lead to p53 accumulation. Prolonged mitosis leads to increased levels of p53 through protein stabilisation. Following mitotic slippage into G_1, p53 induces $p21^{WAF}$ which results in a post-mitotic cell cycle arrest (Blagosklonny, 2006).

There are two major branches of p53 function which prevent cell cycle re-entry: proliferation arrest or apoptosis. p53 induces cell cycle arrest by transactivation of the Cdk-inhibitor $p21^{WAF}$ and apoptosis either by activating membrane-bound death receptors like Fas, DR4 and DR5 or by inducing the expression of pro-apoptotic proteins like Bax (Yu & Zhang, 2005). Cell cycle arrest mediated by $p21^{WAF}$ inhibits apoptosis following p53 expression (Yu & Zhang, 2005). Moreover, $p21^{WAF}$ further effectuates the G_1 arrest by increasing the protein levels of cyclin D1 (Chen et al., 1995; Del Sal et al., 1996), a cyclin typical for the G_1 phase. High cyclin D1 protein levels were also reported to induce $p27^{KIP}$, a $p21^{WAF}$-related Cdk-inhibitor and cell

cycle arrest mediator (Han et al., 1999). Nuclear cyclin D1/Cdk4 complexes are required for the phosphorylation and inactivation of the crucial G_1 checkpoint protein and tumour suppressor Retinoblastoma (Rb). The cytoplasmatic export of cyclin D1 precludes the phosphorylation of Rb and hence the entry into the S-phase (Gladden & Diehl, 2005).

The activation of the post-mitotic G_1 checkpoint after treatment with low concentrations of paclitaxel or depletion of crucial centrosomal proteins can become permanent with cells turning senescent (Blagosklonny et al., 2004; Mikule et al., 2007). However, cells usually can relieve the p53-$p21^{WAF}$ induced G_1 arrest and enter the next replication cycle. There is evidence that Akt kinase positively regulates cell cycle progression by inactivating FOXO transcription factors which are involved in cell cycle inhibition, senescence and apoptosis (Greer & Brunet, 2005). Interestingly, as a second safeguard mechanism, cells which have entered the S-phase despite a post-mitotic G_1 arrest later on additionally arrest prior to mitosis, namely in G_2 (gap phase 2). This checkpoint is also p53-dependent (Vogel et al., 2004).

1.6 TACC3 deregulation in mice and humans

Various mitotic proteins were shown to be vitally required for a correct mitosis. Their suppression usually leads to spindle assembly checkpoint or G_1 checkpoint activation and cell death (Schmit & Ahmad, 2007). On the other hand, their upregulation or increased kinase activity often promotes cellular transformation (Li & Li, 2006).

Several recent reports link elevated expression of TACC3 to human tumours. This includes its identification as a novel prognostic marker in non-small cell lung cancer (Jung et al., 2006), multiple myeloma (Stewart et al., 2004) and the association of TACC3 aberrations with ovarian cancer (Lauffart et al., 2005; Peters et al., 2005). On the other hand, the human TACC3 gene is localised at the sub-telomeric region of 4p chromosome, which deletion accounts for the development of the Wolf-Hirschhorn syndrome. Affected patients suffer among other developmental defects from mental retardation, growth delay and a craniofacial dysmorphy (Bergemann et al., 2005). These epidemiological data imply a critical role of TACC3 in mitosis and cell proliferation during embryonic development.

Indeed, a *knock out* of the *TACC3* gene in mice demonstrated that TACC3 deficiency results in embryonic growth retardation and lethality at mid to late gestation,

associated with aneuploidy, greatly reduced cell numbers and wide-spread apoptotic cell death (Piekorz et al., 2002; Yao et al., 2007). At the same time, $TACC^{+/-}$ heterozygous mice displayed no detectable phenotype. Remarkably, certain defects observed in TACC3 deficient mouse embryos (e.g. craniofacial dysmorphy and growth retardation) correspond to those of Wolf-Hirschhorn patients. In mice, TACC3 proved necessary for cell expansion during embryonic development and haematopoiesis, suggesting an essential and non-redundant role of TACC3 in highly proliferating cells (Piekorz et al., 2002). E.g., fetal liver cells can be easily cultivated in cell culture for up to two weeks when stimulated with growth factors including IL3, IL6 and SCF. However, fetal liver cells derived from $TACC3^{-/-}$ embryos failed to proliferate *ex vivo* (Piekorz et al., 2002). Similar results were obtained for primary mouse embryonic fibroblasts (MEF). Normally, these cells are capable of growing in culture for up to eight passages before undergoing a cell culture shock. There, they nearly cease to divide, but after spontaneous mutations of genes involved in the proliferation arrest (e.g. p53 or Cdk-inhibitor $p16^{INK4\alpha}$), cells re-enter the cycle and can be established as permanent cell lines. TACC3 deficient MEFs, however, displayed a very poor proliferative capability in culture and could hardly be established as cell lines. These data demonstrate the unsuitability of primary cells from TACC3 deficient embryos for further biological studies, since they are largely incapable of growing *ex vivo*.

The reasons for the impaired proliferative capacity of TACC3-deficient cells and the increased apoptosis are largely unknown. Interestingly, the embryonic lethality caused by a constitutive *TACC3* deficiency was partially rescued in mice with a complete loss or reduced levels of the tumour suppressor protein p53, indicating that *TACC3* deficiency activates the p53 checkpoint pathway (Piekorz et al., 2002). Interestingly, it was shown that a mouse line with a hypomorphic TACC3 expression (~5% of the wild-type allele) showed skeletal malformations in growth retarded newborn mice, which was connected to mitotic defects and apoptosis of sclerotomal mesenchymal cells (Yao et al., 2007).

In this thesis, the effects of a conditional depletion of TACC3 on checkpoint activation and cell cycle progression was analyzed in various cell lines. This approach provided the opportunity to study the molecular mechanisms which lead to growth retardation and embryonic lethality of TACC3 deficient mice. Also, the biological outcome of

targeting TACC3 in cancer cell lines, which often have compromised cell cycle checkpoints, was analyzed here for the first time.

2 Aims of the study

The centrosomal protein TACC (transforming acidic coiled-coil) 3 has been implicated in the regulation of mitotic spindle assembly and microtubule dynamics (Gergely et al., 2003; Kinoshita et al., 2005). In mice, the deletion of TACC3 by gene targeting leads to embryonic lethality due to severe growth retardation and widespread apoptosis (Piekorz et al., 2002). However, the molecular mechanisms underlying these defects were unclear. Therefore, the aim of this thesis was to establish cellular models for conditional TACC3 depletion via RNA interference in order to address the following questions:

- What is the role of the p53 mediated G_1 cell cycle checkpoint in cells undergoing mitotic stress through TACC3 depletion?

- What are the consequences of TACC3 depletion for mitotic spindle function, genomic stability and survival in G_1 checkpoint compromised cells?

- Is there a synergistic effect of TACC3 depletion and pharmacological inhibition of mitotic spindle assembly on cell cycle progression and survival?

Answering theses questions would provide novel mechanistical insight into the proliferation and survival defects associated with TACC3 deficiency and hence into the biological role of TACC3. Moreover, since high expression of TACC3 is linked to cancer, this study should clarify the possibility of targeting TACC3 for cancer treatment.

3 Materials

3.1 List of manufacturers and distributors

(1) AppliChem, Darmstadt
(2) Bio-Rad, München
(3) Dako, Glostrup, Denmark
(4) Fermentas, St. Leon-Rot
(5) Fujifilm, Düsseldorf
(6) GE Healthcare Life Sciences, München
(7) Genaxxon Bioscience, Biberach
(8) Invitrogen, Heidelberg
(9) Merck, Darmstadt
(10) MP Biomedicals, Eschwege, Germany
(11) Operon Biotechnologies, Köln
(12) Pierce, Rockford, USA
(13) Qiagen, Hilden
(14) Roth, Karlsruhe
(15) Schleicher & Schuell, Dassel
(16) Serva, Heidelberg
(17) Sigma Aldrich, München
(18) TPP, Trasadingen, Switzerland

3.2 Chemicals

3-[(3-Cholamidopropyl)-dimethylammonio]-1-propansulfonate (CHAPS)	(17)
Acrylamide	(14)
Adenosine-5'-triphosphate (ATP)	(17)
Agarose, "low-melting"	(14)
Ammonium persulfate	(17)
Aprotinin	(17)
Bovine serum albumin (BSA)	(1)
Bromphenol blue	(16)
Bromodeoxyuridine (BrdU)	(1)
Dimethyl sulfoxide (DMSO)	(1)
Dithiothreitol (DTT)	(17)

DNAase	(17)
Doxycycline	(10)
EDTA	(17)
EGTA	(17)
Ethanol	(14)
Etidium bromide	(17)
Glycine	(14)
HCl	(14)
HEPES	(17)
Leupeptin	(17)
Magnesium chloride	(17)
Magnesium acetate	(17)
β-Mercaptoethanol	(17)
Methanol	(14)
N,N,N',N'- Tetramethylethylenediamine (TEMED)	(17)
N,N-Bis (2-hydroxyethyl)-2-aminoethansulfone acid (BES)	(16)
NaCl	(1)
Nocodazole	(17)
Oligodeoxyribonucleotides	(13)
Paclitaxel	(10)
Pepstatin	(1)
Pepsin	(1)
Polybrene	(17)
Ponceau S	(17)
Potassium acetate	(17)
2-Propanol	(14)
Propidium iodide	(1)
Puromycin	(10)
RNAse A	(17)
Saponine	(1)
Sodium dodecyl sulfate (SDS)	(16)
Thymidine	(1)
Tris	(14)
Triton X-100	(17)
Tween 20	(1)
X-Gal	(17)

3.3 Western blotting

ECL Western Blotting Detection System	(8)
Hybond-C-Extra (membrane optimized for protein transfer)	(8)
X-Ray films	(5)
Horseradish peroxidase (HRP) anti-goat IgG	(12)
Horseradish peroxidase (HRP) anti-mouse IgG	(3)
Horseradish peroxidase (HRP) anti-rabbit IgG	(12)
Whatman GF/B blotting paper	(15)
Electrophoresis equipment	(2)
Bradford reagent	(2)

3.4 Cell culture, cell culture media and supplements

Foetal calf serum (FCS)	(8)
L-Glutamine	(7)
D-MEM cell culture medium	(8)
Penicillin/Streptomycin (10,000 U/ml / 10,000 µg/ml)	(7)
McCoy's cell culture medium	(7)
Trypsin/EDTA	(7)
Cell culture plastics	(18)
Trypan blue 0.5% solution	(8)
Dulbecco's phosphate buffered saline (D-PBS)	(7)

3.5 Protein and DNA standards

PageRuler™ prestained protein ladder	(4)
GeneRuler™ DNA ladder	(4)

3.6 DNA and RNA purification kits

Maxi-prep DNA extraction kit	(13)
Mini-prep DNA extraction kit	(13)
JustSpin Gel extraction columns	(7)
Qiazol RNA isolation kit	(13)

3.7 Enzymes

T4 polynucleotide kinase 0.5U/µl	(4)
T4 DNA Ligase 5U/µl	(4)
Restriction enzymes	(4)

3.8 Reagents for confocal microscopy

4',6-diamidino-2-phenylindole (DAPI)	(17)
Alexa 488 anti-mouse IgG	(8)
Alexa 488 anti-rabbit IgG	(8)
Alexa 488 anti-sheep IgG	(8)
Alexa 543 anti-mouse IgG	(8)
Alexa 543 anti-rabbit IgG	(8)
Alexa 594 anti-mouse IgG	(8)
Alexa 594 anti-rabbit IgG	(8)
Alexa 633 anti-mouse IgG	(8)
Alexa 633 anti-rabbit IgG	(8)
Alexa 633 anti-rat IgG	(8)
Fluorescent mounting medium	(3)
Prolong Gold Antifade medium	(8)

All other substances used in this work were purchased from Roth (Karlsruhe) or Sigma-Aldrich (München) with “pro analysi (pA)” grade. X-Ray films were developed on the Agfa Curix 60 developing machine (Agfa, Köln) and DNA bands in agarose gels were detected with the use of DIANA III Camera System (Raytest, Straubenhardt). DNA, RNA and protein photometrical analysis was performed on a DU800 Spectrophotometer (Beckman Coulter, Krefeld). Flow cytometrical analysis was performed on BD FACScalibur (BD, Heidelberg). Confocal analysis was performed on a Leica TCS SP2/AOBS (Leica, Wetzlar) and a LSM510-meta (Zeiss, Jena) confocal microscopes. DNA sequencing was performed by GATC Biotech, Konstanz.

3.9 Original vectors

Lentivectors were provided by Dr. Didier Trono, LVG-Tronolab, Lausanne, Switzerland. Retroviral packaging vector pEQ-PAM3 was provided by Dr. Elio Vanin,

Department of Experimental Haematology, St. Jude Children's Research Hospital, Memphis, TN, USA. Retroviral expression vector S11IP was provided by Prof. Dr. Helmut Hanenberg, Klinik für Kinder-Onkologie, -Hämatologie und Klinische Immunologie, Klinikum der Heinrich-Heine-Universität Düsseldorf. pEGFP-Centrin-2 vector was provided by Dr. Jeffrey Salisbury, Mayo Clinics, Rochester, NY, USA. pCDNA3-histone-2B-YFP vector was provided by Dipl.-Chem. Oleg Fedorchenko and Dr. Antje Gohla, Institut für Biochemie und Molekularbiologie II, Klinikum der Heinrich-Heine-Universität Düsseldorf.

3.10 List of primary antibodies

Directed against (code)	**Specific for** h: H. sapiens m: M. musculus	**Source**
α-tubulin (DM1A)	h, m	Sigma-Aldrich, München, Germany
α-tubulin (YOL1/34)	h, m	Acris Antibodies, Hiddenhausen, Germany
Akt	h, m	Cell Signaling, Danvers, MA, USA
Aurora B	h, m	BD Biosciences, Heidelberg, Germany
β-actin (C4)	h, m	MP Biomedicals, Illkirch, France
Bax (Ab8)	h, m	Lab Vision Corporation, Fremont, CA, USA
Bcl2	h	Dako, Glostrup, Denmark
Bim/BOD (Ab1)	h, m	Lab Vision Corporation, Fremont, CA, USA
BrdU (FITC coupled)		Biomeda, Foster City, CA, USA
BubR1	h	Dr. Stephen S. Taylor, University of Manchester, UK
caspase 3	h	R&D Systems, Bad Nauheim, Germany
Cdk1(cdc2) (sc-54)	h, m	Santa Cruz Biotechnology, Heidelberg, Germany
Cdk4 (Ab6)	h, m	Lab Vision Corporation, Fremont, CA, USA
CREST	h	Immunovision, Springdale, AR, USA
cyclin B1 (Ab3)	h, m	Lab Vision Corporation, Fremont, CA, USA
cyclin B1 (H-433)	h	Santa Cruz Biotechnology, Heidelberg, Germany

cyclin D1 (Ab3)	h, m	Lab Vision Corporation, Fremont, CA, USA
cyclin D2 (Ab4)	h, m	Lab Vision Corporation, Fremont, CA, USA
ERK1/2 (p42/p44)	h, m	Cell Signaling, Danvers, MA, USA
γ-tubulin (GTU-88)	h, m	Sigma-Aldrich, München, Germany
Lamin A/C	h, m	Cell Signaling, Danvers, MA, USA
Ndc80/Hec1 (9G3)	h	Abcam, Cambridge, UK
$p21^{WAF}$	h, m	BD Biosciences, Heidelberg, Germany
$p21^{WAF}$ (F-5)	m	Santa Cruz Biotechnology, Heidelberg, Germany
$p27^{KIP}$ (Ab1)	h, m	Lab Vision Corporation, Fremont, CA, USA
p53 (FL-393)	h, m	Santa Cruz Biotechnology, Heidelberg, Germany
PARP (Ab3)	h, m	Lab Vision Corporation, Fremont, CA, USA
pericentrin (ab4448)	h	Abcam, Cambridge, UK
phospho-Akt-S473	h, m	Cell Signaling, Danvers, MA, USA
phospho-Cdk1-Y15	h, m	BD Biosciences, Heidelberg, Germany
phospho-ERK1/2 (p42/p44)	h, m	Cell Signaling, Danvers, MA, USA
phospho-Foxo3a -T32	h, m	Upstate, Charlottesville, VA, USA
phospho-Histone3	h, m	Cell Signaling, Danvers, MA, USA
phospho-Histone3 (Alexa-488 coupled)	h, m	Beckman Coulter, Krefeld, Germany
Rb	h	BD Biosciences, Heidelberg, Germany
TACC3 (H-300)	h	Santa Cruz Biotechnology, Heidelberg, Germany
TACC3 (N18)	m	Dr. Roland Piekorz, Institut für Biochemie und Molekularbiologie II, Düsseldorf, Germany
Tom20 (FL-145)	h, m	Santa Cruz Biotechnology, Heidelberg, Germany

3.11 Original cell lines

Cell Line	Description	Provided by
HCT116	Human colon carcinoma cell line, near diploid	ATCC® Number: CCL-247
HCT116 $p53^{-/-}$, HCT116 $p21^{WAF-/-}$	Gene deletion through homologous recombination in a HCT116 subclone, neomycine selected	Dr. Bert Vogelstein (John Hopkins Cancer Center, Baltimore, USA)
HCT116 $Mad2^{+/-}$	Gene deletion through homologous recombination in a HCT116 subclone, neomycine selected	Dr. Robert Benezra (Sloan Kettering Cancer Center, NY, USA)
HeLa	Human cervix adenocarcinoma cell line, HP18-virus transformed, hypertriploid to hypotetraploid	ATCC® Number: CCL-2
HeLa KP4	Transgenically expressed tTR-KRAB transrepressor in HeLa, puromycine selected, clone #4	Prof. Dr. Helmut Hanenberg, Düsseldorf
MCF7	Human mammary gland adenocarcinoma cell line, hypertriploid to hypotetraploid	ATCC® Number: HTB-22
MCF7 caspase 3+	Transgenically expressed caspase 3 cDNA, neomycin selected	PD. Dr. Reiner U. Jänicke, Institut für Molekulare Medizin, Heinrich Heine Universität Düsseldorf
NIH3T3	NIH Swiss mouse embryonic fibroblast cell line, more than 5 serial cycles of subcloning, diploid, untransformed	ATCC® Number: CRL-1658
NIH3T3 KP11	Transgenically expressed tTR-KRAB transrepressor in NIH3T3, puromycine selected, clone #11	Prof. Dr. Helmut Hanenberg, Düsseldorf

4 Experimental procedures

4.1 RNA interference as a tool for gene silencing

Gene silencing through RNA interference, also referred to as “knock-down”, is currently a widely accepted method of gene silencing both *in vitro* (primary cells and cell lines) and *in vivo* (animal experiments, attempts of gene therapy in human medicine; Leung & Whittaker, 2005). Unlike a gene “knock out” through homologous recombination, which is irreversible, a *knock-down* is only effective when the so called short interfering RNA oligoribonucleotides (siRNA) are present inside a cell (Tuschl & Borkhardt, 2002).

When a double-stranded RNA is introduced into cells it results in the degradation of a homologous single-stranded mRNA and a consequential silencing of its gene (Tuschl & Borkhardt, 2002). In this process, double-stranded RNA is recognized and cleaved by the Dicer RNAse into catalytically active short intersperse RNA oligoribonucleotides (siRNA oligos), which are between 21 and 23 nucleotides in length. These oligos become incorporated inside a sequence-specific endonuclease complex, named RISC (RNA-induced silencing complex), which cleaves the target mRNA at sites homologous to siRNA sequences.

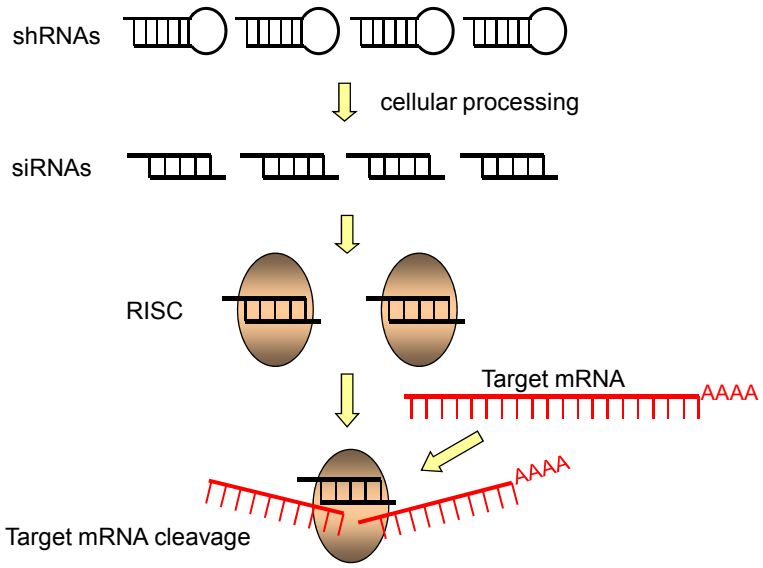

Fig. 5: A model for gene inactivation via RNA interference.

shRNA oligoribonucleotides are processed to 21- to 23-nt long siRNA duplexes intracellular enzymes. The siRNA duplexes are incorporated into a siRNA containing ribonucleoprotein complex, forming the RNA-induced silencing complex (RISC) endonuclease which targets homologous mRNAs for degradation. The RISC mediates sequence-specific target RNA degradation Diagram modified from Tuschl & Borkhardt, 2002.

As a result, the synthesis of the coded protein is largely suppressed without its gene being affected (Tuschl & Borkhardt, 2002). Alternatively, siRNA oligos can be generating from short hairpin RNA (shRNA), single RNA strands consisting of a sense and an anti-sense sequence connected by a short loop of several nucleotides, which allows complementary base-pairing and a production of a hairpin structure. shRNA oligos can be introduced into the cells through transfection or via expression vectors and are processed by cellular enzymes into active siRNA oligos through removal of the loop sequence (Fig. 5).

4.2 Lentiviral shRNA expression vectors

In this work, cellular TACC3 expression was down-regulated using the lentiviral shRNA expression system developed by Drs. Maciej Wiznerowicz and Didier Trono (Wiznerowicz & Trono, 2003). This system allows a delivery of shRNA expression cassettes into the cells by means of lentiviral transduction. The lentivirus used here is derived from human immunodeficiency virus (HIV). It uses the unique infectious capacity of this retrovirus to permeate the nucleus of the target cell and is therefore capable of delivering its genetic information even to non-dividing cells. The lentivector contains a H1 promoter with the upstream tetO (tet-operator) sequence and downstream shRNA sequence.

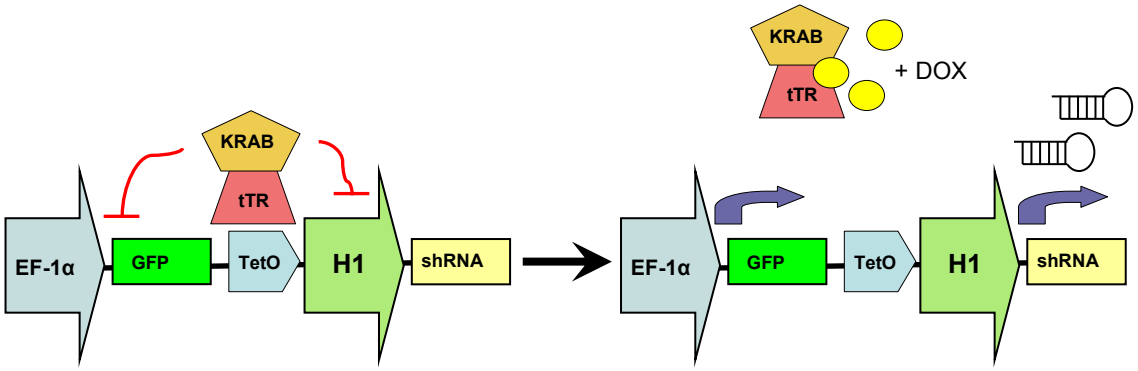

Fig. 6: Mode of action of the DOX-controllable transrepressor tTR-KRAB.

(A) In the absence of DOX, tTR-KRAB binds to tet operator *tetO* and suppresses H1-mediated siRNA transcription, thus allowing normal expression of the cellular target gene (ON). (**B**) In the presence of DOX, tTR-KRAB fails to bind to the *tetO* and hence siRNAs are produced, leading to down-regulation of their target gene (OFF). The internal marker GFP provides an inverse “monitoring device”, as it is ON in the presence of DOX and OFF in its absence. Diagram adapted from Wiznerowicz & Trono, 2003.

Green fluorescent protein (GFP) is used as marker, which expression is controlled by the EF1α-promotor. During reverse transcription by the virus, the U3 region of the 5' LTR is synthesized by using its 3' homologue as a template, which results in a duplication of the siRNA cassette in the provirus and its integration into the genome of target cells. Furthermore, the expression of shRNAs in this particular system can be regulated by the administration of the tetracycline-derivate doxycycline (DOX), provided the cell already expresses the tetracycline-repressor (tTR). Here, tetR from *E. coli* was fused to the KRAB-domain of the human transrepressor Kox1 in order to achieve a significantly higher repression efficiency (Wiznerowicz & Trono, 2003). In absence of DOX, the tTR-KRAB repressor binds to the tetO-sequence and prevents expression of shRNA and the marker gene GFP. When bound to DOX, tTR-KRAB is rendered inactive and the concomitant expression of the shRNA and GFP is induced in a reversible manner (Fig. 6).

4.3 Cloning procedure (shRNA)

Several siRNA sequences of 19 nucleotides targeting murine or human TACC3 were selected according to the siRNA prediction software at the Whitehead Institute for Biomedical Research, Boston, MA. The siRNA sequences employed here are listed in Table 1.

Table 1: Target cDNAs and RNAi sequences used to specifically down-regulate TACC3 expression in cells.

Construct	Target	Accession code (GenBank)	Target sequence	Position in cDNAs (nucleotides)	Down-regulation of TACC3 expression
siRNA2h	human TACC3	BC106071	5'-GTGGATTACCTGGAGCAGT-3'	1728-1746	yes
siRNA3m	murine TACC3	BC003252	5'-GTGGATTATCTGGAGCAGT-3'	1097-1115	yes
siRNA2m	murine TACC3	BC003252	5'-TCTTGACTTCCTCAAGCCT-3'	495-513	no (control)

Number of mismatches: siRNA2h *vs*. murine TACC3: one; siRNA2m *vs*. human TACC3: seven.

DNA oligos flanked by BglII and ClaI restriction sites were custom synthesized (Operon) in order to be aligned as shown in the following example:

mTACC3-2

BglII	sense	loop	antisense	ClaI

5'GATCCCCTCTTGACTTCCTCAAGCCTTTCAAGAGAAGGCTTGAGGAAGTCAAGATTTTTA 3'
3'GGGAGAACTGAAGGAGTTCGGAAAGTTCTCTTCCGAACTCCTTCAGTTCTAAAAATTCGA5'

Lyophilized oligos were dissolved at 10 µM in ddH_2O. For annealing, 2µl of each complimentary oligo were added to 48 µl annealing buffer (100 mM potassium acetate, 30 mM HEPES pH 7.4, 2 mM magnesium acetate), linearized for 4 min at 95°C, incubated at 70°C for 10 min and cooled down at room temperature. For 5' phosphorylation, 5µl annealed oligos were used in 1x T4 Polynucleotide Kinase Buffer B supplemented with 0,5 U/µl T4 Polynucleotide Kinase, 5% (w/v) PEG 6000 solution and 1mM ATP (Fermentas) and incubated at 37°C for 30 min. The enzyme was then heat inactivated at 70°C for 20 min.

Phosphorylated oligos were first ligated into pBluescript vector already containing a Histone H1-Promoter, digested with BglII and HindIII, then purified through ethanol-sodium acetate precipitation and dissolved in 10 mM Tris-Cl pH8. Ligation was performed overnight at 12°C using T4 DNA Ligase (5 U/µl; Fermentas) and transformed into chemocompetent *E. coli* DH5α. 50 µl bacteria were pre-incubated with 20 µl ligation mixture for 30 min on ice, heat-shocked in a water bath at 42°C for 30 sec, put back on ice and then shaken for 1h at 37°C in antibiotics-free SOC-medium and finally plated onto LB-agar plates containing 50 µg/ml ampicillin and grown at 37°C for 24h. Plasmids from growing clones were prepared using a Qiagen mini-prep kit according to manufacturer's instructions, digested with EcoR1/ClaI and fragments were separated on 2% agarose gel. DNA was stained with ethidium bromide and analyzed using a DIANA III Camera System (Raytest).

Positive clones were recognized by the appearance of a 290 bp DNA fragment (H1-shRNA cassette) on the agarose gel as compared to the 230 bp DNA fragment from an empty pBluescript vector (H1 cassette). Since chemically synthesized siRNA oligos were used, their sequence fidelity needed to be insured. Plasmids from positive E. coli clones were hence sent for sequencing (GATC Biotech) using T7 primer provided by GATC Biotech (TAATACGACTCACTATAGGG). Only plasmid clones without any mismatches in the siRNA region as proved through sequencing were used for further processing. Next, the H1-shRNA cassette was cloned into the

lentiviral vector pLVTH, which main characteristics are depicted in Fig. 7 and which was provided by Dr. Didier Trono (LVG-Tronolab).

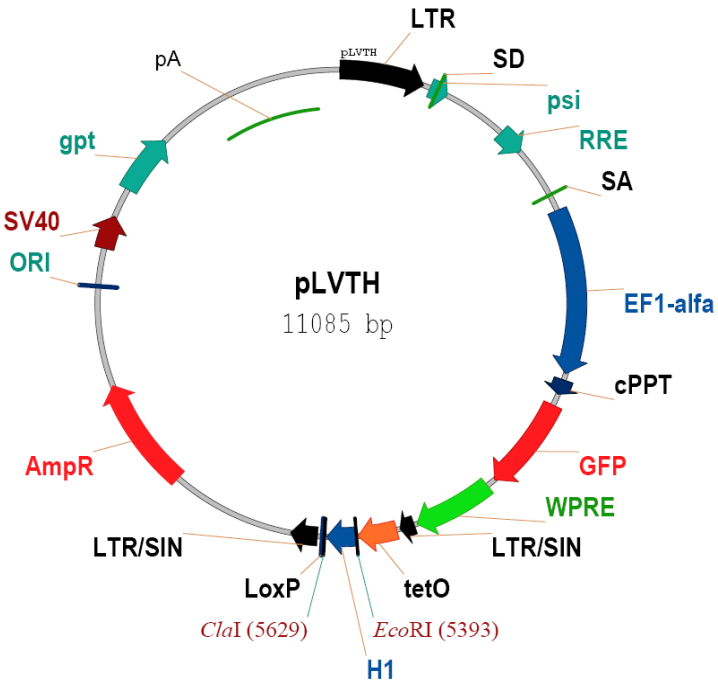

Fig. 7: Schematic structure of the pLVTH lentiviral expression vector.

The H1 insert was replaced with the H1-shRNA cassette through cloning using the Cla I and Eco RI restriction sites (from http://tronolab.epfl.ch/ website).

For cloning, pBluescript-H1-shRNA vector was digested with ClaI and EcoRI and run on a 2% agarose gel. Gel fragments containing the H1-shRNA cassette were excised under UV-light and DNA was purified using the Qiagen gel purification kit according to manufacturer's instructions. The fragments were dissolved in 10 mM Tris-Cl (pH 8). The target vector pLVTH was cut in the same way, thus losing its own H1-promotor cassette, and then purified as described above.

Ligations, transformations and restriction screens (ClaI/EcoRI) were performed similarly to the protocol described above. Positive clones carrying respective shRNA-LVTH plasmids (Table 1) were amplified in 500 ml LB-medium containing 50 µg/ml ampicillin at 37°C for 16 h. Plasmid-DNA was prepared using a Qiagen maxi-prep kit according to manufacturer's instructions and finally dissolved in 10 mM Tris-Cl (pH 8.0).

4.4 Cloning procedure (tTR-KRAB transrepressor)

HeLa and NIH3T3 cell lines expressing the tTR-KRAB repressor were originally provided by the laboratory of Prof. Dr. Hanenberg (Klinik für Kinder-Onkologie, -Hämatologie und Klinische Immunologie, Klinikum der Heinrich-Heine-Universität Düsseldorf). However, an expression vector for tTR-KRAB with a selection cassette was required in order to create new cell lines for conditional TACC3 depletion. For that, the tTR-KRAB cDNA was cloned into a retroviral expression vector containing a puromycin-resistance cassette. The tTR-KRAB cDNA was obtained through XhoI/SmaI digest from the lentiviral vector pLV-tTRKRAB-Red, provided by Dr. Didier Trono (Fig. 8).

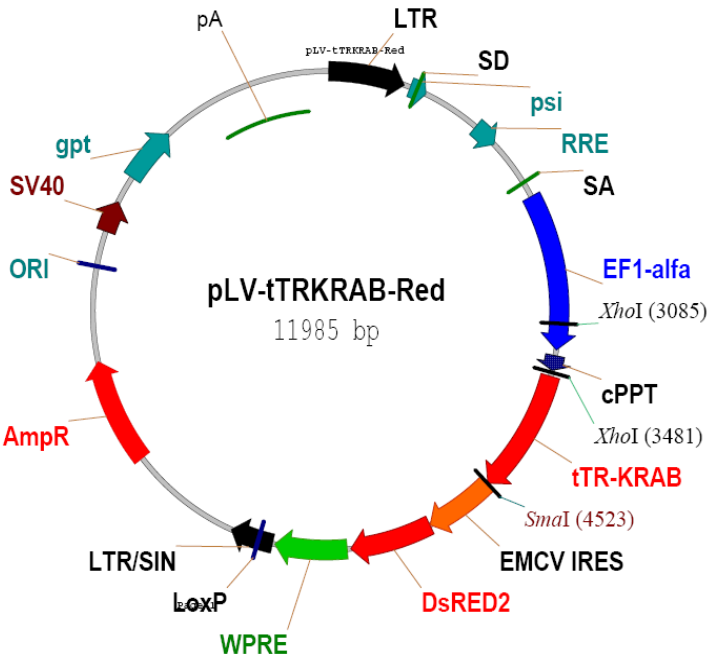

Fig. 8: Schematic structure of the pLV-tTRKRAB-Red lentiviral expression vector.
The tTR-KRAB cassette was excised using XhoI and SmaI (from http://tronolab.epfl.ch/ website).

The digested vector was run on a 0.8 % agarose gel and the gel fragment containing the tTR-KRAB DNA was excised on a UV-table and purified on JustSpin Gel Extraction columns (Genaxxon Bioscience) according to manufacturer's instructions. In parallel, the shuttle vector pBluescript (Fig. 9) was also digested with XhoI/SmaI. Ligation of the tTR-KRAB fragment into the pBluescript vector was performed overnight at 12°C using 5 U T4 DNA Ligase.

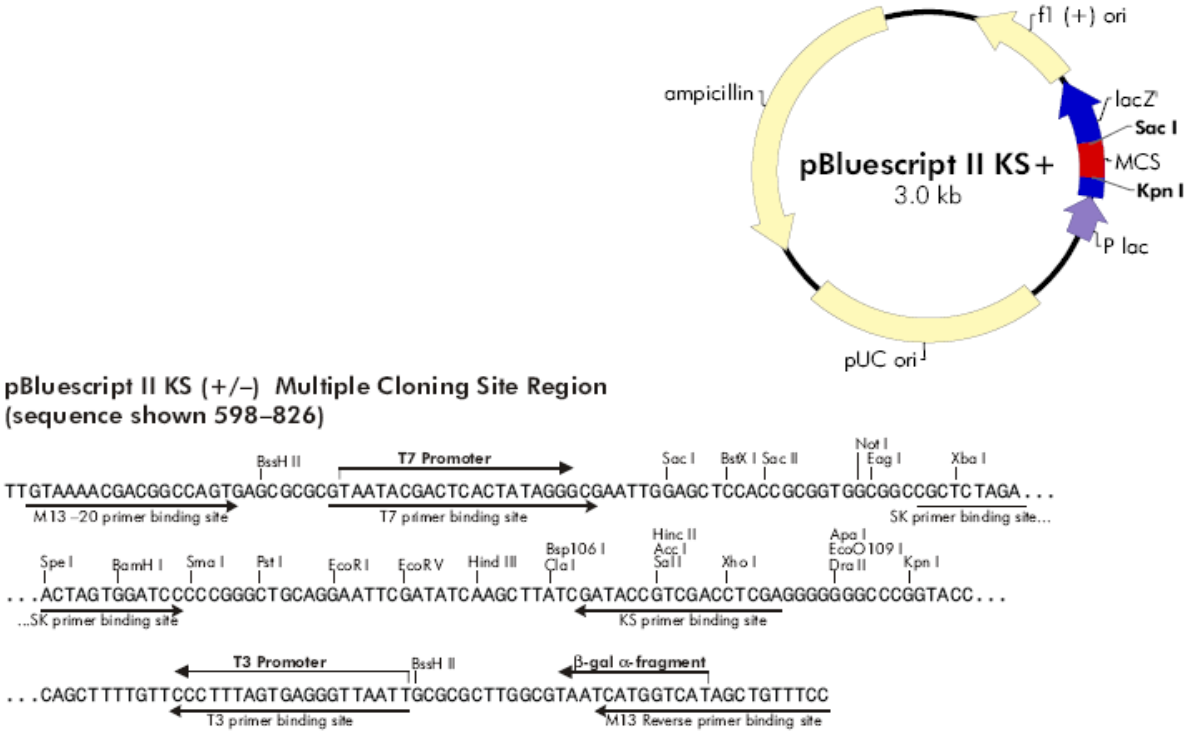

Fig. 9: Schematic structure and the multiple cloning site region of the pBluescript cloning vector.

From the www.stratagene.com website.

One positive clone was selected, amplified in 500 ml LB-medium and the pBS-tTR-KRAB plasmid DNA was prepared using the Qiagen maxi-prep kit according to manufacturer's instructions. Next the tTR-KRAB fragment was excised from pBluescript vector with ApaI/BamHI following the protocol described above. As a target vector the retroviral expression construct S11IP (provided by Prof. Dr. Helmut Hanenberg; Klinik für Kinder-Onkologie, -Hämatologie und Klinische Immunologie, Klinikum der Heinrich-Heine-Universität Düsseldorf; Fig. 10) was used.

This IRES (internal ribosome entry site sequence) containing vector enables the simultaneous expression of the puromycin acetyltransferase gene and a target gene cloned into the MCS under the same promoter. It can be used for retrovirus production and transduction of proliferating cells. S11IP was cut with NotI (producing the same overhangs as ApaI) and BamHI and purified from agarose as described above. Ligation of the tTR-KRAB fragment into S11IP vector was performed overnight at 12°C with 5 U T4 DNA Ligase. Clones were screened through several digests, using BamHI, SalI, XhoI and NdeI. These digests demonstrated a loss of a

5'-terminal sequence of the tTR-KRAB insert, which could be explained by an unexpected exonuclease activity of any enzyme involved.

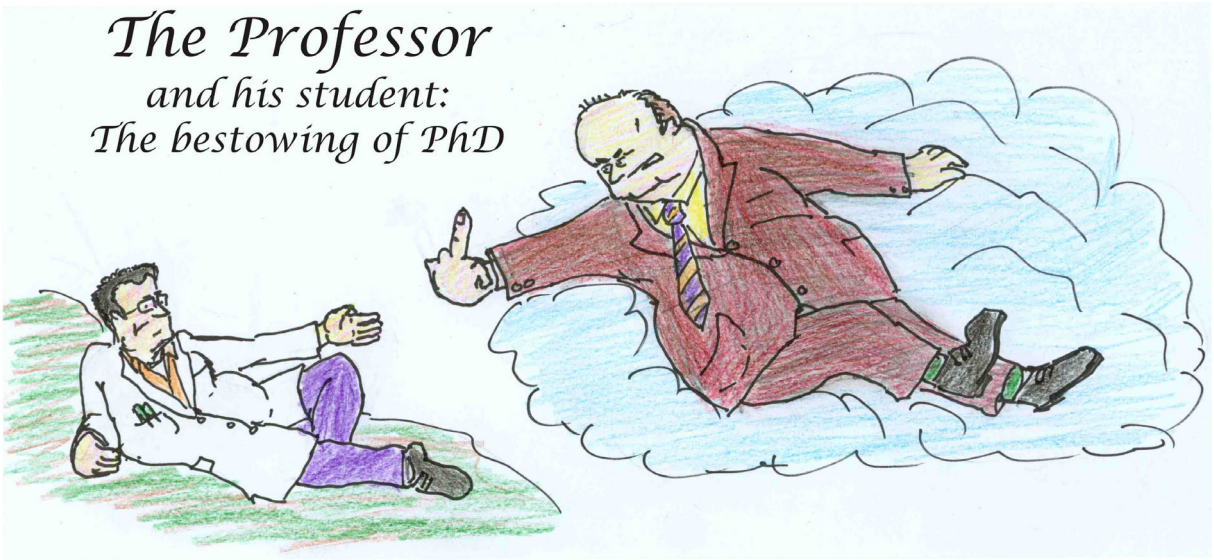

Fig. 10: Schematic structure of the retroviral expression vector S11IP.

The PCMV promoter drives the expression of an IRES sequence containing mRNA encoding the cDNA cloned into the MCS and the puromycine-resistance cDNA.

These 5' deletions were also confirmed by sequencing (GATC Biotech) using a specifically designed primer (5'-GTGTTGTCTCTGTCTGACGTGG-3'). However, one plasmid clone could be found where the 5' deletion did not reach the ATG start codon, thus still enabling translation of the tTR-KRAB protein. This particular vector was named tTR-KRAB-S11IP #23 and amplified with the use of Qiagen maxi-prep kit according to manufacturer's instructions.

4.5 Cell culture, viral transduction and isolation of stably transduced subclones

HEK 293T, NIH3T3, HeLa and MCF7 cells were cultured in Dulbecco's modified Eagle's Medium supplemented with 10% FCS (Invitrogen), 2mM L-glutamine, 100U/ml penicillin and 100µg/ml streptomycin (Genaxxon) at 5% CO_2 and 37°C in a standard cell culture incubator. HCT116 cell lines (provided by Dr. Bert Vogelstein) were cultured under the same conditions using McCoy's 5A Medium (Genaxxon). All cell lines were grown on standard cell culture dishes (TPP) and passaged for further cultivation every 3-4 days in the ratio of 1:6. In brief, culture medium was removed, cells washed with calcium and magnesium free D-PBS (Dulbecco's phosphate buffered saline; Genaxxon) and incubated with trypsin-EDTA (0.05% Trypsin with

EDTA-4Na; Invitrogen) for 5 min at 37°C. Trypsin was neutralized by addition of cell culture medium and detached cells were brought into a single cell suspension by repeated pipetting. When required, the number of viable cells was routinely determined by trypan blue (0.05%) exclusion. For that, single cell suspension was diluted with D-PBS, supplied with trypan blue, counted under the microscope using the Neubauer chamber. Average cell numbers per square were multiplied with 10^4 and the dilution factor in order to assess the number of cells per millilitre of cell suspension.

Lentivirus was generated by transient transfection of human embryonic kidney 293T cells plated on the previous day at a density of 4.5 x 10^6 cells per 10 cm dish. A lentiviral siRNA expression vector (pLVTH-siRNA), a packaging vector (psPAX2, provided by Dr. Didier Trono) and an envelope vector (pCR-VSV-G) were co-transfected at 10 µg each. For that, DNA at concentration of 1 µg/µl was dissolved in 533 µl ddH_2O and 62.5 µl of a 2.5 M calcium chloride solution was added. Building of precipitate complexes of calcium and DNA phosphate residues was induced by addition of 625 µl of 2x BBS solution (50 mM BES, 280 mM NaCl, 1.5 mM Na_2HPO_4, pH 7.02). Transfection mixtures were incubated at room temperature for 5 min and pipetted into the culture medium of 293T cells. Cells were put back in the incubator for approx. 16 hrs. Medium was next replaced by fresh medium supplemented with 10 mM sodium butyrate for 6 hrs in order to enhance lentivirus production, then replaced again. Supernatants containing recombinant lentiviral particles were harvested 24 hrs later and cellular debris was removed by filtration through sterile 0.45 µm filters. Virus-containing supernatants were supplied with 7 µg/ml polybrene (Sigma-Aldrich) and directly used to transduce target cells for a period of 24 hrs, which were seeded on the previous day at a density of 3.5x10^4 cells per 3.5 cm plate

Puromycin-selected NIH3T3 and HeLa cell lines stably expressing the tTR-KRAB transrepressor were provided by Dr. Paula Rio and Prof. Dr. Helmut Hanenberg. In order to create further cell lines (MCF7 and HCT116) capable of controllable siRNA expression, these cells needed to be first transduced with the retrovector tTR-KRAB-S11IP #23 which encodes the tTR-KRAB transrepressor and also confers puromycin resistance. Retroviral particles were produced following the same procedure as described for the lentiviral transduction method. A single retroviral packaging vector was used, namely pEQ-PAM3, provided by Dr. Elio Vanin (Persons et al., 1998). Two days after transduction, cells were subjected to positive selection through treatment

with 2 µg/ml puromycin (MP Biomedicals) into the cell culture medium for 3-4 days. Surviving cells proven to be positive for tTR-KRAB transrepressor were further used for siRNA lentivirus transduction.

From bulk populations of cells carrying the DOX-controllable siRNA-expression system individual clones were isolated. For that, $1 \cdot 10^3$ cells were seeded onto a 10 cm culture dish and allowed to form clonal colonies for several days. Colonies were then picked with a pipette, trypsinised into a single cell suspension and further expanded on 24 well plates. For each siRNA various subclones were analyzed in this study. From individual clones and also from bulk populations cryostocks were made by supplementing cell suspensions with 10% v/v DMSO, slow freeze down to -80°C and subsequent storage in liquid nitrogen. To bring cells back in culture, cryostocks were rapidly thawed, diluted with warm medium 1:10 and centrifuged at 1000x g. Cell pellets were then resuspended and seeded in appropriate medium onto culture dishes.

Induction of the siRNA expression in all cell lines was achieved by addition of 5 µg/ml DOX to the cell culture medium.

4.6 Cell synchronisation

HeLa cells were subjected to synchronization in G_1/S by a double thymidine block protocol (Piekorz et al., 2002). Cells were seeded at a density of $8x10^3/cm^2$ and treated at day 2 of DOX treatment (5 µg/ml) with 2 mM thymidine (Sigma-Aldrich) in culture medium for 24 h. After a triple wash with D-PBS thymidine-free medium was added for 10 h followed by another treatment with 2 mM thymidine for 16 h. Cells were then washed trice with D-PBS and released into thymidine-free medium.

For arresting cells in prometaphase, cells were also seeded at a density of 8 x $10^3/cm^2$ in cell culture flasks. Two days later cells were exposed to 100 nM nocodazole (Sigma-Aldrich) in culture medium for 16 h. Mitotic cells were harvested by mechanical shake-off, i.e. the flask was gently bounced several times at its side. By this method only round mitotic cells went in suspension and could be collected with the supernatant. Mitotic cells were then washed trice with D-PBS, released into nocodazole free medium, seeded in cell culture dishes and analysed at given time points. When stated, cells were supplied upon release with 20 µM of the pan-

caspase inhibitor N-(2-quinolyl)valyl-aspartyl-(2,6-difluorophenoxy)methylketone (Q-VD; MP Biomedicals).

4.7 Flow cytometry

Cell cycle analysis was performed on a Becton-Dickinson FACScalibur using CellQuest software. For determination of cell cycle distribution, cells were collected by trypsinisation together with culture medium in order to retain dead cells, centrifuged at 1400x g, washed with D-PBS, placed into a FACS tube and centrifuged again. FACS tubes with the cell pellets were placed onto the vortexer, dissolved in Nicoletti's staining solution (50 µg/ml propidium iodide, 0.1% w/v sodium citrate, 0.1% v/v Triton X-100 and 40 µg/ml RNAse) and kept until analysis on ice in the dark. The DNA content and percentage of cells in different phases of the cell cycle (G_1/S/G_2M) and aneuploid cells (near G_1 DNA content) were assayed by flow cytometry and quantified in a linear mode (FL2-A). The percentage of cells undergoing apoptotic DNA fragmentation (<2N, sub-G_1) or polyploidisation (>4N) was determined in a logarithmic mode (FL3-H).

For determination of the mitotic index through detection of the mitosis-specific phosphorylation of histone H3 at Ser10, cells were collected and washed as described above. Cells were then fixed on ice for 30 min in 90 % methanol (rapid addition of 900 µl ice-cold methanol to 100 µl cell suspension in D-PBS while vortexing). Cells were then washed with D-PBS (all centrifugations of fixed cells were performed at 1500x g) and blocked with 0.5 % BSA in D-PBS. Stainings were performed using an Alexa488-coupled anti-phospho-histone H3 (Ser10) antibody (Beckman Coulter) at a dilution of 1:10 in 0.5 % BSA/D-PBS at 4°C overnight in the dark. After a washing step with D-PBS DNA was counterstained with propidium iodide (20 µg/ml in 0.5 % BSA/D-PBS containing 40 µg/ml RNAse A). Phospho-Histone H3-positive cells and DNA content were assessed in a logarithmic mode (FL1-H) or in a linear mode (FL2-A), respectively.

For intracellular cyclin B1 staining, cells were collected and washed as described above and fixed on ice for 60 min in 70% ethanol (rapid addition of 1 ml ice-cold 96% ethanol to 400 µl cell suspension in D-PBS while vortexing). Thereafter, cells were washed, permeabilised with 0.2% Triton X100/D-PBS, washed again and blocked in 0.5% BSA/D-PBS. Stainings were performed with a monoclonal anti-cyclin B1

antibody (1:50; Ab3; Labvision) in 0.5% BSA/D-PBS at 4°C overnight. Next, cells were washed with D-PBS and the secondary FITC-conjugated antibody (1:40 in 0.5% BSA/D-PBS; Dako) was applied for 1h at room temperature in the dark. After washing with D-PBS DNA was counterstained with propidium iodide as described above. Cyclin B1-positive cells were assessed in a logarithmic mode (FL1-H) and DNA content in a linear mode (FL2-A).

BrdU (Bromodeoxyuridine) labelling of DNA-replicating cells was achieved by addition of the thymidine analogue BrdU (AppliChem) into the culture medium at a final concentration of 10 µM for 30 min. Cells were then harvested and fixed according to the procedure described for cyclin B1 staining. After centrifugation, cell pellets were resuspended in 200 µl pepsin solution (0.4 mg/ml pepsin in 0.1 M HCl) and incubated for 20 min at 37°C. Next, DNA was denaturated by incubating cell nuclei in 2M HCl for 20 min at 37°C. After centrifugation, the residual HCl was neutralized by the addition of borax buffer (0.1 M sodium tetraborate, pH 8.5). Cell nuclei were then washed with 0.5% BSA/D-PBS and stained overnight at 4°C in the dark with FITC-conjugated anti-BrdU antibody (Biomeda), diluted 1:10 in 0.5% BSA/D-PBS. After washing with D-PBS, DNA was counterstained with propidium iodide as described above. BrdU-positive cells were assessed in a logarithmic mode (FL1-H) and DNA content in linear mode (FL2-A).

FACS measurements were evaluated with Apple MacOS operated Becton-Dickinson FACSCalibur CellQuest software and assessed for presentation using WinMDI 2.8 software for Microsoft Windows.

4.8 Confocal laser scanning microscopy

Cells were seeded at densities of $8x10^3$ cells/cm^2 on round 15mm coverslips in a 12-well plate and grown in media containing 5 µg/ml DOX. After the indicated periods of time, cells were washed with PBS, fixed with ice-cold methanol/acetone (1:1) for 20 min at -20ºC, washed with PBS again and subsequently incubated in IF buffer (4% BSA, 0.05% saponine in PBS) for 1 hr. Cells were then stained at 4°C overnight in IF buffer with the following primary antibodies at the indicated dilutions: mouse-anti-α-tubulin (DM1a, 1:500, Sigma-Aldrich) or rat-anti-α-tubulin (YOL1/34, 1:500, Acris Antibodies); anti-γ-tubulin (GTU-88, 1:100, Sigma-Aldirch); anti-pericentrin and anti-Ndc80/Hec1 (ab4448 resp. ab3613, 1:500, Abcam); anti-centromer serum (CREST

serum, 1:500, Immunovision); anti-cyclin B1, (H-433, 1:200, Santa Cruz Biotechnology); anti-Aurora B (1:100; BD) and anti-BubR1 (1:1000; kindly provided by Dr. Stephen S. Taylor). Thereafter, cells were washed trice with PBS and labelled with secondary antibodies (4 µg/ml; Alexa 488-, Alexa 568- or Alexa 594-coupled anti-mouse, anti-rabbit, anti-rat or anti-human antibodies; Invitrogen, 1:400 in IF buffer) for at least 3 hrs. Cells were again washed trice with PBS and DNA was detected using DAPI (4,6 diamidino-2-phenylindole, 1 µg/ml in PBS; Sigma-Aldrich) staining. The coverslips were finally mounted onto microscope slides using fluorescent mounting medium (Dako) or Prolong Gold Antifade medium (Invitrogen). Analyses were performed with a Leica TCS SP2/AOBS confocal laser scanning microscope (cLSM) equipped with a HCX PL APO 63x immersion objective and excitation wavelengths of 405nm, 488 nm 594 nm and 633 nm. Confocal pictures were taken where indicated as projections of recorded z-stacks of various dimensions. Alternatively, cells were analyzed on a LSM510-Meta confocal microscope (Zeiss) equipped with 40x/1.3 or 63x/1.4 immersion objectives and excitation wavelengths of 364 nm, 488 nm, 543 nm and 633 nm.

For determining the percentage of cells with more than one nucleus or of cells with more than two centrosomes, cells were visualized by combined α-tubulin/DAPI or γ-tubulin/DAPI staining, respectively, as described above.

4.9 Intracellular labelling and transfections

For labelling and detection of centrioles within centrosomes, the centrin-2 cDNA was excised with BglII/BamHI from its original vector (provided by Dr. Jeffrey Salisbury, D'Assoro et al., 2001) and subcloned into the MCS of the pEYFP-C1 vector (Fig. 11), which was cut also with BglII and BamHI. This pEYFPC1-centrin2 vector allowed the expression of a N-terminal YFP-centrin-2 fusion protein in cells.

For intracellular chromosome labelling, an expression vector for the Histone-2B-YFP fusion protein was used. This expression plasmid, based on the pCDNA3 vector (Invitrogen), was provided by Oleg Fedorchenko and Dr. Antje Gohla (Institut für Biochemie und Molekularbiologie II, Klinikum der Heinrich-Heine-Universität Düsseldorf). HeLa cells were transiently transfected with pEYFPC1-Centrin-2 or pCDNA3-Histon-2B-YFP vector using the ExGen 500 reagent (Fermentas) according to the manufacturer's instructions. Next day after transfection, cells were re-seeded

at densities of 8 x 10^3 cells/cm^2 and treated with DOX (5 µg/ml) to induce siRNA expression and used for cLSM analysis.

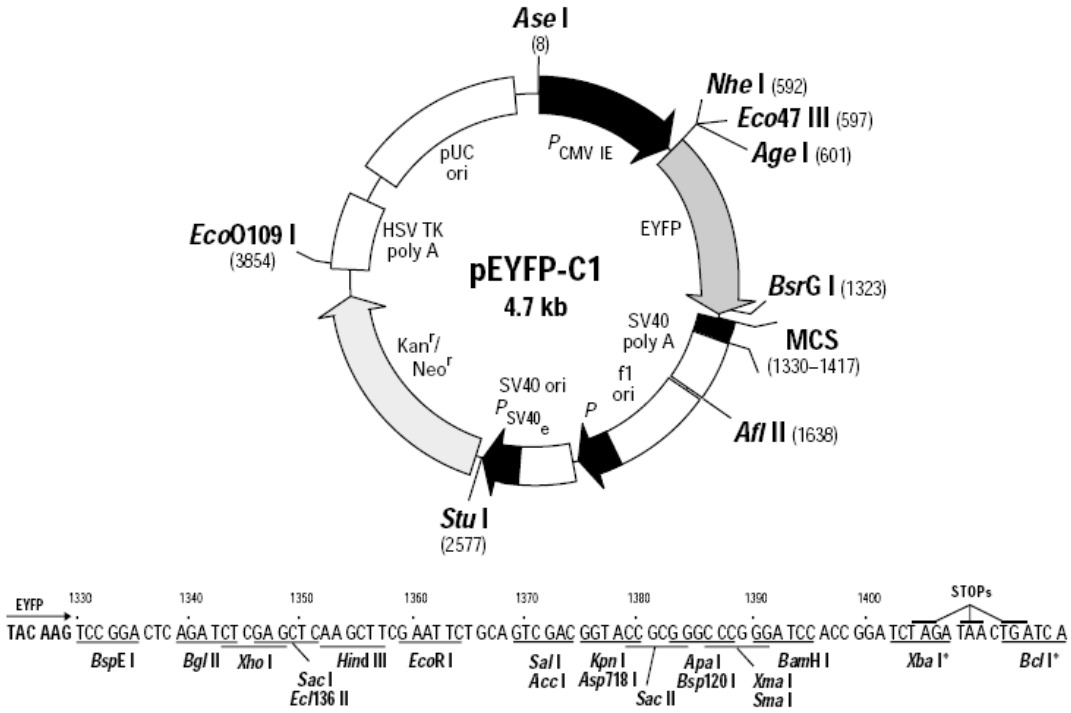

Fig. 11: Schematic structure and sequence of the multiple cloning site of the pEYFP-C1 expression vector.

From the www.bdbiosciences.com website.

4.10 Senescence-associated β-Galactosidase (β-Gal) staining

Cells were grown in 6 well plates under continuous DOX treatment (5 µg/ml). The protocol for histochemical detection of the lysosomal β-galactosidase activity at pH 6.0 has been initially described (Dimri et al., 1995). In brief, cells were fixated for 4 min with 2% formaldehyde / 0.2% glutaraldehyde (Applichem) in PBS, washed with PBS and stained with β-Gal staining solution (2 mM $MgCl_2$, 150 mM NaCl, 5 mM $K_4Fe(CN)_6$, 5 mM $K_3Fe(CN)_6$, 40 mM citric acid pH 6.0, 1 mg/ml X-Gal (5-Bromo-4-Chloro-3-Indolyl α-D-Galactopyranoside) at 37°C for 24 hrs. Cells were washed again with PBS and the characteristical blue staining of senescent cells was documented by standard microscopy using a Zeiss imaging system.

4.11 Reverse transcriptase-PCR expression analysis

Total cellular RNA was isolated using the Qiazol RNA isolation kit (Qiagen). First strand cDNAs were generated from 2 µg RNA in a total volume of 20 µl by oligo dT priming using Omniscript reverse transcriptase (Qiagen). Primer sets and PCR conditions used to amplify fragments of individual human TACC isoforms have been previously published (TACC1: 5'-CGGGGATCCATGGCGTTCAGCCCGTGGCA-3' and 5'-GGATTCGGGGAGAGGTGTGCCCTCCACAG-3'; Conte et al., 2002 ; TACC2: 5'-CTTTATTCTTCTGCTCCAGCGTCCTTTCCA-3' and 5'-TTTTAAATCCCA AGCCTCTTTGAGATCC-3'; Pu et al., 2001 ; TACC3: 5'-CCAAAGCTGAAATCCAGA A-3' and 5'-GATCTCCTCGTTTGCCA-3'; McKeveney et al., 2001). PCR amplification was carried out for 30 cycles on 1.3 µl (TACC2 and TACC3) or 3.9 µl (TACC1) of the reverse transcription mixture, and samples were analysed on 1.2% agarose gels.

4.12 Subcellular fractionation

Frozen cell pellets were homogenized through 1 ml syringes with No. 20 needles in 500 µl ice-cold extraction buffer (EB; 10 mM HEPES-KOH (pH 8.0), 0.32 M sucrose, 1 mM EGTA, 25 mM KCl, 5 mM $MgCl_2$, 0.1 mM DTT, 1 mM DNase, 1 mM PMSF, Complete Protease Inhibitor Cocktail (Roche)). The crude nuclear pellet was isolated by centrifugation (600x g, 10 min), re-suspended in 3 ml nuclear buffer 1 (NE1; 0.25 M sucrose, 10 mM $MgCl_2$), and transferred onto 3 ml NE2 (0.35 M sucrose, 0.5 mM $MgCl_2$) in a fresh tube and centrifuged (1450x g, 5 min). Pellets were re-suspended in 300-400 µl EB containing 2% CHAPS and retained as the nuclear fraction. The cytosolic supernatant containing mitochondria from the initial centrifugation step (600x g, 10 min) were transferred into a fresh tube and centrifuged (10,000x g, 30 min). The crude mitochondrial (pellet) fraction was washed in EB (10,000x g, 30 min), then re-suspended in 100 µl EB containing 2% CHAPS. The crude cytosolic (supernatant) fraction was centrifuged (10,000x g, 30 min) to pellet out residual mitochondria. The resulting supernatant was transferred into a fresh tube and retained as the soluble cytosolic fraction.

4.13 Immunoblotting

For protein extraction cells were harvested and washed as described for Flow Cytometry (p. 38). Cell pellets were shock-frozen in liquid nitrogen and stored at -80°C. Total cell lysates from pellets were prepared in NP40-lysis buffer (1% NP-40, 50 mM Tris/Cl pH 8.0, 150 mM NaCl, 2 mM EDTA, 1 mM DTT, 0.1 mM Na_2VO_4 and Complete Protease Inhibitor Cocktail (Roche)) by incubating on 4°C under constant agitation. Lysates were centrifuged for 5 min at 13000x g. Supernatants were collected and analyzed for protein concentration using the Bradford assay (BioRad). For that, a calibration curve of BSA standards was prepared (ranging from 1 to 15 µg/µl). The photometrical analysis was performed in micro-cuvettes at 595 nm using the DU800 Spectrophotometer and Application Software (Beckman Coulter).

For SDS-PAGE, samples with equal protein amount (in µg) were dissolved in Laemmli loading buffer (64mM Tris-Cl pH 6.8, 6% v/v glycerol, 0.1% w/v bromphenol blue, 0.03% w/v SDS and 20% β-mercaptoethanol), denaturated at 95°C for 5 min and loaded on SDS-PAGE gels. Proteins were separated by gel electrophoresis using the Bio-Rad mini gel apparatus (Bio-Rad). Thereafter proteins were transferred in blotting buffer (containing 20% methanol) to a nitrocellulose membrane (Hybond C, GE Healthcare Life Sciences) using the Bio-Rad mini blot apparatus (60 min at 300mA). Western blot membranes were stained for equal protein loading with Ponseau S (0.2% in 5% acetic acid) and documented. Afterwards blot membranes were blocked in 5% skimmed milk powder in TBS (Tris-buffered saline, pH 7.4) for 1h at room temperature. Primarily antibodies (see pp. 25-26) were applied at dilutions of 1:500-1:1000 (or 1:10000 for α-tubulin, β-actin and Lamin A/C) in 5% BSA/PBS and incubated overnight at 4°C under constant agitation. Membranes were then washed trice for 5 min with TBS-T (0.1% Tween 20 in TBS) and probed for 1 h with HRP (horseradish peroxidase) labelled secondary antibodies, diluted in 5% skimmed milk/TBS according to the manufacturer's instructions. After a triple 5 min wash with TBS-T western blot membranes were treated with the ECL detection system (GE Healthcare Life Sciences) and exposed to X-ray films. Films were developed using the Agfa Curix 60 developing machine.

4.14 Statistical analysis

To evaluate statistical significance, Student's *t* tests were performed using the Sigma Plot 9 software. Results are given as means ± S.D. *p*-values below 0.05 were considered significant.

5 Results

5.1 Establishing cellular models for conditional TACC3 silencing

TACC3 deficiency in mice results in embryonic lethality and the failure of primary *knock out* cells to grow *ex vivo* (Piekorz et al., 2002). In order to address the molecular and cellular role of TACC3 in proliferation, a system for drug inducible, hence conditional, TACC3 depletion via RNA interference was developed. In this system, the expression of siRNAs and the marker gene GFP is suppressed by binding of the tTR-KRAB transrepressor to the tetO-DNA sequence proximal to the promoter (Fig. 6). After addition of doxycycline (DOX, 5 µg/ml), the inhibition of transcription is relieved due to the incapacity of DOX-bound tTR-KRAB to associate with the Tet-operator.

The resulting siRNA expression was indirectly confirmed by the production of GFP protein in the cells, which is demonstrated here for murine NIH3T3 cells by flow cytometric analysis (Fig. 12A). Expression of the TACC3 specific siRNA (siRNA3m) led to an efficient depletion of the TACC3 protein in NIH3T3 cells already at day 3 of DOX treatment, while the control siRNA (siRNA2m) did not have any detectable effect (Fig. 12B). Furthermore, the concept of inducible siRNA-mediated TACC3 withdrawal allows also the study of TACC3 function in human cells. Hence, human cancer cell lines were used in order to down-regulate TACC3. For instance, in the cervix carcinoma cell line HeLa TACC3 could be nearly totally depleted by TACC3 specific siRNA (siRNA2h) expression already at day 2 of DOX treatment, as demonstrated by western blot analysis of total TACC3 protein levels (Fig. 12C). The reduction of TACC3 mRNA upon siRNA expression was confirmed by semi-quantitative RT-PCR (Fig. 12D). Importantly, mRNA levels of the other TACC isoforms (TACC1 and TACC2) were not affected by TACC3-siRNA expression. This finding was confirmed by co-transfection of siRNA-lentivectors and expression vectors for the three murine TACC-isoforms into 293T cells. When the TACC3 specific siRNA3m was expressed, protein levels of transiently expressed TACC1 and TACC2 remained high, while the expression of TACC3 was largely suppressed (Fig. 12E). In summary, TACC3-siRNA expression cassettes could be delivered by lentiviral vectors to various cell lines and used for drug-controlled inhibition of TACC3 expression.

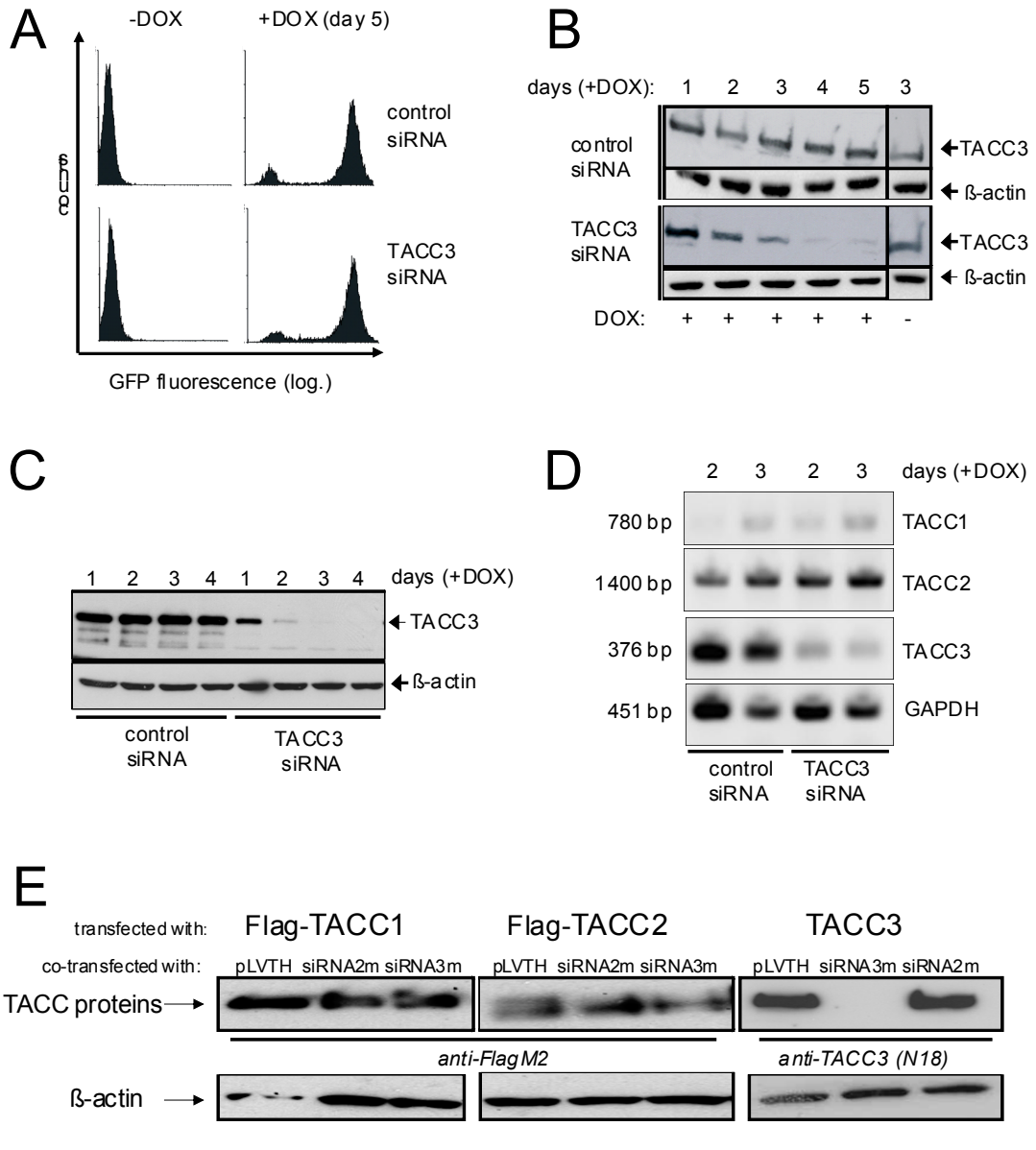

Fig. 12: Inducible and efficient depletion of TACC3 in various cell lines.

(**A**) Upon addition of DOX (5 µg/ml), GFP marker is expressed indicating co-expression of the induced siRNAs. Flow cytometric analysis of murine NIH3T3 cells, stably transduced with control (siRNA2m) or TACC3 siRNA (siRNA3m) expression vectors. (**B**) Downregulation of TACC3 expression in NIH3T3 cell clones, transduced with lentiviral vectors encoding a control or TACC3-specific siRNA. TACC3 protein levels were determined by immunoblot analysis after the indicated period of DOX treatment. Expression of β-actin served as a control for protein loading. (**C**) Similar as in (B), TACC3 protein is strongly and rapidly depleted in human HeLa cells after DOX addition. (**D**) Isoform-specific TACC3 depletion. Total cellular RNA was isolated from TACC3-specific or control siRNA expressing HeLa cells treated with DOX (5 µg/ml) for two or three days. The presence of transcripts for human TACC isoforms was determined semiquantitatively by reverse transcriptase-polymerase chain reaction analysis. GAPDH-specific primers were employed as a control for cDNA integrity. (**E**) Isoform-specific suppression of transient TACC3 expression in 293T cells by siRNA3m. 293T cells were transfected by the calcium-phosphate method with expression vectors for murine TACC3 or FLAG-labeled murine TACC1 and TACC2 together with the empty pLVTH vector or pLVTH plasmids expressing siRNA2m or siRNA3m. Total cell lysates were analyzed by western blotting using the indicated antibodies.

5.2 Consequences of TACC3 depletion for cell cycle progression in checkpoint proficient cells

Cell cycle checkpoints, especially the p53-dependent G_1-checkpoint, are activated as response to various stress and DNA-damage events and are crucial for the maintenance of chromosomal stability and hence for the prevention of cellular transformation (Pietenpol & Stewart, 2002). In order to elucidate the molecular and cellular mechanisms associated with the defects observed in TACC3-deficient mouse embryos, the effects of a conditional depletion of the mitotic protein TACC3 were studied in G_1 checkpoint proficient cells lines. For that, the murine fibroblast line NIH3T3 and the human breast carcinoma cell line MCF7 were employed. It is widely accepted that NIH3T3 represents an untransformed cell line and that both NIH3T3 and MCF7 cells display a fully functional p53-$p21^{WAF}$ response.

5.2.1 Aneuploidy and inhibition of proliferation in NIH3T3 cells upon TACC3 depletion

After DOX-mediated induction of TACC3-siRNA expression in NIH3T3 fibroblasts a strong inhibition of cell proliferation was observed, which was not seen when the control siRNA was expressed (Fig. 13). Experimentally, an equal number of control and TACC3 siRNA expressing cells was seeded every four days and the cumulative cell number was assessed when cells were passaged.

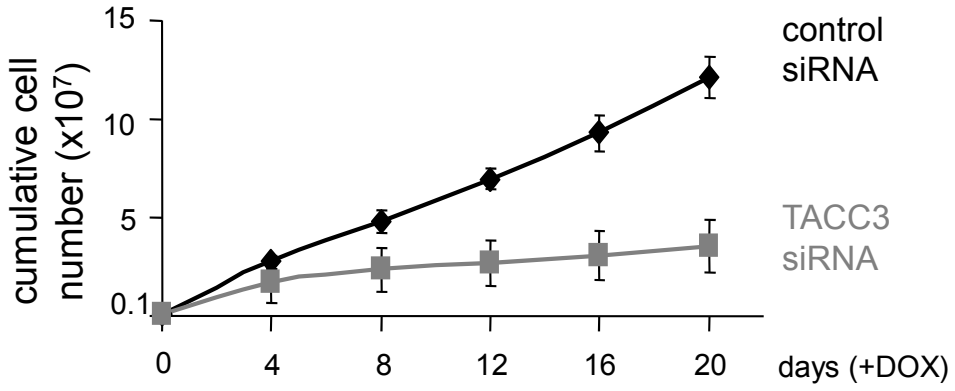

Fig. 13: TACC3 depletion inhibits proliferation of NIH3T3 fibroblasts.

Cell proliferation of siRNA expressing NIH3T3 clones in the absence of TACC3. An equal number of cells ($6x10^3/cm^2$) was re-plated every four days and cumulative cell numbers were determined prior to each passage. Long term cumulative growth with two control siRNA and two TACC3 siRNA expressing clones was analyzed in two experiments (mean ± SD).

In particular, at day 12 of continuous DOX treatment and re-passaging, the cumulative numbers of cells expressing a functional (siRNA3m) and non-functional siRNA (siRNA2m) differed by 2.5-fold, increasing to an average 3.4-fold difference by day 20 (Fig. 13).

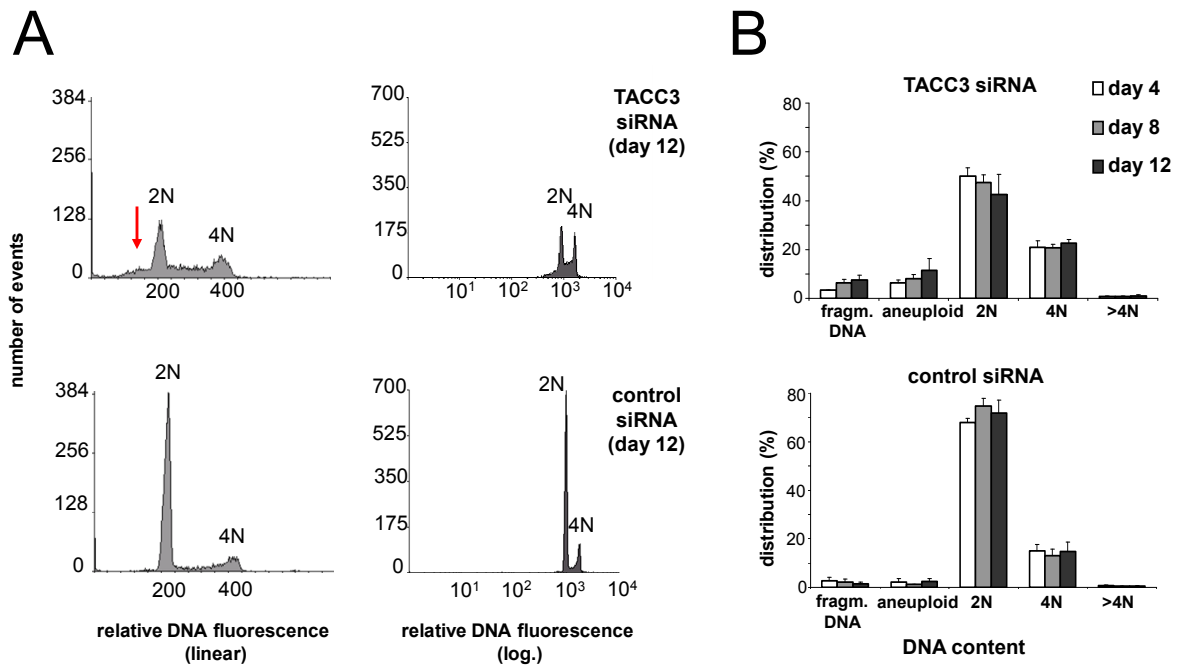

Fig. 14: TACC3 depletion causes aneuploidy in NIH3T3 cells.

(**A**) Analysis of cellular DNA content by propidium iodide staining and flow cytometry. Cells were passaged as described and and the percentage of cells with various DNA contents indicative of cell death (DNA fragmentation in sub-G_1, detected in a logarithmic mode), aneuploidy (nearly 2N; arrow, detected in a linear mode) and polyploidy (>4N) were determined. A representative experiment at day 12 of DOX treatment is shown. (**B**) Kinetics and statistical evaluation of the propidium iodide staining and DNA content analysis as shown in (A).

At the cell cycle level, the diminished proliferation capacity of TACC3-depleted cells was characterized by a progressive decrease of cells with a normal diploid (2N) DNA content, whereas more cells were present in 4N (Fig. 14). Thus, an elevated 4N/2N ratio indicated an accumulation of tetraploid (4N) cells following TACC3 depletion. Cell death was slightly increased following TACC3 depletion as indicated by the percentage of cells undergoing DNA fragmentation within a logarithmic sub-G_1 window. Most importantly, a significant percentage of TACC3 depleted cells became aneupoid, containing less then a DNA content (nearly 2N) and affecting nearly 12% of cells at day 12 of DOX treatment (Fig. 14B). These findings therefore suggest that the withdrawal of TACC3 affects equal separation of chromosomes thus resulting in

aneuploidy and inhibition of cellular proliferation. In the following, the mechanistical interdependence between these two phenotypes was studied.

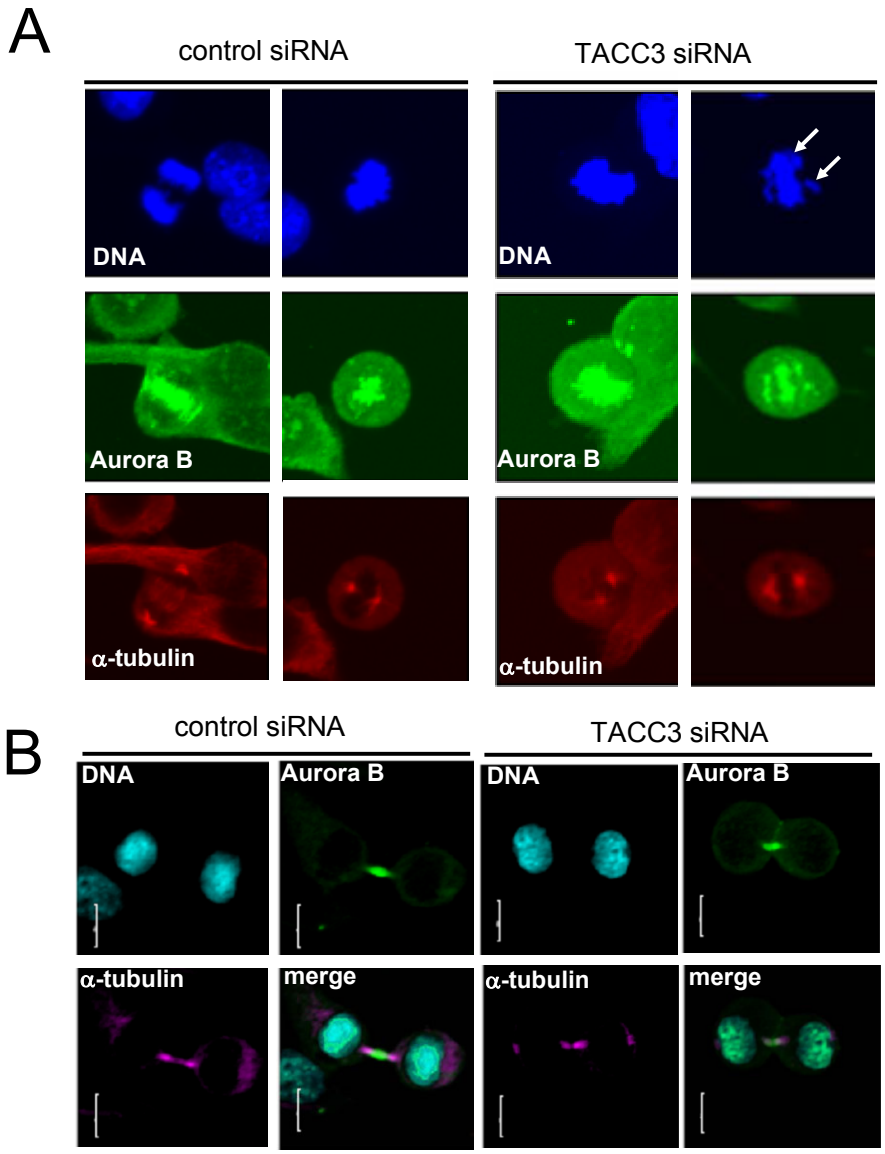

Fig. 15: Aneuploidy, but lack of major mitotic defects in TACC3-depleted NIH3T3 cells.

(**A**) Mitotic localization of Aurora B, a major regulator of chromosomal alignment and cell division at kinetochores was visualized by immunocytochemistry and confocal microscopy. Control and TACC3-depleted cells were co-stained for Aurora B (green) and α-tubulin (red) using specific antibodies. Note that TACC3-depleted cells in metaphase show unattachted chromosomes (arrows). (**B**) TACC3-depleted cells perform cytokinesis without obvious abnormalities, with normal Aurora B localization at mitotic bridges. Cells undergoing cell division were analyzed as described in (A). DNA in (A) and (B) was visualized by DAPI staining (blue), Aurora B (green), α-Tubulin (violet). Representative confocal images are shown. Bar: 7.8 µm.

Errors in the process of mitotic chromosomal segregation are widely accepted to be the origins of aneuploidy (Bharadwaj & Yu, 2004). TACC3 expression is cell cycle

dependently regulated and sets on in G_2 phase, peaking at mitosis where the protein localizes to the centrosome and the mitotic spindle (Piekorz et al., 2002). Consistent with its function in mitosis, TACC3 depletion resulted in chromosomal misalignment and segregation defects.

As representatively shown in Fig. 15A, most TACC3 depleted NIH3T3 cells displayed signs of chromosomal misalignment at metaphase. However, the defects in spindle assembly in TACC3 depleted cells were of a moderate severity, since these cells did not show a decreased delocalisation of the regulatory mitotic kinase Aurora B from kinetochores (Fig. 15) as opposed to TACC3 depleted HeLa cells (shown in Fig. 27). During mitotic progression, Aurora B first localises to kinetochores and at the anaphase transition to the midbody, which becomes the mitotic bridge at cytokinesis. As indicated in Fig. 15, Aurora B localised normally during the corresponding mitotic phases when TACC3-depleted as well as control siRNA expressing NIH3T3 cells were analyzed by cLSM. The observed defects in chromosomal alignment in TACC3 depleted NIH3T3 cells apparently caused only a transient mitotic delay. Flow cytometrical analysis of cells quantitatively stained for the mitotic marker phospho-histone 3 (PH-3) revealed a significantly increased but still relatively low mitotic index for TACC3-depleted cells (3.2±1.1% PH-3 positive cells in TACC3 siRNA expressing cultures as compared to 1.3±0.9% in control cells; mean ± SD; p=0.01). In summary, mitotic defects in TACC3 depleted NIH3T3 cells lead to chromosomal misalignment but do not suffice to induce a sustained mitotic arrest.

5.2.2 Activation of the p53-p21^{WAF} pathway and G_1/G_2 arrest upon TACC3 depletion in NIH3T3 cells

G_1-checkpoint proficient cells usually respond to aberrant mitosis and the consequential unequal DNA distribution by post-mitotic arrest in G_1 and G_2 in a p53-dependent manner (Blagosklonny, 2006; Vogel et al., 2004). Indeed, embryonic growth retardation and even the embryonic lethality of TACC3 deficient mice could be in part genetically rescued by lowering p53 expression (Piekorz et al., 2002). Therefore, the inhibited proliferation of TACC3 depleted NIH3T3 cells could possibly originate from a p53-p21^{WAF} mediated arrest, which is activated as a response to an aberrant mitosis (Blagosklonny, 2006).

As demonstrated in Fig. 16A, TACC3 depletion in NIH3T3 cells led to a robust and lasting increase in the levels of the G_1-checkpoint proteins p53 and $p21^{WAF}$ (Schneider et al., 2007b). In addition, the $p21^{WAF}$-related Cdk-inhibitor $p27^{KIP}$ was found slightly elevated in TACC3 depleted cells. Remarkably, these inductions appeared in most cases to become stronger with every passage, indicating a proportionally increasing percentage of G_1 arrested cells in the time course of TACC3 siRNA expression.

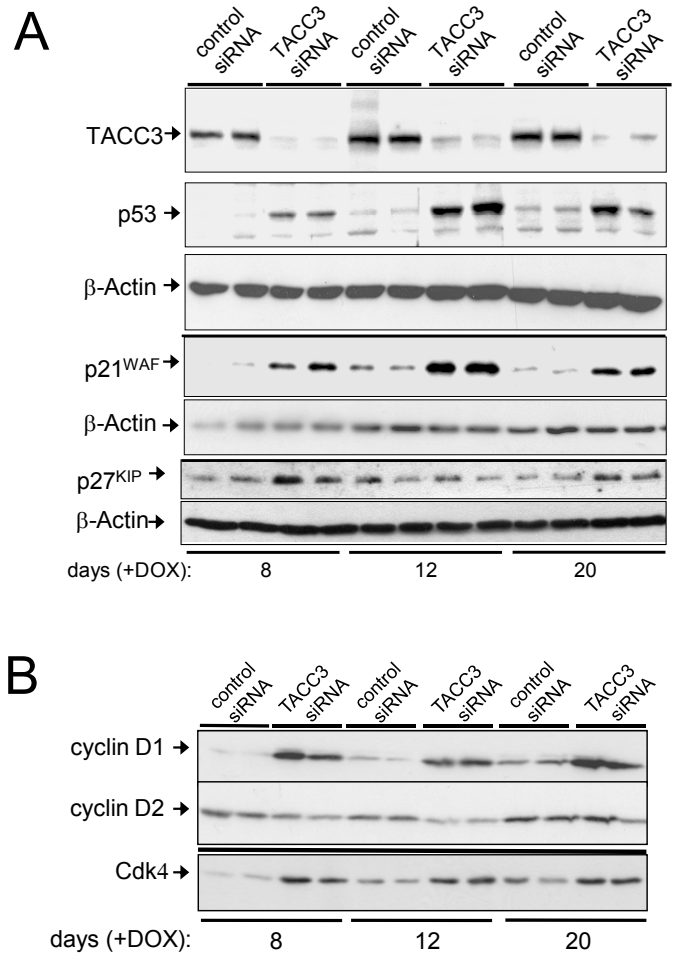

Fig. 16: Sustained activation of the p53-$p21^{WAF}$ pathway and G_1 arrest in TACC3-depleted NIH3T3 cells.

(**A**) Immunoblot analysis of extracts from TACC3 depleted cells and control siRNA expressing cells after treatment with DOX for a period of eight, twelve and twenty days. Cells were re-passaged every fourth day as indicated in Fig. 13. Antibodies specific for TACC3, p53, $p21^{WAF}$ and $p27^{KIP}$ were employed in this representative immunoblot analysis. (**B**) Cells were treated as in (A) and protein levels for the G_1 markers cyclin D1 and its corresponding kinase Cdk4 were determined. Staining for β-actin (A) or cyclin D2 (B) was used to control protein loading.

In order to further determine whether TACC3 depletion first arrests NIH3T3 cells in G_1, the expression of cyclin proteins was analyzed. Each phase of the cell cycle is

characterised by the expression of its specific cyclins. D-type cyclins, which regulate the kinases Cdk4 and Cdk6 are typically associated with the late G_1 phase. Therefore, the occurance of a post-mitotic G_1 arrest in TACC3 depleted NIH3T3 cells is supported by the elevated protein levels of the G_1-type specific regulators cyclin D1 and Cdk4 (Fig. 16B).

The elevated expression of cell cycle specific cyclins in TACC3 depleted NIH3T3 cells does not only indicate an arrest in G_1. Furthermore, elevated protein levels of cyclin B1, which is specifically expressed in G_2/M, point to an additional checkpoint activated in TACC3 depleted cells (Fig. 17A).

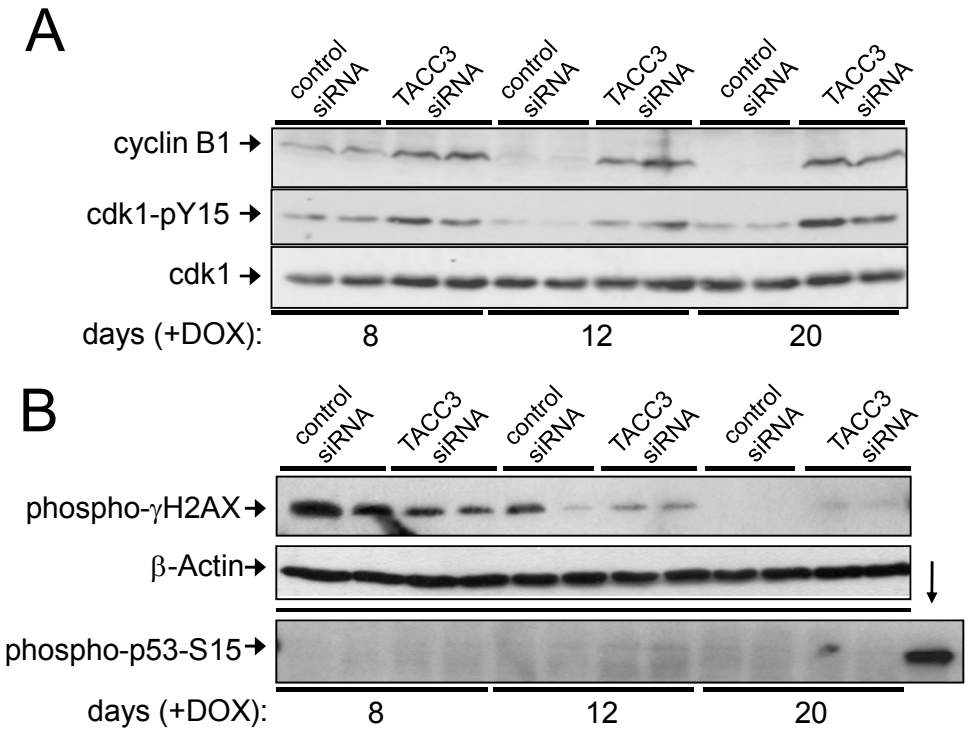

Fig. 17: G_2 arrest in TACC3-depleted NIH3T3 cells.

(A) G_2/M transition arrest upon TACC3 depletion as indicated by elevated levels of cyclin B1 and Y15-phosphorylated (i.e. inactive) Cdk1 kinase. Expression of β-actin served as a control for equal protein loading. (**B**) A classical activation of the G_2 checkpoint by DNA damage can be excluded, since neither γ-H2AX nor p53-Ser15 phosphorylation (both typical markes for DNA damage) were increased in TACC3 depleted cells (arrow: positive control for the DNA-damage marker p53-pSer15. Here, NIH3T3 cells were treated with the DNA damaging agent Actinomycin D at 1 µg/ml).

This additional arrest in G_2 is further verified by increased amounts of Cdk1 (=cdc2) phosphorylated at Tyr-15 (Fig. 17A). This regulatory phosphorylation is performed in G_2 primarily by *wee1*- and *mik1*-encoded tyrosine kinases and prevents the activation of the Cdk1-cyclin B1 complex required for mitotic entry (Gould & Nurse, 1989;

Nurse, 1990). Thus, these data indicate that TACC3-depleted cells, which eventually escaped G_1 arrest, became once more arrested prior to the G_2/M transition. The notion that this G_2 arrest is caused through the slippage from G_1 arrest and not by activation of classical DNA damage pathways (Motoyama & Naka, 2004) was supported by the lack of increased p53 phosphorylation at Ser15 and histone γ-H2AX phosphorylated at Ser139 (Fig. 17B). Both phosphorylated molecules are classical markers for a G_2 arrest resulting from DNA damage (Motoyama & Naka, 2004).

5.2.3 Reversibility of the post-mitotic arrest in TACC3 depleted NIH3T3 cells by TACC3 re-expression

The activation of the p53-pathway can cause either apoptosis or cell cycle arrest (Yu & Zhang, 2005). In NIH3T3 cells, TACC3 depletion failed to cause a strong cell death response (Fig. 14) and resulted predominantly in a $p21^{WAF}$ dependent cell cycle arrest (Fig. 16). This arrest did not become permanent and was actually functioning in a reversible manner, as indicated in Fig. 18A.

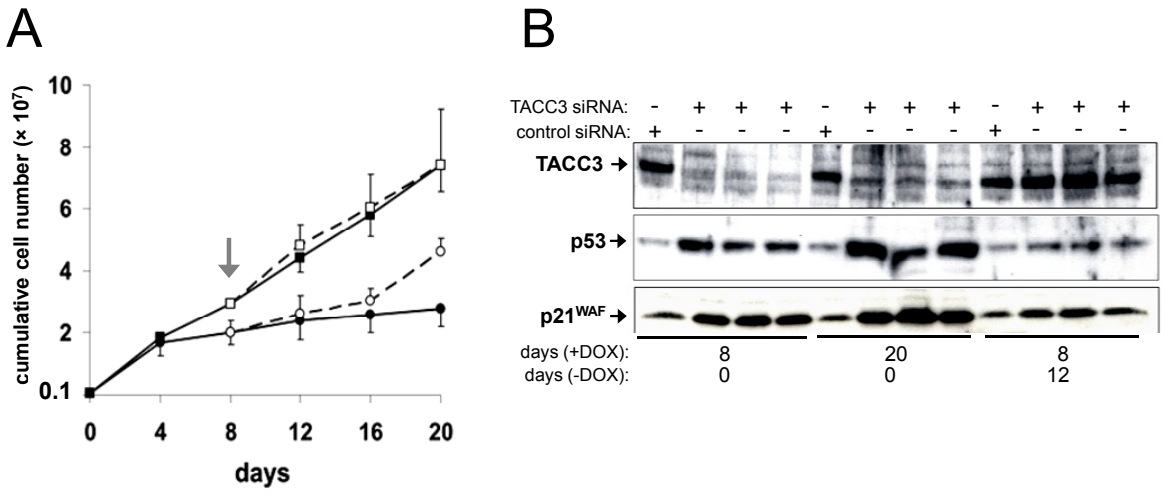

Fig. 18: Cell cycle inhibition following TACC3 depletion in NIH3T3 fibroblasts is reversible.

(**A**) NIH3T3 cell clones expressing a control siRNA (squares) or the TACC3-specific siRNA (circles) were analyzed as indicated in Fig. 13 and the cumulative increase in cell numbers was determined over a period of twenty days. The black lines show the number of cells in the continuous presence of DOX, and the dashed lines the cell number after DOX withdrawal from day eight on (arrow). Values shown are the means ± SD from two experiments analyzing each two different control and TACC3 siRNA-expressing clones. (**B**) Immunoblot analysis of extracts from TACC3-depleted cells and controls with and without DOX treatment using TACC3-, p53- and $p21^{WAF}$-specific antibodies. The last four lanes show cells grown in absence of DOX for 12 days following a previous period of treatment with DOX of 8 days.

In this experiment, NIH3T3 cells were cultured for eight days in the presence of DOX, thus inducing TACC3-siRNA expression and TACC3 depletion. Thereafter, cells were either further kept on DOX or the siRNA expression was discontinued through DOX removal. Indeed, proliferation of “DOX-free” cells could fully recover after 12 days and became comparable to the rate of control siRNA expressing cells (Fig. 18A). At the same time, protein levels for the p53 and $p21^{WAF}$ levels declined while TACC3 expression was restored (Fig. 18B). Thus, TACC3 depletion-induced mitotic stress causes a transient p53-$p21^{WAF}$-associated inhibition of cell cycle progression, which is reversible and is not sufficient to cause a widespread cell death as indicated by an only moderate increase in the percentage of cells with fragmented DNA (Fig. 14).

5.2.4 TACC3 depletion and treatment with low doses of paclitaxel activate similar signalling pathways in a synergistic manner

The previous data implies that mitotic stress through TACC3 depletion activates the p53 dependent post-mitotic G_1 checkpoint. Interestingly, this has been also reported for the mitotic spindle poison paclitaxel (Taxol®) when applied in low nanomolar concentrations (Giannakakou et al., 2001). Paclitaxel is a widely used chemotherapeutic agent, which impedes microtubule dynamics by binding to β-tubulin subunit at the plus-end of microtubules. This results in stabilization of microtubules and hence impairment of a proper attachment of microtubules to the kinetochores. Treatment of cells with low paclitaxel concentrations (~10 nM) results in a misaligned chromosome phenotype (Abal et al., 2003), similarly as observed in TACC3 depleted NIH3T3 cells (Fig. 15). Therefore, the molecular pathways activated by mitotic stress, i.e. through paclitaxel treatment or TACC3 depletion, were investigated and compared in greater detail. In particular, the outcome of a combined treatment (i.e. paclitaxel treatment of TACC3-siRNA expressing cells as opposed to treatment of control-siRNA expressing cells) on G_1 checkpoint activation was studied in NIH3T3 cells.

Indeed, both paclitaxel treatment and TACC3 depletion resulted in the activation of similar molecular pathways. In TACC3 depleted NIH3T3 cells, treatment with a low concentration of paclitaxel (10 nM) had profound effects on G_1 checkpoint activation. As indicated in Fig. 19A, the p53-$p21^{WAF}$ response was potentiated, i.e. increased

protein levels of p53-p21^{WAF} and also elevated cyclin D1 and p27^{KIP} protein concentrations could be detected. Furthermore, the G_1 regulator cyclin D1 accumulated in the cytoplasm as required for an efficient arrest (Fig. 19B). Only nuclear cyclin D1/Cdk4 complexes are able to inactivate the Rb protein and thus initiate progression into S-phase (Gladden & Diehl, 2005). Importantly, the sub-cellular localisation pattern of p53, p21^{WAF} and cyclin D1 in TACC3 depleted cells was not altered by additional paclitaxel treatment (Fig. 19B), which supports a synergistic model, describing the combined impact of TACC3 depletion and paclitaxel treatment.

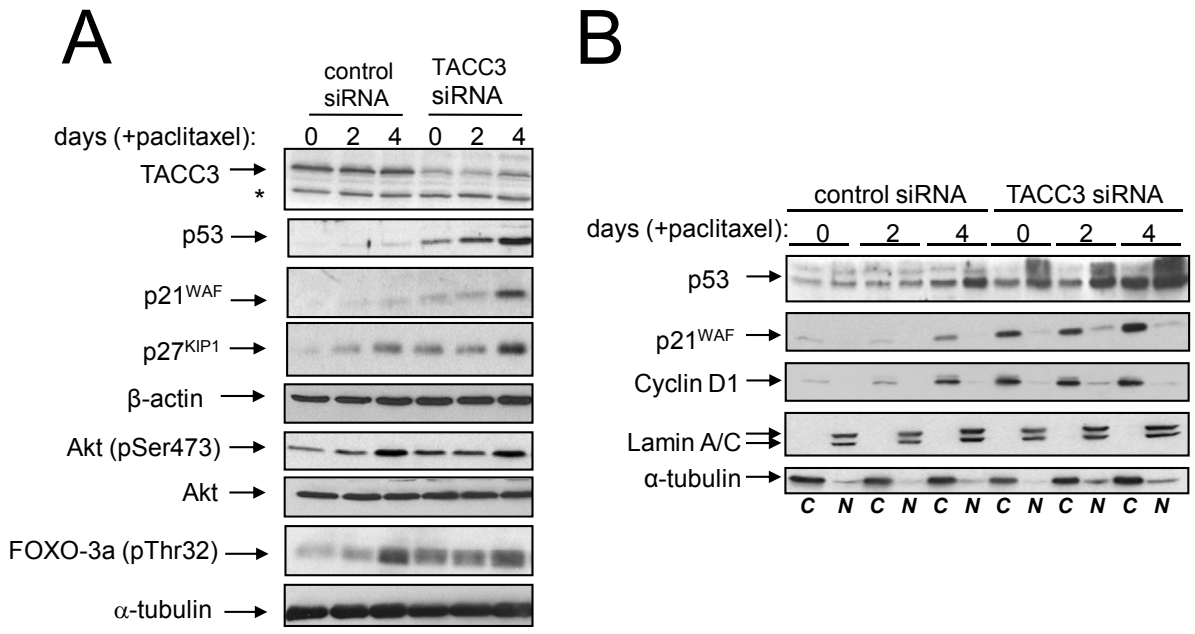

Fig. 19: TACC3 depletion strongly increases the expression of various cell cycle effectors upon low dose paclitaxel treatment.

(**A**) Immunoblot analysis of extracts from TACC3 depleted cells and control cells without paclitaxel treatment (day 0) or after treatment with 10 nM paclitaxel for two or four days. The expression of p53, p21^{WAF}, p27^{KIP} as well as of Ser-473 phosphorylated Akt and the Akt phosphorylation target FOXO-3a (Thr32) and β-actin/α-tubulin as loading controls was determined by immunoblot analysis using specific antibodies. The unspecific signal recognised by the anti-TACC3 antibody (N18) is indicated by the asterisk. (**B**) Upregulation and cytoplasmatic accumulation of p21^{WAF} and cyclin D1 increases in TACC3-depleted cells upon paclitaxel treatment. Nuclear and cytoplasmatic extracts were prepared and analyzed as indicated in (A). Lamin A/C and α-tubulin were used as markers for nuclear (*N*) and cytoplasmatic fractions (*C*), respectively.

Upon TACC3 depletion and/or treatment with low doses of paclitaxel, p53 was predominantly found in the nucleus, corresponding to its function as a transcriptional effector, while p21^{WAF} was highly induced and localized to the cytosol rather than to the nucleus. It was reported that the cytosolic retention of p21^{WAF} upon treatment with

low paclitaxel concentrations depends on the phosphorylation of $p21^{WAF}$ by the PI3K regulated kinase Akt/PKB (Heliez et al., 2003). Indeed, the levels of Ser-473 phosphorylated (i.e. active) Akt were also elevated upon TACC3 depletion and/or paclitaxel treatment (Fig. 19A). Activation of the PI3K/Akt pathway ensures cell cycle progression and cellular survival upon treatment with low paclitaxel concentrations (Pushkarev et al., 2004). Correspondingly, the levels of phosphorylated FOXO-3a, an Akt substrate and transcription factor, were higher in TACC3 depleted and/or paclitaxel treated NIH3T3 cells (Fig. 19A) as compared to untreated control siRNA expressing cells. Transcription factors of the FOXO family are key regulators involved in the induction of cell cycle arrest and apoptosis. This activity is regulated by subcellular localization. Mechanistically, phosphorylation of FOXO-3a by Akt results in its exclusion from the nucleus and hence its functional inactivation (Greer & Brunet, 2005).

Overall, these data indicate a mechanistical similarity of the molecular G_1 checkpoint response evoked by the two mitotic stress conditions, depletion of the centrosomal protein TACC3 and treatment with the microtubule interfering agent paclitaxel.

5.2.5 TACC3 depletion in MCF7 cells results in G_1 arrest and cellular senescence

The post-mitotic G_1 arrest upon TACC3 depletion in the untransformed cell line NIH3T3 is transient and reversible, thus allowing these cells to continue cycling, albeit slowly. Interestingly, in the breast carcinoma cell line MCF7, expression of TACC3 siRNA rapidly led to a permanent G_1 arrest and cellular senescence. Prior to that, TACC3 depleted MCF7 cells displayed a strong inhibition of proliferation. This was detected by determining the incorporation rate of the thymidine analogue BrdU (bromodeoxyuridine) during DNA-replication in S-phase (Fig. 20A).

Already at day 2 and more prominently at day 4 of TACC3 siRNA expression, MCF7 cells revealed a strongly reduced DNA-replication rate as compared to control siRNA expressing cells and became arrested in G_1. In contrast, control siRNA expressing cells which continued cycling without any alteration in their proliferative capacity. Concomitantly, between day 4 and 6 of DOX treatment MCF7 cells showed a flattened and enlarged appearance and the activity of the lysosomal β-galactosidase (SA-β-gal) as indicated by colorimetric detection using 5-bromo-4-chloro-3-indolyl α-

D-galactopyranoside (X-Gal) as a substrate for the SA-β-gal enzyme (Fig. 20B). The occurrence of SA-β-gal activity serves as a specific and widely accepted marker for cellular senescence (Dimri et al., 1995).

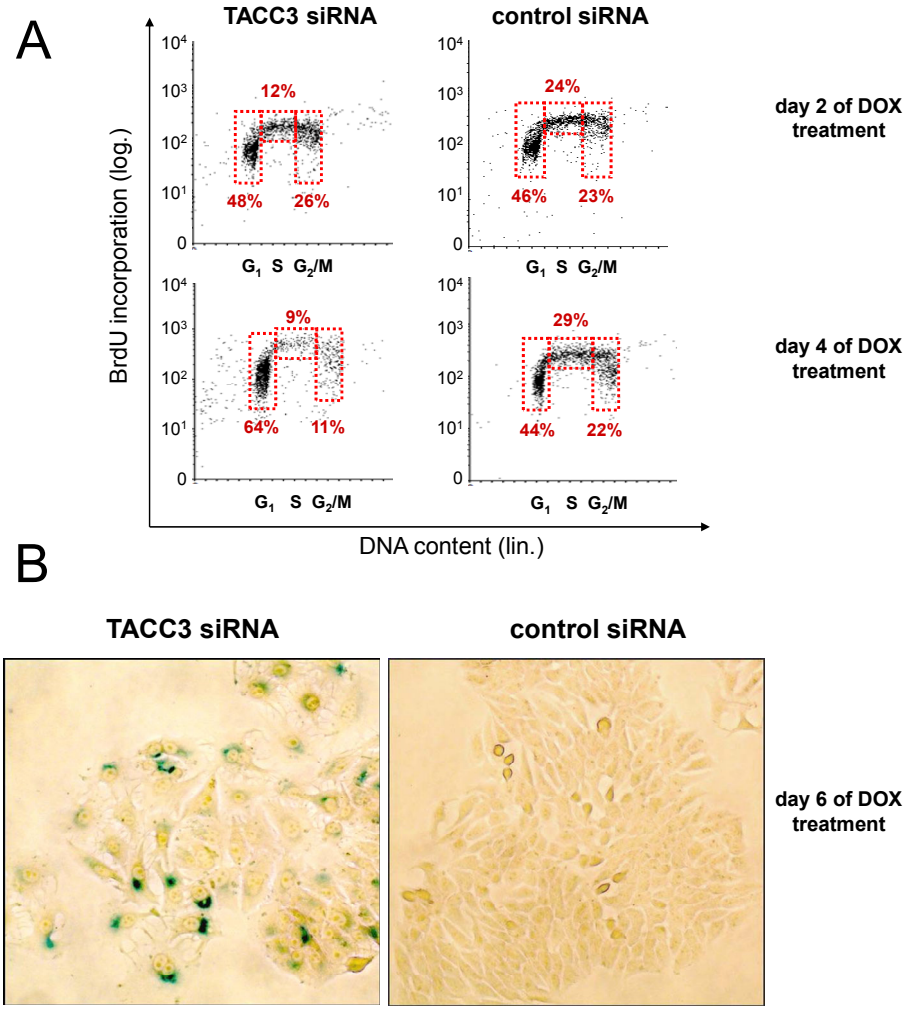

Fig. 20: TACC3 depleted MCF7 cells stop proliferating and become senescent.

(**A**) Cells at given days of DOX treatment were pulsed with 10 µM BrdU for 30 min prior to fixation. Cells were stained with anti-BrdU antibody coupled with FITC. DNA was detected using propidium iodide staining. (**B**) At day 6 of DOX treatment, cells were fixed and stained for β-galactosidase activity (SA-β-gal) as indicated by the occurance of blue coloured cells. Images were taken with a 10x objective.

These findings provided definitive criteria for a cellular senescence process (Blagosklonny, 2003), which took place in MCF7 cells upon TACC3 down-regulation. In contrast, occurrence of senescent cells in the control siRNA expressing population was hardly detectable. Induction and maintenance of senescence relies on the activation of the p53-p21^{WAF} pathway in response to various stress stimuli, such as

DNA-damage or cytostatic drug action (Ben-Porath & Weinberg, 2005; Blagosklonny, 2003; Roninson et al., 2001).

Indeed, TACC3 *knock down* in MCF7 cells was also associated with the activation of the post-mitotic p53-p21^{WAF} G_1-checkpoint. Accordingly, p53 accumulated in the nucleus (Fig. 21A) and the concentrations of p21^{WAF} and cyclin D1, a G_1-type cyclin, concomitantly increased with the senescent phenotype. At the same time, a rapid decline of the G_2/M type cyclins A and B1 was detectable, further confirming the observed cell cycle occurring exit occurring post-mitotically in G_1 (Fig. 21).

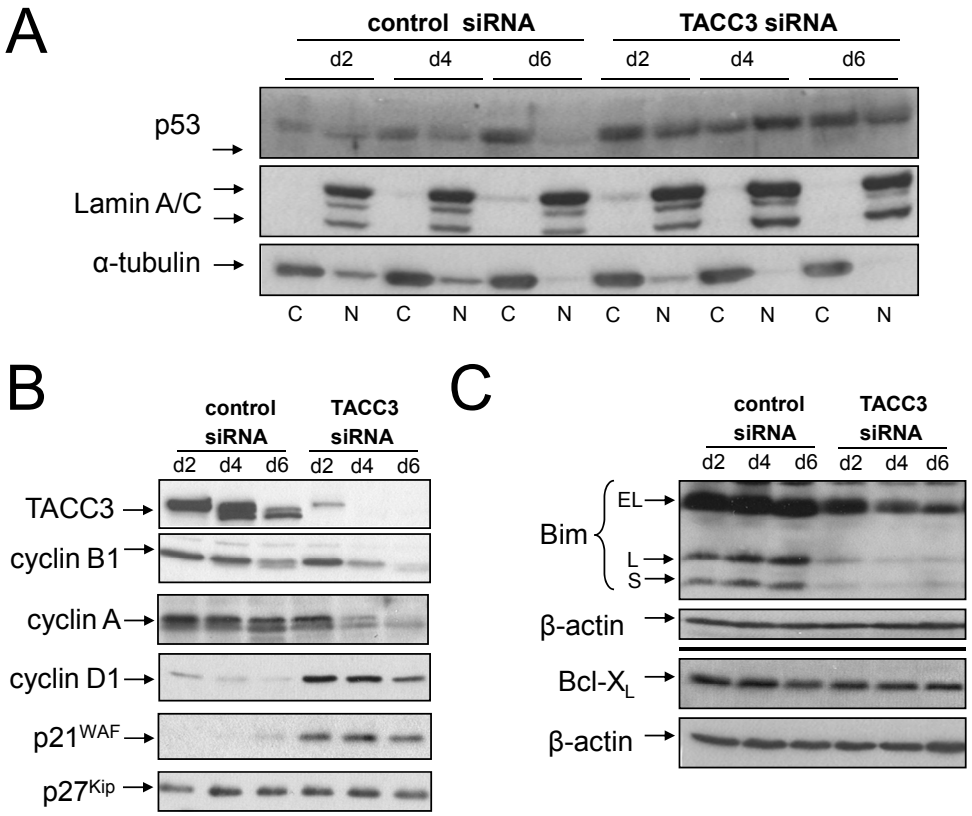

Fig. 21: Activation of the post-mitotic G_1 checkpoint in TACC3 depleted MCF7 cells.

(**A**) Subcellular fractionation revealed p53 accumulation in the nucleus upon TACC3 depletion. α-Tubulin and Lamin A/C were used as markers for cytosolic (C) resp. nuclear (N) fractions. siRNA expression was induced for the indicated period of days (d2, d4, d6). (**B**) G_1 arrest and senescence in TACC3 depleted cells as shown by elevated cyclin D1 and p21^{WAF} levels and decreased cyclin A and B1 protein amounts. (**C**) Decline of all 3 isoforms of the pro-apoptotic protein Bim upon TACC3 depletion, while the protein levels of the anti-apoptotic Bcl-X_L remained unaffected.

Interestingly, the permanent G_1 arrest in TACC3 depleted MCF7 cells led also to the suppression of apoptosis, as indicated by the low DNA fragmentation rate (DNA content <2N, Fig. 20A) and by the decresed protein levels of the pro-apoptotic Bcl-2

family member Bim (Fig. 21C). Bim binds to mitotic spindle microtubules and is released upon mitotic stress, leading to the induction of apoptosis (Mollinedo & Gajate, 2003). Therefore, the decline of Bim protein levels in MCF7 cells experiencing mitotic stress through TACC3 depletion is consistent with a suppression of apoptotic pathways which is typical and required for the development of cellular senescence.

Taken together, depletion of the mitotic spindle protein TACC3 results in the activation of the post-mitotic G_1 checkpoint. This checkpoint is p53-$p21^{WAF}$ dependent and responsible for the induction of a G_1 arrest and hence for inhibition of cellular proliferation.

5.3 Consequences of TACC3 depletion in G_1 checkpoint deficient cells

The previous data clearly implied the importance of the post-mitotic, p53-$p21^{WAF}$-dependent G_1 checkpoint in the cellular response of TACC3 depleted cells. As shown in the following, the protective (i.e. anti-apoptotic) role of this pathway became particularly obvious when TACC3 siRNA was expressed in cell lines with an impaired G_1 checkpoint and hence uncontrolled cell cycle progression beyond G_1. In the following studies cell line models were employed which lack key components of the post-mitotic G_1 checkpoint. The consequences of prolonged TACC3 depletion for cell survival became graver with a perturbed p53-$p21^{WAF}$ function, withcervix carcinoma HeLa cells being particularly susceptible due to their fully ablated G_1-checkpoint response.

5.3.1 Differential roles of p53 and $p21^{WAF}$ in survival upon TACC3 depletion

In order to investigate a direct role of p53 and $p21^{WAF}$ in G_1 checkpoint function and cell survival upon TACC3 depletion, expression of TACC3 was downregulated in the human colon carcinoma cell line HCT116 (which has a functional G_1 checkpoint) and its p53- or $p21^{WAF}$-deficient isogenic derivates, i.e. HCT116 $p53^{(-/-)}$ and HCT116 $p21^{(-/-)}$ cells.

As demonstrated in Fig. 22A and B, the percentage of apoptotic cells (i.e. cells with fragmented DNA in sub-G_1) was significantly higher in TACC3-depleted wild-type

HCT116 cells as compared to p53$^{(-/-)}$ cells. In contrast, a p21^{WAF}-deficient background strongly enhanced polyploidisation and concomitant apoptosis following TACC3 depletion, as indicated by the lack of viability of TACC3 siRNA-expressing HCT116 p21$^{WAF(-/-)}$ cells beyond day five of DOX treatment (Fig. 22A,B).

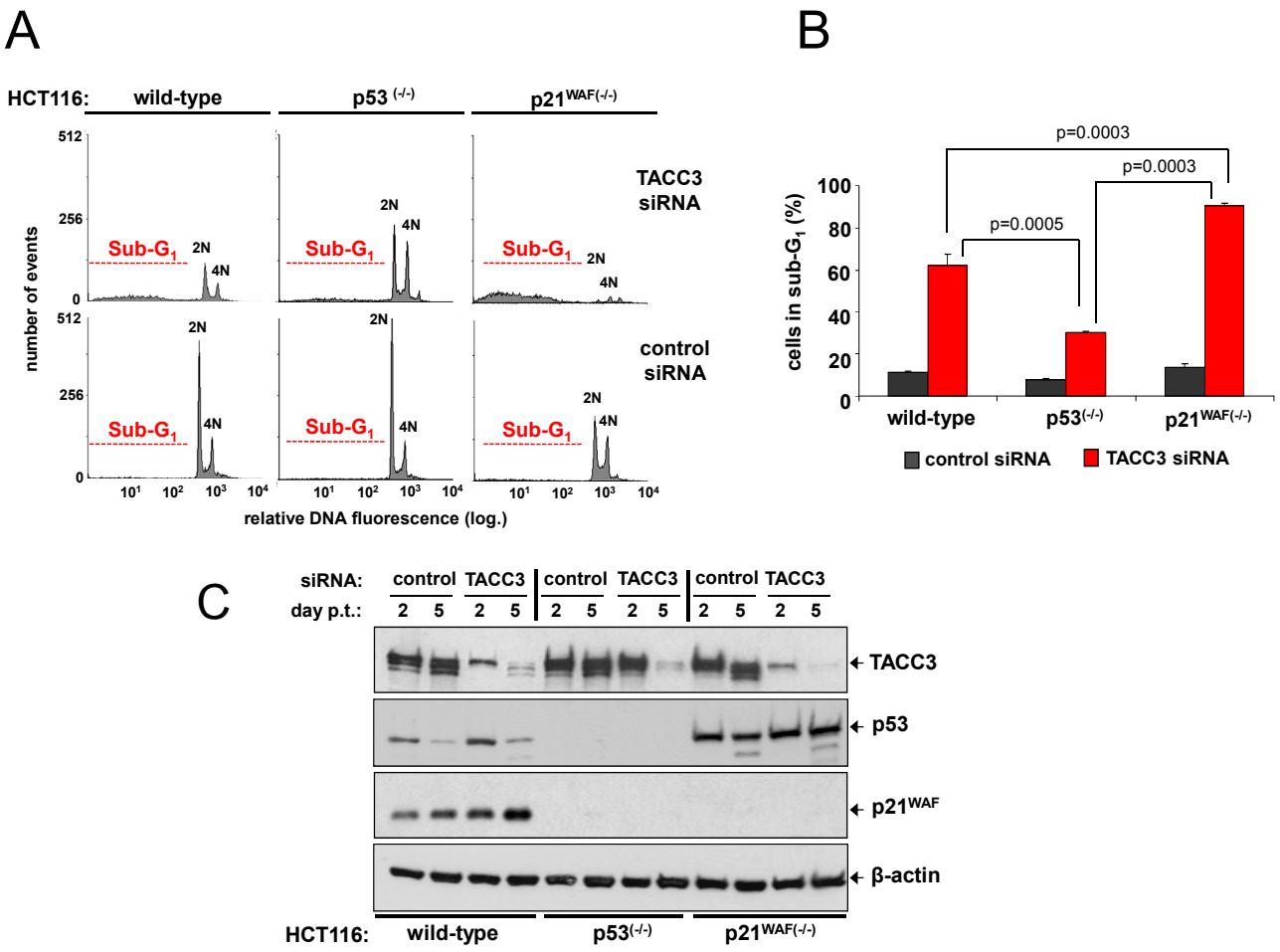

Fig. 22: p53 deficiency ameliorates, whereas p21^{WAF} deficiency accelerates cell death in TACC3-depleted human HCT116 colon carcinoma cells.

HCT116 cells and their p53- or p21^{WAF}-deficient sub-lines were transduced in parallel with lentiviral constructs expressing either a human TACC3-specific siRNA or a control siRNA. (**A**) DNA content and the percentage of apoptotic cells (<2N, sub-G_1 gate) were analyzed five days after transduction using propidium iodide staining and flow cytometry. (**B**) Quantification of apoptotic cells with fragmented DNA as analyzed in A. Values show the means ± SD from one typical experiment performed in triplicate. The transduction efficiency was greater than 90% as determined by flow cytometric GFP staining on day 2. (**C**) p53 and p21^{WAF} protein expression upon TACC3 depletion in HCT116 cells and mutants. Immunoblot analysis of cellular extracts using antibodies against TACC3, p53 and p21^{WAF}. Staining against β-actin was used as a loading control. p.t., post transduction.

These data suggest that p21^{WAF}, which is up-regulated in a p53-dependent manner upon TACC3 depletion (Fig. 22C), exerts a key anti-apoptotic and protective role in the absence of TACC3 function by inducing a post-mitotic and largely protective cell

cycle arrest. However, $p21^{WAF}$ deficient HCT116 cells already displayed elevated p53 levels (Fig. 22C) and are therefore particularly prone to p53-induced apoptosis upon cellular stress.

Thus, cell death through TACC3 depletion in HCT116 colon carcinoma cells is augmented by p53 function and largely prevented by its transcriptional target $p21^{WAF}$.

5.3.2 Progressive prometaphase arrest in TACC3 depleted HeLa cells

The human cervix carcinoma cell line HeLa is known for a suppressed p53-$p21^{WAF}$ pathway. Additionally, HeLa cells lack the G_1-checkpoint Retinoblastoma (Rb) protein, which is also involved in the induction of the G_1 arrest following mitotic stress (Margolis et al., 2003). These checkpoint defects in HeLa cells are due to the oncogenic DNA integration of the human papilloma virus HPV18. The expression of the viral proteins E6 and E7 leads to the degradation of p53 protein and suppression of Rb gene expression (Hu et al., 1995).

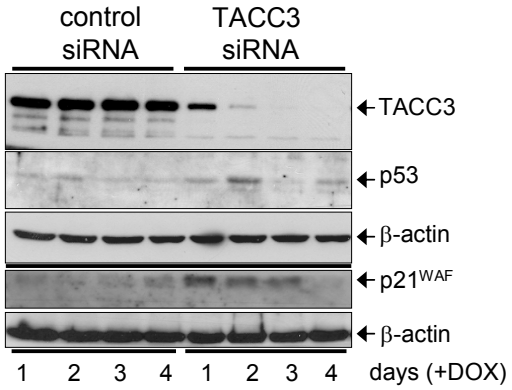

Fig. 23: Downregulation of TACC3 protein expression and the suppressed p53-$p21^{WAF}$ checkpoint in HeLa cells.

Levels of the indicated proteins were determined by immunoblot analysis of TACC3-specific or control siRNA-expressing HeLa cells treated with DOX (5 µg/ml) for a period of 1 to 4 days. Depletion of TACC3 in HeLa cells caused only a minimal increase in p53 and $p21^{WAF}$ proteins, as shown by the immunoblot analysis of cellular extracts using antibodies against TACC3, p53 and $p21^{WAF}$. Staining against β-actin was used as a loading control.

As indicated in Fig. 23, the TACC3 protein could be very efficiently depleted in HeLa cells already at day 2 of DOX treatment. However, unlike as in the G_1-checkpoint proficient cell lines analysed before, HeLa cells did not display any functional increase in p53 protein and consequentially virtually no activation of its target and cell cycle inhibitor $p21^{WAF}$ (Fig. 23).

With their G_1-checkpoint being compromised and hence allowing cells to progress into the next cell cycle, HeLa cells unfolded a particularly strong phenotype when

expression of TACC3-siRNAs was induced. A progressive mitotic arrest of TACC3 depleted cells was revealed using subcellular α-tubulin/cyclin B1/DNA staining and cLSM analysis. The mitotic cyclin B1 identifies cells from late G_2 to metaphase and is degraded during anaphase (Pines, 2006), offering an excellent marker for the analysis and quantification of mitotic progression.

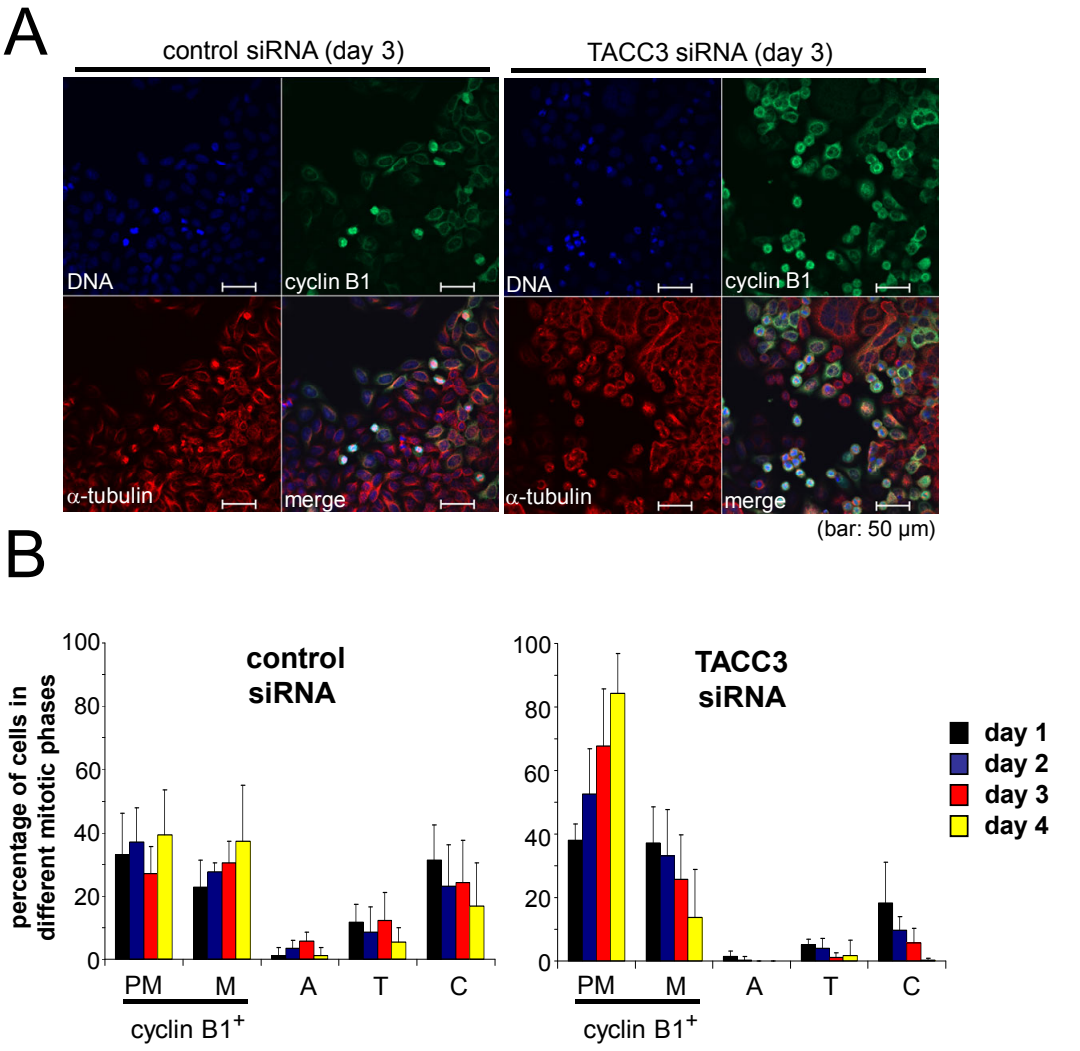

Fig. 24: TACC3-depleted HeLa cells accumulate prior to anaphase.

(**A**) TACC3-depleted and control cells were analyzed by immunocytochemistry and confocal microscopy using cyclin B1 (green) and α-tubulin (red) specific antibodies. DNA was visualized by DAPI staining (blue). (**B**) Quantification of the percentage of control and TACC3-depleted HeLa cells in various mitotic phases during a period of treatment with DOX for four days. The criteria used to analyse mitotic cells were DNA and spindle morphology as well as cyclin B1 positivity. PM, prometaphase; M, metaphase; A, anaphase; T, telophase; C, cytokinesis. Values are means ± SD from two experiments analyzing each two control and three TACC3 siRNA-expressing cell clones. For each time point of DOX treatment ~80-100 control cells and ~200-450 TACC3 siRNA-expressing cells were scored.

Typically, TACC3-siRNA expressing cells arrested in a cyclin B1-positive stage (Fig. 24A) and were also positive for the mitotic marker phospho-histone 3 (8.8±3.0% upon

TACC3 depletion *vs.* 2.6±0.4% for control cells as determined by FACS analysis; day 3 of DOX treatment).In particular, upon prolonged DOX-treatment, TACC3-depleted HeLa cells rapidly accumulated in prometaphase with a concomitant decrease of the percentage of cells in all successive mitotic stages, i.e. metaphase, anaphase and telophase (Fig. 24B). Also, the percentage of cells undergoing cytokinesis decreased progressively upon TACC3 knockdown as compared to control siRNA expressing cultures.

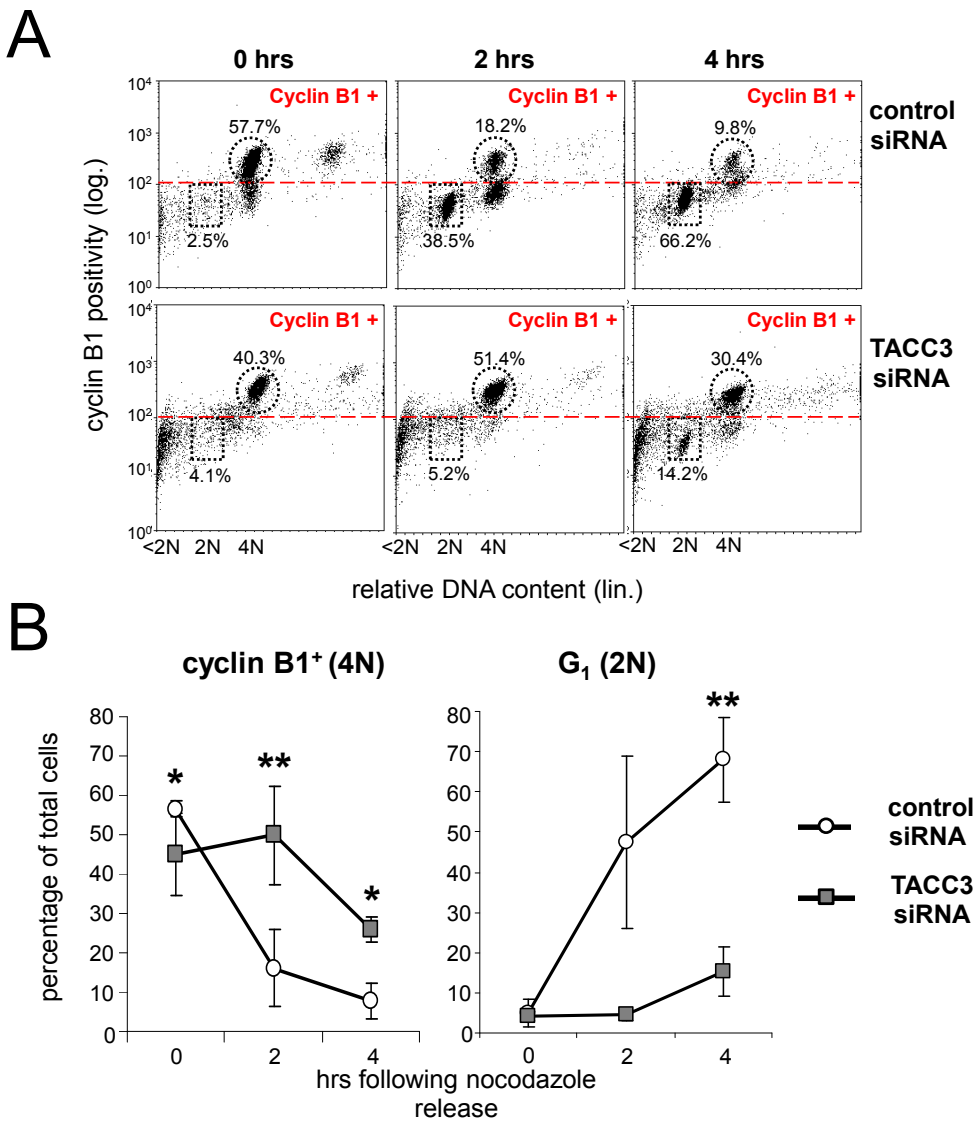

Fig. 25: Impaired mitotic division and progression into G_1 in TACC3 depleted HeLa cells.

(**A**) Determination of mitotic progression by intracellular cyclin B staining and FACS analysis. Nocodazole-arrested cells were collected by mitotic shake-off and replated into nocodazole-free medium. Cyclin B expression and DNA content (2N: rectangles; 4N: circles) were analyzed by flow cytometry at the indicated time points following nocodazole release. (**B**) Quantification of the percentages of cyclin B1-positive mitotic cells and cells which entered the next G_1 phase following nocodazole release. Values shown are means ± SD (* $p<0.05$; ** $p<0.005$) from at least three experiments.

In order to confirm the observation of the prometaphase arrest upon TACC3 depletion, control and TACC3 siRNA expressing HeLa cells were quantitatively synchronized in prometaphase by nocodazole treatment and their mitotic progression was monitored after washing and release in nocodazole-free medium using an intracellular cyclin B1 staining protocol and FACS analysis. Within the first two hours of release, TACC3-depleted cells failed to degrade cyclin B1 and hence to proceed into anaphase, whereas the majority of control cells completed mitosis and progressed into the next G_1-phase (Fig. 25A and B).

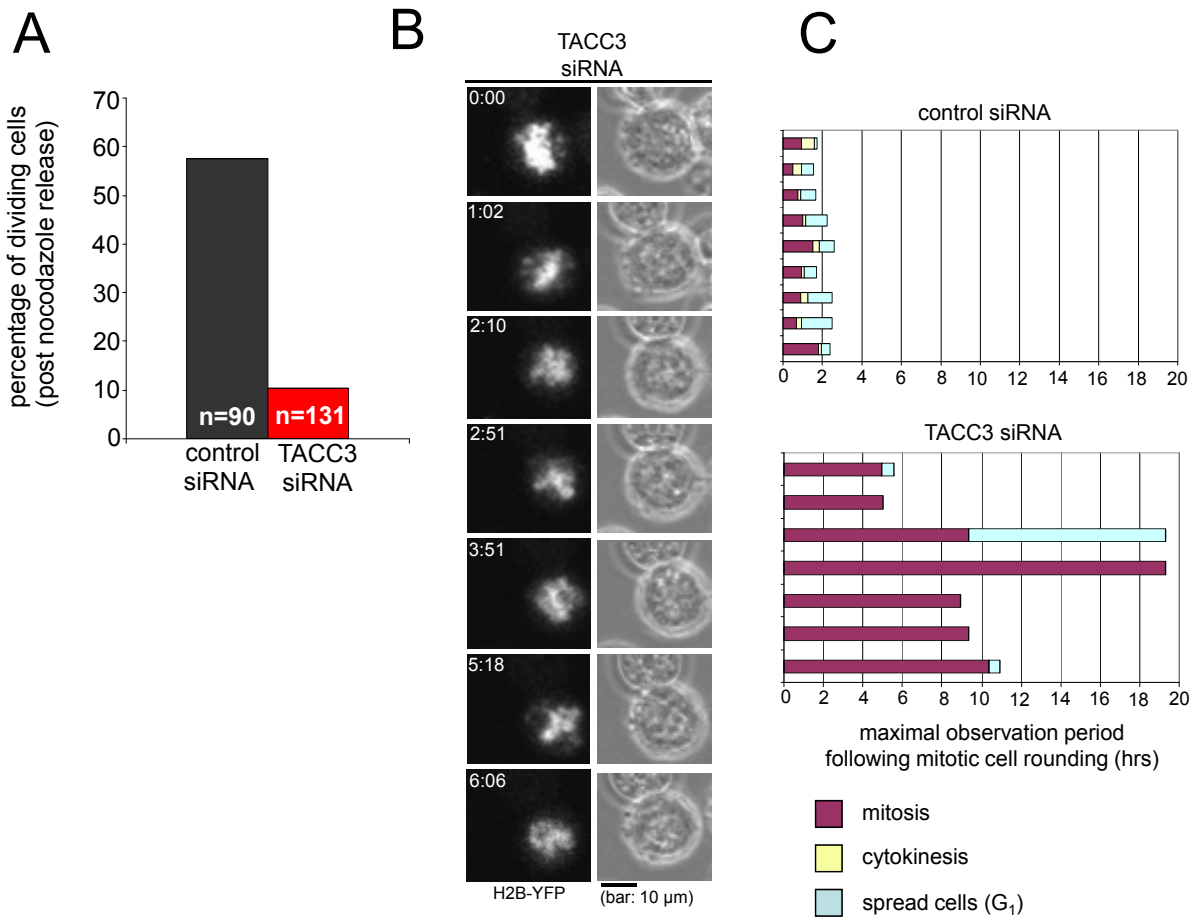

Fig. 26: Impaired division of HeLa cells following TACC3 depletion – live cell imaging.

(**A**) Nocodazole-arrested cells were collected by mitotic shake-off, washed and released into nocodazole-free medium. Live cell imaging (LCI) was performed for a period of 5 hrs in order to study the completion of mitosis and to determine the percentage of dividing cells. (**B**) Time lapse study of a TACC3 depleted cell expressing the chromosome marker YFP-Histone 2B. Note that the cell failed to properly align its chromosomes and to progress into anaphase for at least 6 hrs. Time is indicated in hh:mm following mitotic cell rounding (at 0:00). (**C**) Cells were synchronized by a double thymidine block in G_1/S, released into the cell cycle and analysed by LCI. Cell rounding was defined as the onset of mitosis (T=0 hrs). Cytokinesis and cell spreading (cells in G_1) were also defined by observation of the cell shape. A total of 9 control siRNA expressing (upper panel) and 7 TACC3 siRNA expressing cells (lower panel) from different experiments were analyzed.

Most of the TACC3 depleted HeLa cells remained in a cyclin B1 positive state for up to 8 hrs after release from nocodazole, thus indicating the severity of the molecular defects leading to the mitotic arrest.

Lastly, the cell division defects in TACC3 depleted cells were further confirmed on a cellular level. Nocodazole synchronized cells were released into nocodazole-free medium and their mitotic progression was monitored by live cell imaging. Within observation period of five hour following nocodazole release only ~10% of the analysed TACC3-siRNA expressing cells completed cell division, as opposed to nearly 60% of control-siRNA expressing HeLa cells (Fig. 26A).

For further studies, cells were transiently transfected with a Histone 2B-YFP expression vector to visualize chromosomal dynamics. These experiments additionally demonstrated that the mitotic arrest of TACC3 depleted HeLa cells was apparently caused by their failure to congress their chromosomes at the metaphase midplate during the observation period as indicated in Fig. 26B. Comparable results were obtained when HeLa cells were synchronized by a double thymidine block in G_1/S and then released into the cell cycle (Fig. 26C). Following entrance into the mitotic phase, TACC3 siRNA-expressing HeLa cells lastly failed to enter anaphase during an observation period of up to 20 hours. In contrast, control siRNA expressing cells usually performed cell division within a period of one to two hours following mitotic cell rounding and progressed into G_1, recognizable by their final adhesion onto the culture plate. TACC3 siRNA expressing HeLa cells which eventually entered anaphase often failed to complete cytokinesis, thus yielding binucleated cells (Fig. 26C). Taken together, these overall findings demonstrate that TACC3 *knock-down* inhibits mitotic progression of HeLa cells by inducing chromosomal misalignment and a severe mitotic arrest prior to anaphase (Schneider et al., 2007a).

5.3.3 Delocalization of structural and checkpoint proteins at kinetochores of TACC3 depleted HeLa cells

On the molecular level, mitotic arrest is mediated through the spindle assembly checkpoint (SAC) which senses defects in spindle structure, in particular unattached kinetochores and the resulting misalignment of chromosomes (Brito & Rieder, 2006; Weaver & Cleveland, 2005). Phenotypically, following induction of TACC3-siRNA expression, mitotic HeLa cells showed after a progressing disarrangement of

chromosomal attachment to microtubules and a deterioration of the mitotic spindle structure (Fig. 27).

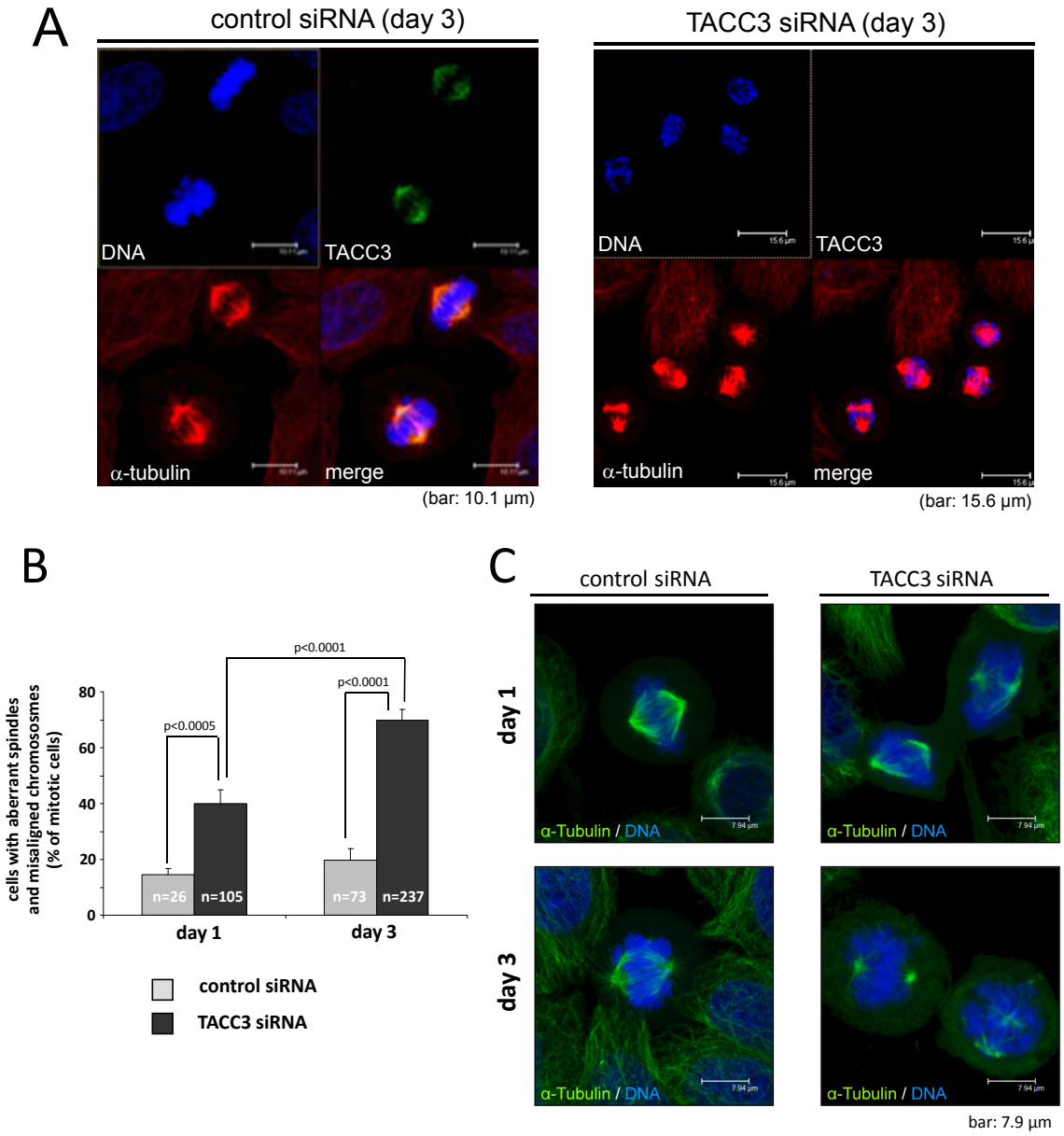

Fig. 27: Chromosomal misalignment and reduced spindle stability in TACC3 depleted HeLa cells.

(**A**) Control and TACC3-depleted HeLa cells were stained using TACC3 (green)- and α-tubulin-specific antibodies (red) and analyzed by cLSM. (**B**) Quantification of the percentage of control cells and TACC3-depleted mitotic cells displaying abnormal spindles and misaligned chromosomes. The number of cells scored on days 1 and 3 of DOX-treatment is indicated. (**C**) Assay of spindle stability by cold treatment. Control and TACC3 siRNA-expressing cells were transferred to 4°C for 2 hrs and then allowed to recover at 37°C for 25 min. Cells were stained using α-tubulin antibodies (green) and analyzed by cLSM. Note that already on day 1 of DOX treatment and TACC3 depletion cells failed to efficiently regrow their spindle microtubules following cold treatment as compared to control cells. DNA in *A* and *C* was visualized by DAPI staining (blue). Representative experiments are shown.

In contrast to control cells, the chromosomal arrangement in TACC3 depleted cells was clearly perturbed in (pro)metaphase and often accompanied by an aberrant spindle morphology and multipolar spindles as visualised by DNA and α-tubulin staining (Fig. 27A). An abnormal spindle morphology was already evident in ~40% of TACC3 depleted cells at day 1 of DOX treatment as assessed by a combined analysis of spindle architecture and chromosomal alignment (Fig. 27B). The percentage of cells with affected spindles increased to ~70% by day 3 of TACC3 siRNA expression. In addition, TACC3 depleted cells, as compared to control cells, were not capable of reassembling functional mitotic spindles at 37°C after microtubule depolymerisation through cold treatment (Fig. 27C). Again, microtubule destabilization was already prevalent at day 1 of TACC3 siRNA expression. These findings altogether indicate that TACC3-regulated spindle function is essential for proper chromosomal alignment and hence mitotic progression beyond metaphase.

The observed chromosomal misalignment and the reduced spindle stability in TACC3 depleted HeLa cells led to the important question whether the absence of the mitotic spindle associated protein TACC3 affects spindle dependent kinetochore protein assembly and function. Therefore, studies addressing the mitotic localization of Aurora B, BubR1 and Ndc80 were performed in control and TACC3 depleted HeLa cells. These three proteins are essential representatives of three functionally important kinetochore associated complexes, namely of the chromosomal passenger complex (1), the spindle assembly checkpoint (2) and outer kinetochore scaffold (3), respectively.

Typically, Aurora B is seen at kinetochores and the chromosomal midplate in (pro)metaphase and anaphase cells, respectively. However, as shown in Fig. 28A, Aurora B failed to accumulate to normal levels at these target structures in TACC3-depleted cells. The reduction of Aurora B signal intensity at kinetochores became increasingly prominent following day two of DOX-dependent TACC3 depletion. By day four of DOX-treatment, the majority of mitotically arrested TACC3-depleted cells had strongly reduced Aurora B signals at kinetochores. Concomitantly, a reduced kinetochore staining of BubR1 in TACC3 depleted cells was observed (Fig. 28A). Kinetochore localization of BubR1 is per se dependent on Aurora B in order to control chromosomal alignment (Ditchfield et al., 2003).

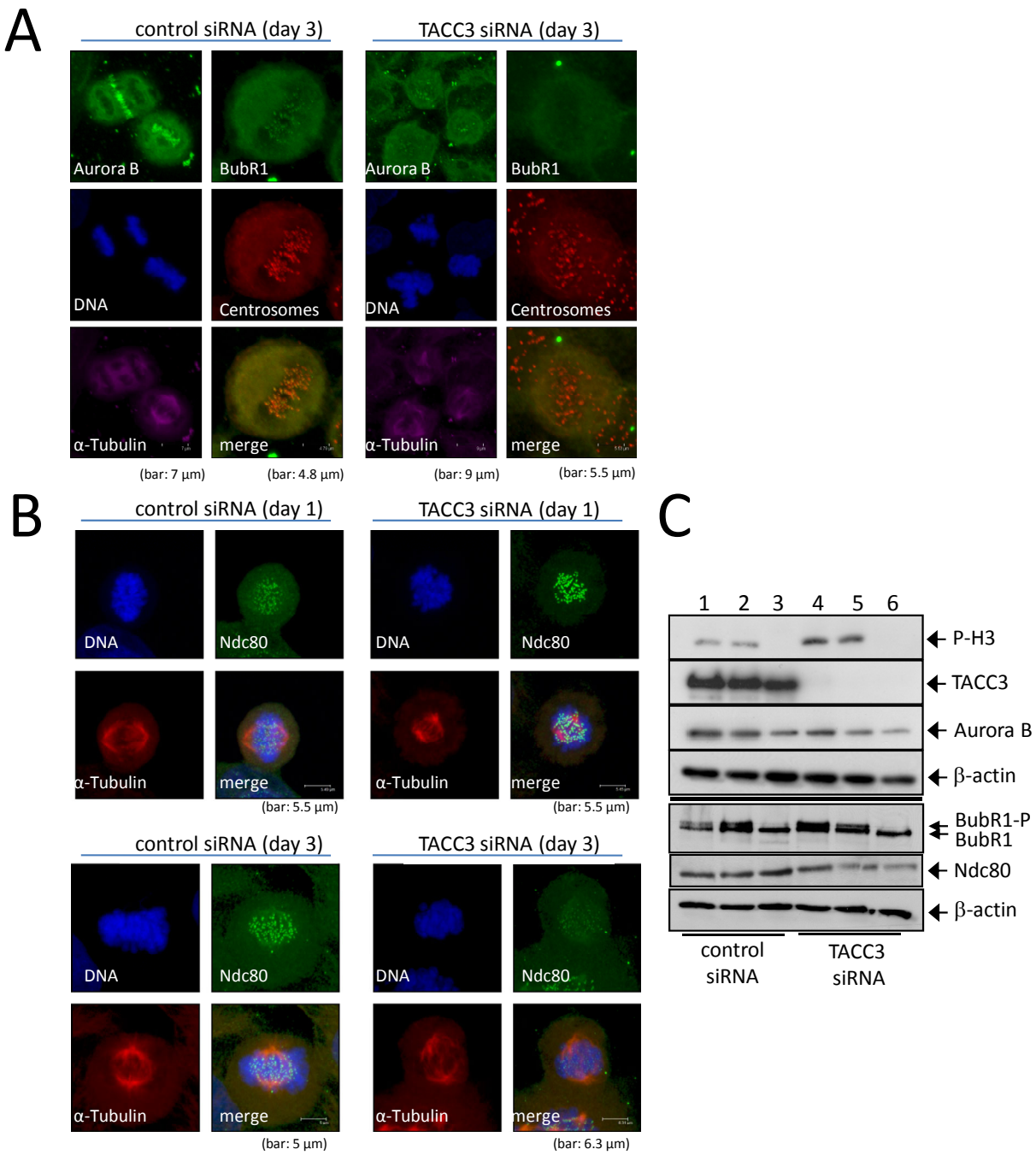

Fig. 28: Reduced mitotic localization of checkpoint proteins at kinetochores of TACC3-depleted HeLa cells.

Visualization of Aurora B and BubR1 localization by immunocytochemistry and cLSM. (**A**) Control and TACC3-depleted HeLa cells were costained for Aurora B (green) and α-tubulin (violett) using specific antibodies. Centromeres (red) and BubR1 (green) were detected using a CREST antiserum and BubR1-specific antibodies. (**B**) Visualization of the structural kinetochore component Ndc80 in control and TACC3-depleted HeLa cells. Ndc80 (green) and α-tubulin (red) were detected using specific antibodies. DNA in A and B was visualized by DAPI staining (blue). Cells were analysed at day 1 (upper panels) and day 3 (middle and lower panels) of control siRNA and TACC3 siRNA expression. Representative experiments are depicted. (**C**) Immunoblot analysis of phospho-histone 3, TACC3, Aurora B, BubR1 and Ndc80 expression in cells obtained by mitotic shake off (lanes 1,2 and 4,5) and in non-mitotic cells (lanes 3 and 6). P-H3, phospho-histone H3; BubR1-P, phosphorylated BubR1. Probing for β-actin was used as loading control.

Interestingly, the localization of Ndc80, a structural protein at the outer kinetochore crucial for the attachment of microtubules to chromosomes (Ciferri et al., 2007) and a

phosphorylation target of Aurora B (DeLuca et al., 2006), was also affected by TACC3 depletion, albeit not at day 1. However, by day 3 of DOX treatment, the fluorescence signal of Ndc80 was remarkably reduced at kinetochores of TACC3-depleted (pro)metaphase cells as compared to control cells (Fig. 28B). This phenotype of decreased/reduced kinetochore protein localization was already observed in bipolar TACC3 depleted cells with only few misaligned chromosomes and rather normally appearing spindles. Immunoblot analysis revealed that Aurora B and phosphorylated BubR1 were expressed in TACC3-depleted mitotic HeLa cells at levels comparable to controls. Interestingly, the total protein levels of Ndc80 were rather diminished both in mitotic and non-mitotic TACC3 depleted cells as compared to controls (Fig. 28C).

Taken together, the obvious reduction of Ndc80, Aurora B and BubR1 at kinetochores by day 3 of TACC3 depletion, combined with the observed chromosomal misalignment indicates a progressive deterioration of the spindle and kinetochore architecture in the course of TACC3 depletion (Schneider et al., 2007a).

5.3.4 Caspase-dependent mitotic cell death of TACC depleted HeLa cells

The observed deterioration of the mitotic spindle apparatus upon TACC3 depletion was accompanied by a rapidly increasing cell death rate. As a consequence, TACC3-siRNA expressing HeLa cells could only be maintained in cell culture for few days. Upon TACC3 depletion, the loss of viability became experimentally evident in FACS studies by an elevated number of cells with apoptotic DNA fragmentation in sub-G1 (DNA content <2N) together with a progressive reduction of cells in G_1 (Fig. 29A). Furthermore, TACC3 depletion typically resulted in processing and the activation of caspase-3 as well as in the cleavage of its substrate PARP (Poly (ADP-ribose) polymerase; Fig. 29B). Consequentially, the apoptotic cell death of TACC3 siRNA expressing HeLa cells was almost completely abolished by the pan-caspase inhibitory peptide Q-VD-OPH (Q-Val-Asp-OPH), as indicated by the strong decrease of the percentage of cells with DNA fragmentation (<2N; Fig. 29C).

Next, the origin of the apoptotic cell death of TACC3 depleted HeLa cells was addressed in order to differentiate between a mitotic arrest and death vs. post-mitotic events. HeLa cells were synchronized in prometaphase by nocodazole treatment, washed and released into nocodazole-free medium with or without Q-VD-OPH.

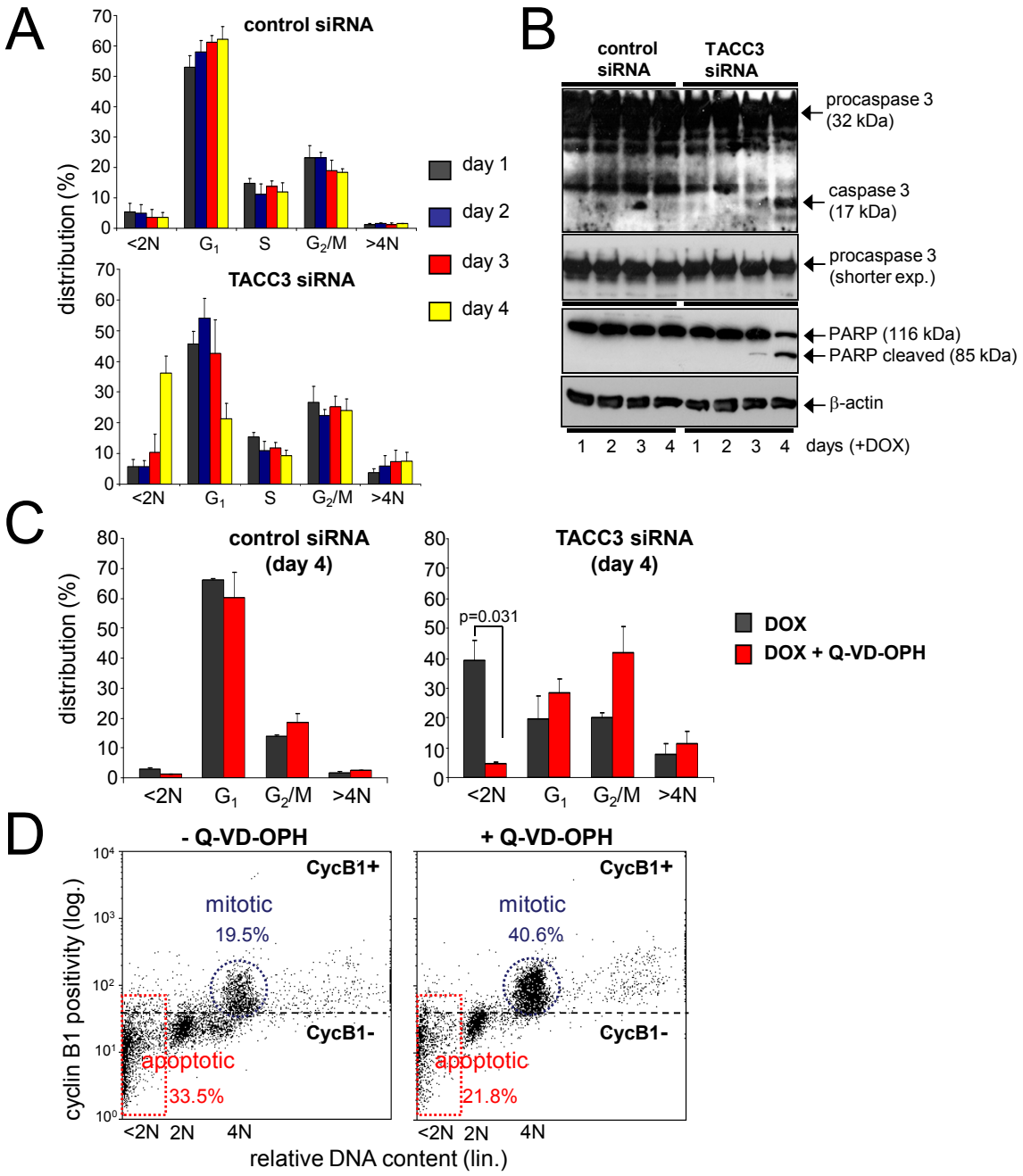

Fig. 29: Apoptotic cell death of HeLa cells following TACC3 depletion is initiated during mitosis and is caspase-dependent.

(**A**) DNA content analysis of TACC3 depleted HeLa cells. The percentage of cells in different cell cycle phases was determined by FACS analysis and calculated as means ± SD. Apoptotic cells with fragmented DNA and polyploid cells are characterized by a DNA content of <2N (sub-G_1) and >4N, respectively. (**B**) Caspase-3 activation and PARP cleavage indicates apoptosis induction upon TACC3 depletion. Immunoblot analysis was performed using Caspase 3 and PARP specific antibodies. Probing for β-actin was used as loading control. (**C**) Addition of the pan-caspase inhibitor Q-VD-OPH during DOX treatment strongly impairs apoptosis following TACC3 depletion. Cells were analyzed as indicated in (A). (**D**) TACC3-depleted HeLa cells were subjected to synchronization by nocodazole treatment and collected by mitotic shake-off. The cells were equally divided and immediately re-plated into nocodazole-free medium with or without Q-VD-OPH for a period of 4 hours. Thereafter, cyclin B1 expression and DNA content were analyzed by flow cytometry. The percentages of cyclin B1-positive cells (circles) or cells with fragmented DNA (<2N; squares) are indicated.

In the presence of this caspase inhibitor, as compared to its absence, significantly less TACC3-siRNA expressing cells underwent apoptosis from mitosis, as detected by an increased percentage of viable cyclin B1-positive cells in the 4N gate and a decreased fraction of cells with fragmented DNA in sub-G1 (<2N; Fig. 29D). These data demonstrate that TACC3 depletion in HeLa cells initiates caspase-dependent cell death already during mitosis. This mitotic cell death is p53 independent (Mansilla et al., 2006) and is obviously not a post-mitotic event, since HeLa cells lack a functional p53-dependent G_1 checkpoint response.

5.3.5 Requirement of the spindle assembly checkpoint for induction of mitotic cell death upon TACC3 depletion

Mitotic apoptosis is executed when cells become indefinitely arrested in metaphase through the sustained activity of the spindle assembly checkpoint (SAC; Kadura & Sazer, 2005). The mitotic proteins BubR1 and Mad2 are essential components of the SAC complex and required to arrest cells in mitosis when chromosomes are unattached to one or more microtubules (Weaver and Cleveland, 2005). Considering that these regulators possibly determine the cellular outcome following depletion of TACC3, siRNA against TACC3 was expressed in the human colon carcinoma cell line HCT116 and its isogenic derivate HCT116-Mad2$^{+/-}$. Due to haploinsufficiency for Mad2 expression, HCT116 Mad2$^{+/-}$ cells are characterized by a defective SAC function uponn defects in chromosomal attachment (Michel et al., 2001).

As indicated in Fig. 30A, HCT116 wild-type cells underwent cell death upon TACC3 depletion as measured by an increased fraction of cells with DNA fragmentation in sub-G_1 and a concomitantly decreased percentage of cells in G_1 (2N) at day four of DOX-treatment. In contrast, the absence of a functional spindle checkpoint in HCT116-Mad2$^{+/-}$ cells protected them against cell death following TACC3 knock-down as indicated by a significantly decreased percentage of apoptotic cells in the sub-G_1 gate (Fig. 30B). Therefore, these findings point to a requirement of a functional SAC in order to uphold mitotic arrest and induce cell death upon TACC depletion.

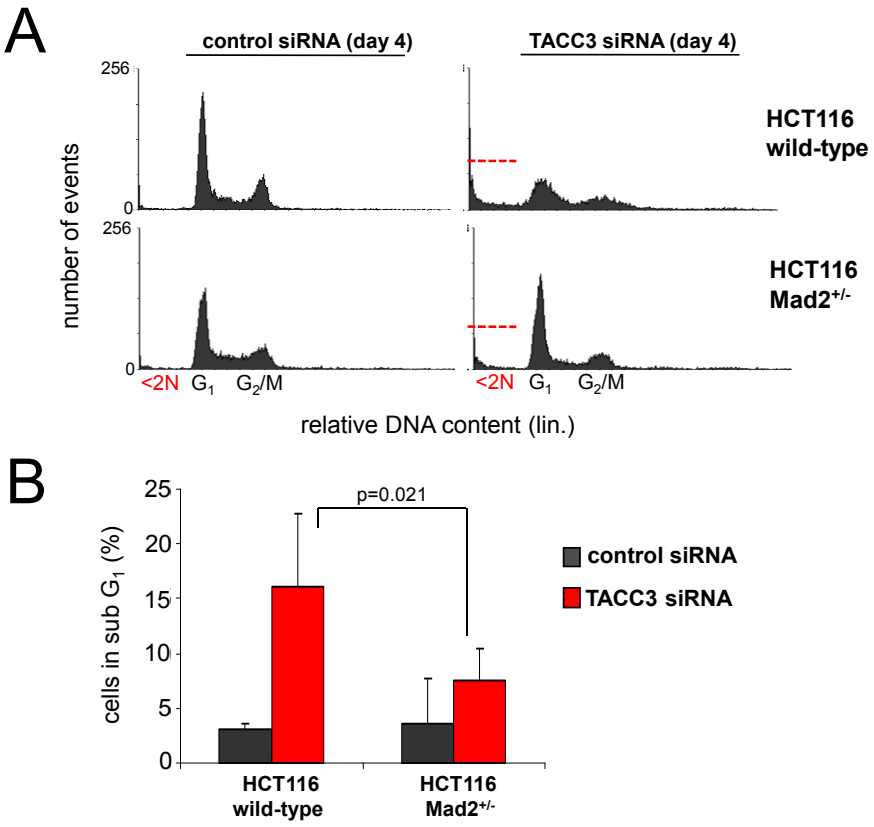

Fig. 30: Activation of the spindle assembly checkpoint is necessary for TACC3 depletion-induced mitotic cell death.

(**A**) Flow cytometric cell cycle analysis of HCT116 wild-type and *Mad2*$^{(+/-)}$ cells following TACC3 depletion, day 4 of DOX treatment. Apoptotic cells with fragmented DNA (<2N) are indicated by the red line. (**B**) Quantification of the percentage of apoptotic cells in sub-G_1 (<2N) as indicated in A. Values were assessed by analyzing HCT116 wildtype or Mad2$^{+/-}$ cell lines which expressed either TACC3- or control siRNAs (means ± SD from four experiments).

5.3.6 Mitotic checkpoint slippage in TACC3 depleted HeLa cells results in polyploidization and centrosome amplification

Mitotic cells arrested by the SAC can avoid mitotic cell death by escaping from this block through a process termed mitotic slippage (Brito & Rieder, 2006; Weaver & Cleveland, 2005). Indeed, live cell imaging expreiments indicated that TACC3 depleted HeLa cells can aberrantly exit mitosis after a prolonged arrest, resulting in cytokinesis failure and tetraploidy (Fig. 26C). Upon prolonged TACC3 depletion not only apoptotic cells with fragmented DNA (<2N; Fig. 29A), but also polyploid cells (DNA content >4N) became increasingly detectable in HeLa cultures.

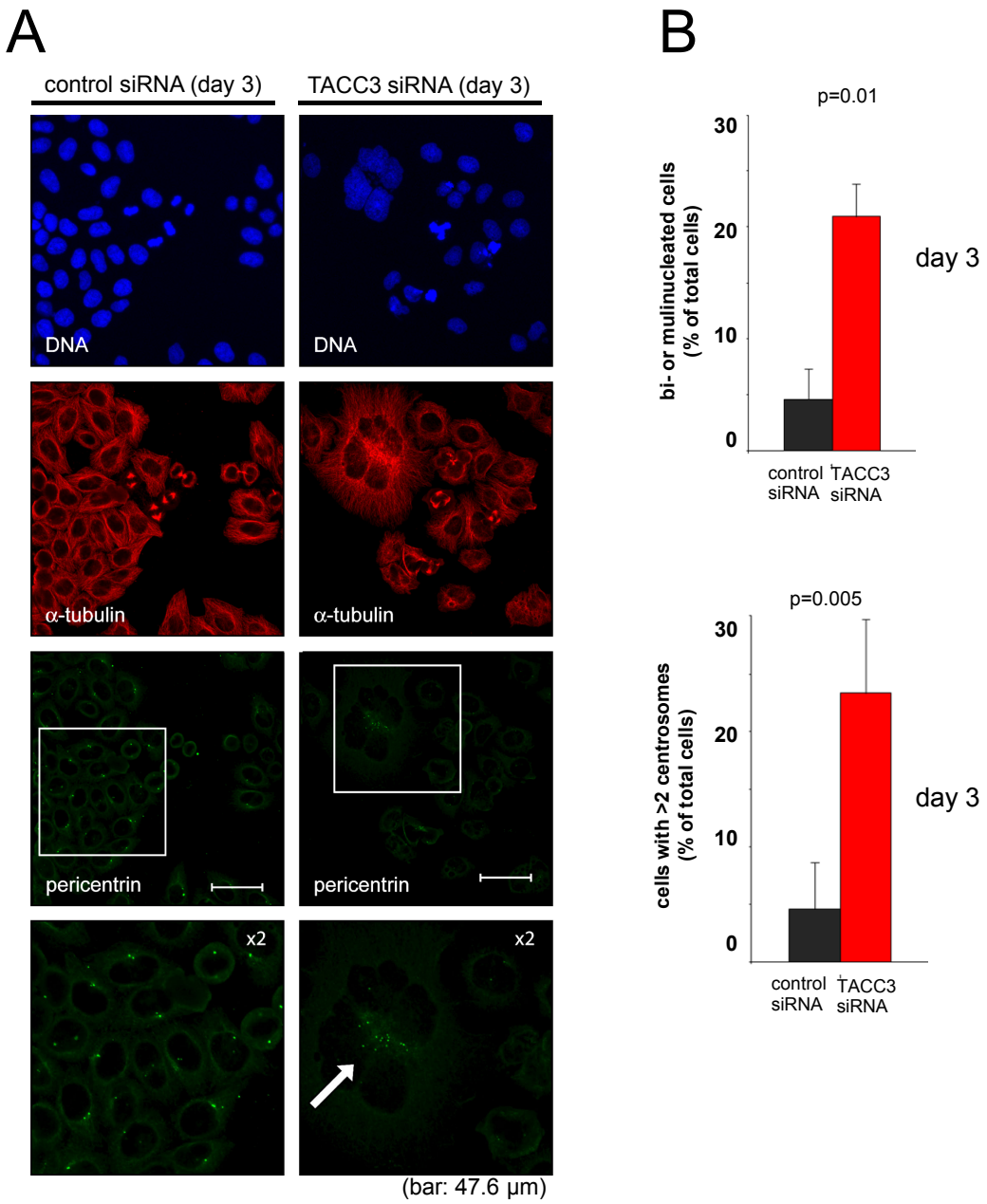

Fig. 31: Polyploidy and centrosomal amplification in TACC3 depleted HeLa cells.

(**A**) Visualization of microtubules (red) and centrosomes (green) using α-tubulin and pericentrin-specific antibodies, respectively. DNA was detected by DAPI staining (blue). Note the accumulation of centrosomes in the highly polyploid HeLa cell enlarged in the lower panel as indicated by the arrow. (**B**) Quantification of the percentage of bi- or polynucleated HeLa cells and cells with more than two centrosomes following TACC3 depletion (analysis at day three of DOX treatment). Here, centrosomes were detected using pericentrin-specific antibodies and DNA was visualised using DAPI staining. Values are means ± SD from scoring ~300 control siRNA or TACC3 siRNA expressing cells in three experiments.

As indicated in Fig. 31, downregulation of TACC3 (day 3 of DOX treatment) was associated with a profound increase in the percentage of bi- or multinucleated cells. In particular, within the first day of DOX treatment, this percentage was already 2.2-fold higher in TACC3 siRNA expressing cultures as compared to control siRNA

expressing cells. This difference increased progressively to 7.6-fold on day four of DOX treatment (a total of ~1200 to 1500 control siRNA and TACC3 siRNA expressing HeLa cells were scored microscopically in two independent experiments).

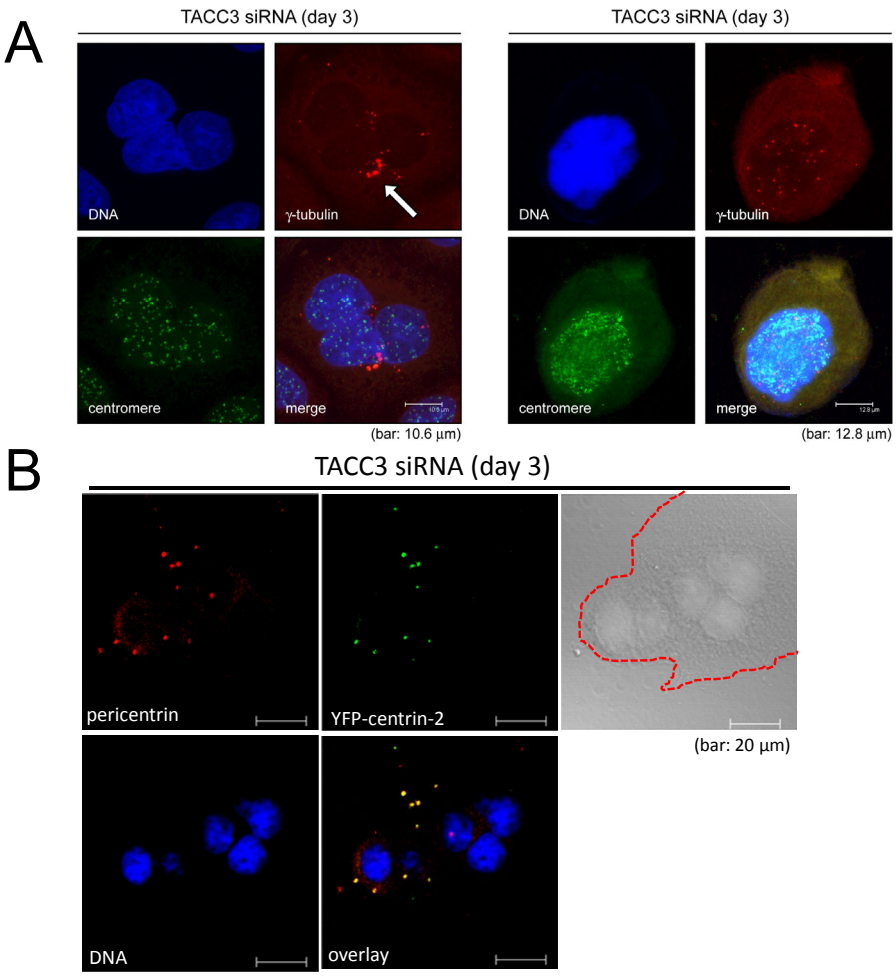

Fig. 32: Accumulation of centrosomes in TACC3 depleted polyploid HeLa cells.

(**A**) Visualization of centromeres (green) and centrosomes (red, arrow) using CREST- and γ-tubulin-specific antibodies, respectively. DNA was detected by DAPI staining (blue). (**B**) Colocalization of the centriole marker YFP-centrin-2 (green) and pericentrin (red) on supernumerary centrosomes in TACC3-depleted cells. HeLa cells transiently expressing YFP-centrin-2 were subjected to DOX treatment for three days and subsequently analyzed by cLSM using a 63x objective. DNA was detected by DAPI staining (blue). Cell boundary is indicated by the red line.

In addition, the polyploidy in TACC3-depleted HeLa cells was accompanied by supernumerary centrosome as visualised by staining of γ-tubulin (Fig. 32A) or detection of the PCM (pericentriolar material)-specific marker pericentrin (Fig. 31A and Fig. 32B). Quantitatively, at day three of DOX-treatment, 23.4±6.3% of TACC3-depleted cells contained more than two centrosomes as compared to 4.6±4.1% of

cells in control cultures; mean±SD). At the same time point, this finding reflected the degree of bi- and multi-nucleation in cultures of TACC3 siRNA-expressing cells (Fig. 31B).

Different processes including fragmentation of the PCM, overduplication of centrosomes or cell division failure have been implicated in the occurrence of numerical centrosome aberrations (Nigg, 2006). Centrosomes harbour one or two centrioles which are characterized by centrin-2, a protein required for centriole duplication during the cell cycle (Salisbury et al., 2002). In order to address the origin of the centrosomal accumulation following TACC3 depletion, HeLa cells were transfected with an expression construct for the YFP-centrin-2 fusion protein and subjected to DOX-induced TACC3 depletion. In multinucleated cells, the majority of supernumerary centrosomes, as detected by staining for pericentrin, co-stained with YFP-centrin-2 (Fig. 32B). These findings indicate that the multiple centrosomes observed in TACC3-depleted polyploid HeLa cells indeed harbour centrioles and therefore apparently represent complete centrosomes rather than “centrosome-related bodies” (Nigg, 2006). Since supernumerary centrosomes were predominantly found in multinuclear cells, these findings point to cell division failure as the likely mechanism for the accumulation of centrosomes upon TACC depletion.

Taken together, the functionality of the G_1 checkpoint is decisive for the cellular response to TACC3 depletion. In checkpoint proficient cells like NIH3T3 fibroblasts, TACC3 depletion led to a relatively moderate aneuploidy and reversible growth arrest. In contrast, unrestricted cycling of checkpoint compromised cells like HeLa following TACC3 depletion caused an accumulation of mitotic defects and consequently a strong SAC activation. As a consequence, cells either underwent mitotic cell death or became polyploid following mitotic slippage.

5.4 TACC3 depletion highly sensitises cells to low dose paclitaxel treatment

Therapeutic interference with the mitotic spindle apparatus is an established and widely used rationale for the treatment of tumours. The taxane paclitaxel is among the most effective chemotherapeutic agents for patients with prostate, breast and non-small cell lung cancer (Jordan & Wilson, 2004). Unfortunately, resistance and a decreased sensitivity to paclitaxel represents an emerging problem in chemotherapy

(Abal *et al.,* 2003). Paclitaxel stabilizes microtubules and suppresses their dynamics, resulting in disruption of the microtubule network required for mitosis and cell proliferation. Different concentrations of paclitaxel can trigger distinct effects on both the microtubule network and biochemical pathways. At low nanomolare concentrations, paclitaxel causes p53-$p21^{WAF}$-dependent arrest following mitotic delay (Ikui *et al.,* 2005). Since paclitaxel apparently triggers a phenotype which is similar to that of TACC3 depletion, the effect of the latter on the sensitivity of cells to paclitaxel treatment was further investigated. Indeed, the combination of low, subtoxic, doses of paclitaxel with concomitant TACC3 depletion caused a much stronger increase in protein levels of the post-mitotic G_1-checkpoint proteins p53 and $p21^{WAF}$ (Fig. 19) and had very profound synergistic effects on proliferation and viability. In particular, as shown in the following, treatment with low doses of paclitaxel trigerred in cell death in TACC3 depleted NIH3T3 cells and accelerated onset of cellular senescence in TACC3 depleted MCF7 cells.

5.4.1 TACC3 depletion sensitizes to paclitaxel-induced cell death

The synergistic effects of TACC3 depletion and treatment with low doses of paclitaxel on cell cycle progression and survival was first investigated by FACS based DNA content analysis. As indicated in Fig. 33, treatment of TACC3 depleted NIH3T3 cells with paclitaxel resulted in elevated aneuploidy, polyploidy, and cell death, while the same paclitaxel concentrations alone, i.e. in control siRNA expressing NIH3T3 cells, had none or very minute effect (Schneider et al., 2007b). In particular, aneuploidy, already markedly present in TACC3 depleted cells, was significantly increased in its extent already after one day of paclitaxel treatment. By day four of paclitaxel treatment, surviving cells usually displayed an abnormal DNA content.

Importantly, prolonged incubation of TACC3 depleted cells with paclitaxel at a low concentration of 10 nM caused excessive polyploidy and potentiated cell death as demonstrated by the determination of the percentage of cells undergoing DNA fragmentation (Fig. 33A). Typically, these cells were strongly enlarged in size and often contained multiple nuclei, as visualised by microtubule/DNA staining and cLSM analysis (Fig. 33B).

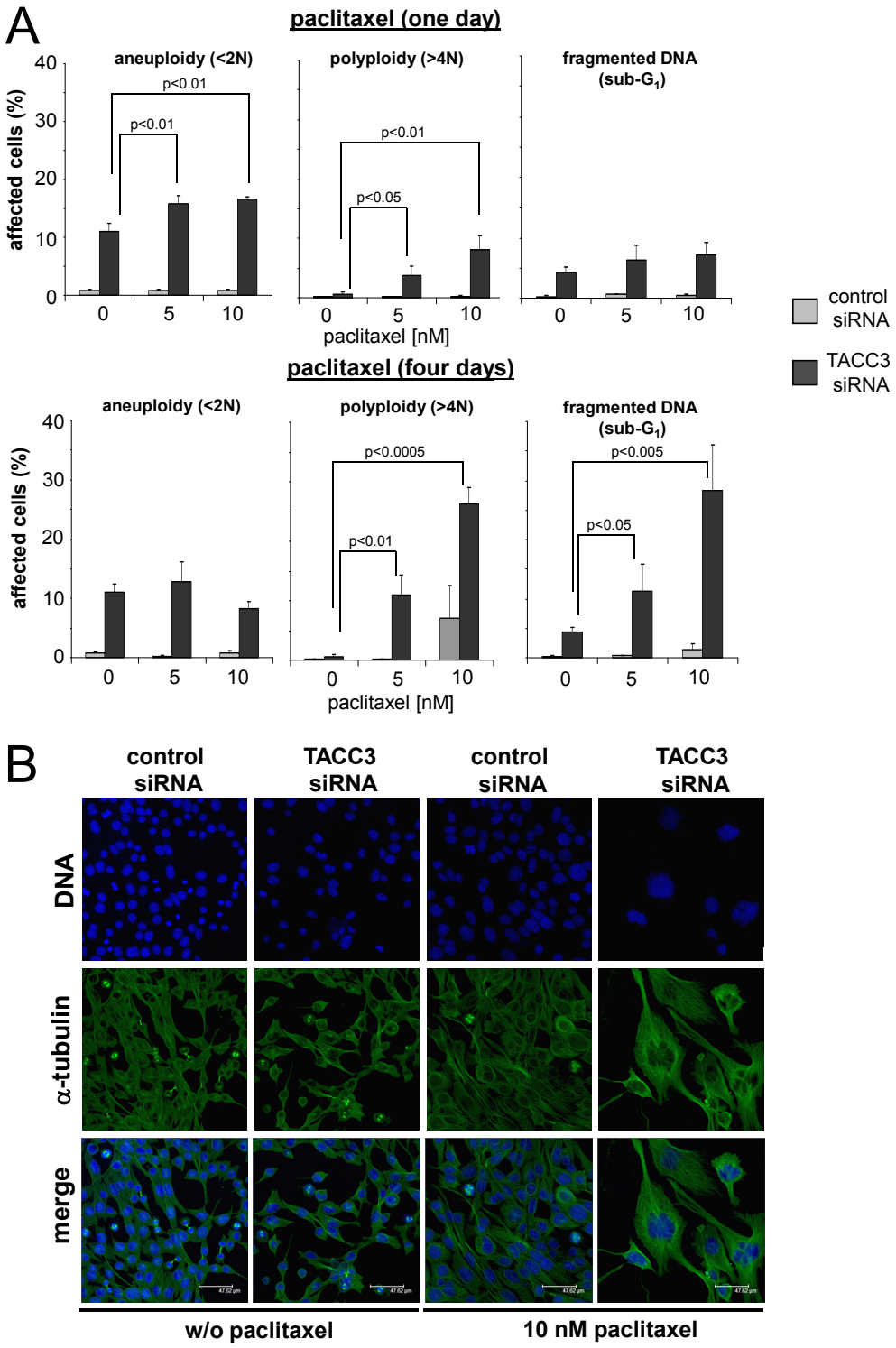

Fig. 33: TACC3 depletion sensitizes NIH3T3 cells to the effects of low dose paclitaxel treatment.

(**A**) After four days of DOX treatment, control siRNA and TACC3 siRNA expressing cells were either left untreated or treated with the indicated concentrations of paclitaxel. Following further incubation for one or four days the number of aneuploid cells (nearly 2N) and cells undergoing polyploidization (>4N) or DNA fragmentation (sub-G_1) was determined by flow cytometry. Values shown are the means ± SD from three experiments. (**B**) TACC3 depleted cells and control cells were treated with 10 nM paclitaxel for three days and thereafter subjected to confocal laser scanning microscopy. Microtubules (green) were detected using α-tubulin-specific antibodies. DNA was visualized by DAPI staining (blue). Bar: 47.6 µm. Representative confocal images are shown.

Taken together, simultaneous downregulation of TACC3 expression and low paclitaxel treatment led to increased mitotic stress beyond a threshold sufficient to cause severe polyploidisation and cell death.

TACC3 depletion led to a strong activation of the p53 pathway (Fig. 16A), which could be further increased by additional paclitaxel treatment (Fig. 19). The induction of $p21^{WAF}$ mediated cell cycle arrest in TACC3 depleted NIH3T3 cells largely suppressed the apoptotic branch of p53. In particular, p53 mediates cell death through the transcriptional activation of the pro-apoptotic factor Bax, which counteracts the anti-apoptotic function of Bcl-2 (Yu & Zhang, 2005). Elevated Bax levels predispose cells towards apoptosis, since activated Bax translocates into mitochondrial membrane in order to initiate cytochrome C release and apoptosis (Willis & Adams, 2005).

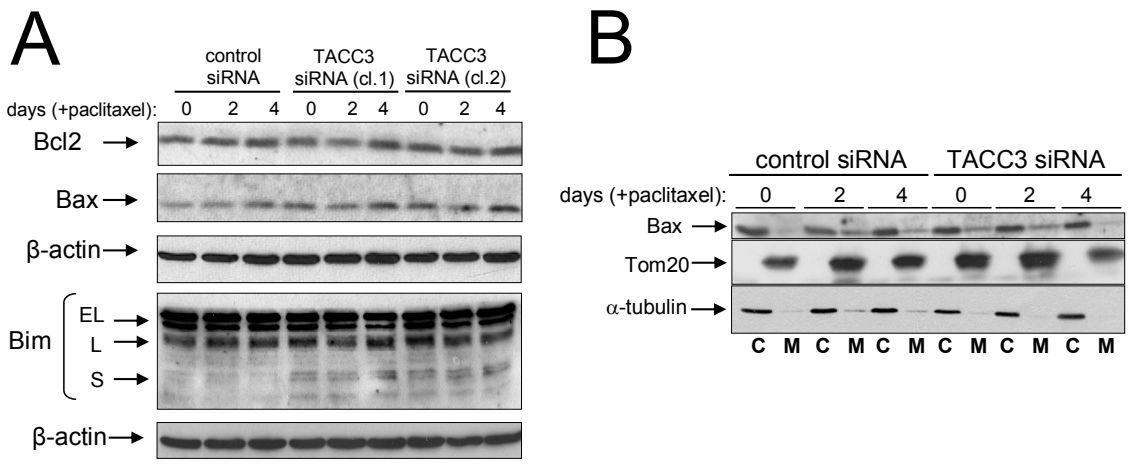

Fig. 34: Increased Bim-S protein levels indicate a predisposition of TACC3 depleted cells towards paclitaxel induced cell death, while the Bax pathway remains unaffected.

(**A**) Immunoblot analysis of extracts from TACC3 depleted cells and control cells without paclitaxel treatment (day 0) or after treatment with 10 nM paclitaxel for two or four days. The expression of Bcl-2, Bax, Bim, and β-actin as loading control was determined by immunoblot analysis using specific antibodies. (**B**) Paclitaxel treatment of TACC3 depleted cells does not lead to increased apoptosis-associated translocation of Bax to mitochondrial membrane. Subcellular fractions were subjected to Immunoblot analysis, using Bax specific antibodies. Tom20 and α-tubulin were used as markers for mitochondrial (M) and cytoplasmic fractions (C), respectively.

However, the protein levels of Bax were not overtly altered in TACC3 depleted cells upon paclitaxel treatment (Fig. 34A). Consistent with this, no significant increase in the apoptosis-associated translocation of Bax to the mitochondrial membrane was

visible in these cells (Fig. 34B) by Immunoblot analysis of subcellular fractions, despite the fact that these cells underwent cell death as shown by apoptotic DNA-fragmentation (Fig. 33A).

An important pro-apoptotic protein activated by microtubule-disrupting agents in a p53-independent fashion is Bim (Ley et al., 2005; Mollinedo & Gajate, 2003). Its activation can be triggered by stress to the mitotic spindle. In particular, the Bim-S splice form is considered to be the most pro-apoptotic form of all three expressed Bim splicing isoforms (O'Connor et al., 1998). The possibility that increased Bim-S protein concentrations are associated with the cell death phenotype of TACC3 depleted/paclitaxel treated NIH3T3 cells was addressed by immunoblot analysis. Indeed, the protein levels of Bim-S were increased in TACC3 depleted cells and remained elevated upon paclitaxel treatment, while in control siRNA expressing cell Bim-S was at all times nearly undetectable (Fig. 34A). Thus, TACC3 depletion predisposes NIH3T3 cells to spindle poison-induced cell death, which occurs despite the high concentrations of the anti-apoptotic cell cycle inhibitor $p21^{WAF}$. This cell death is apparently Bax-independent and possibly Bim-S associated. Overall, the data presented above indicate that inhibiting the function of the centrosomally localised and microtubule stabilising factor TACC3 sensitises cells to the effects of the chemotherapeutic agent paclitaxel (Schneider et al., 2008).

5.4.2 Paclitaxel accelerates the onset of senescence in TACC3 depleted MCF7 cells

In contrast to the other cell lines analyzed in this study, MCF7 cells display a suppressed apoptotic response and are relatively insensitive towards many chemotherapeutic agents (Simstein et al., 2003). Remarkably, all isoforms of the pro-apoptotic protein Bim became downregulated in MCF7 cells upon TACC3 depletion (Fig. 21C). Also, while TACC3 depleted NIH3T3 cells underwent polyploidisation and cell death when treated with paclitaxel virtually no apoptosis was detected in MCF7 cells under similar conditions (Fig. 20A). Instead, the onset of cellular senescence was accelerated when cells were treated with low doses of paclitaxel. As indicated in Fig. 35A, after 2 days of paclitaxel treatment, up to 50% of TACC3 depleted MCF7 cells stained positive for senescence-associated β-galactosidase (SA-β-gal) activity, while paclitaxel treated control siRNA expressing cells and also untreated TACC3

depleted cells showed little SA-β-gal activity at this stage. At day 5 of paclitaxel treatment, close to 90% of TACC3 depleted cells displayed detectable SA-β-gal activity, though the TACC3 depletion per se already resulted in 75 % senescent cells (Fig. 35B). At the same time, control siRNA expressing cultures showed maximally ~20% senescent, i.e. SA-β-gal positive, cells.

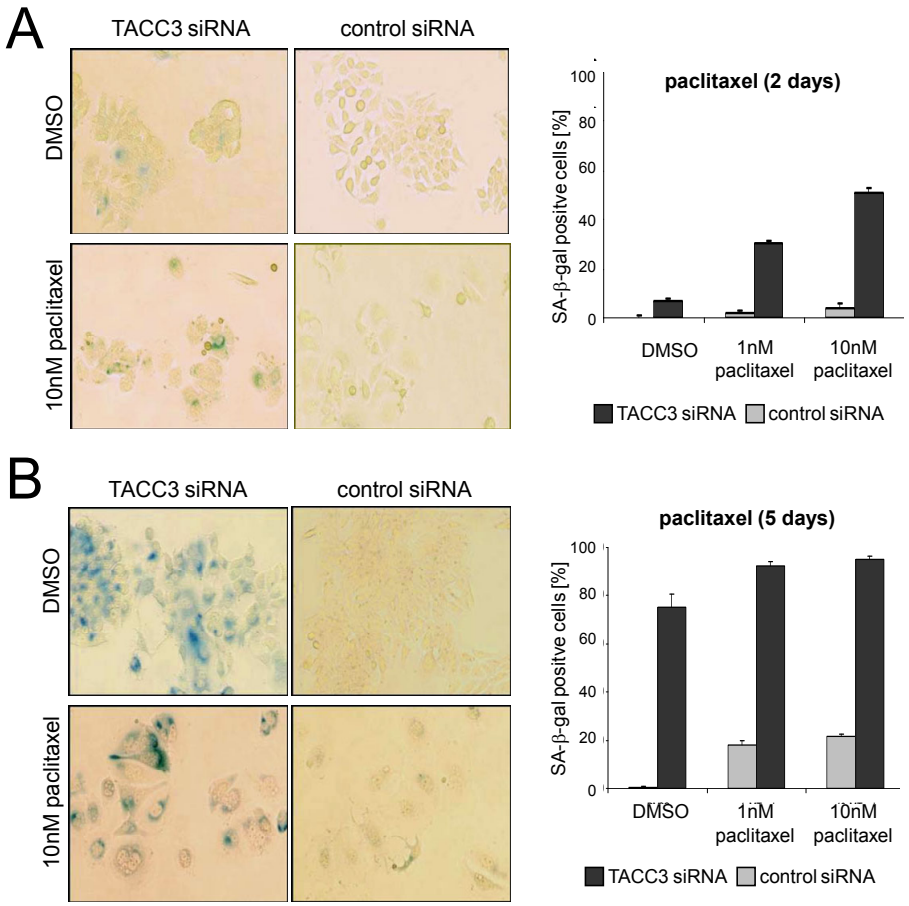

Fig. 35: Treatment of TACC3 depleted cells with low doses of paclitaxel accelerates the onset of senescence.

At day 1 of DOX treatment (i.e. control or TACC3 siRNA expression), cells were supplied with 1 or 10 nM paclitaxel or DMSO as control. (**A**) After two days, cells were stained for SA-β-gal activity and analyzed by standard microscopy (10x objective, left panel). For each value, a triplicate of approx. 400 cells each was scored for SA-β-gal (blue) positivity (right panel). (**B**) Fllowing 5 days of paclitaxel treatment control and TACC3 siRNA expressing cells were analyzed as in A.

These experiments demonstrate that paclitaxel is a weak inducer of cellular senescence in TACC3 proficient MCF7 cells. However, when TACC3 is depleted, the effect is potentiated by even low paclitaxel concentrations, leading to accelerated senescence. In contrast, in cells with functional apoptotic pathways like NIH3T3 cells, low doses of paclitaxel lead to polyploidy and cell death when combined with TACC3 depletion.

6 Discussion

In this thesis, the role of the centrosomal protein TACC3 in cell cycle progression and cellular survival was analyzed by characterizing the molecular and cellular effects of its silencing on the integrity of the mitotic spindle apparatus and the resulting activation of mitotic and post-mitotic checkpoints.

TACC proteins contribute to the stability of the mitotic spindle apparatus. Mechanistically, in *Xenopus laevis* and *Drosophila melanogaster*, TACC proteins are required to recruit the microtubule stabilizing protein ch-TOG/XMAP215/Msps in an Aurora A kinase-dependent manner to the centrosome and thereby to counteract the microtubule-destabilizing activity of the kinesin XKCM1/MCAK (Kinoshita et al., 2005; Peset et al., 2005). It was previously shown that TACC3 plays an essential role in maintaining survival of highly proliferating cells during embryonic development (Piekorz et al., 2002). Here, the molecular mechanisms possibly underlying the *in vivo* defects observed in embryonically lethal TACC3-deficient mice were elucidated in greater detail. Furthermore, the consequences of defective cell cycle checkpoints, often characteristic for cancer cells, were addressed in the context of TACC3 depletion. This offers a perspective for a possible role of TACC3 as a molecular target for tumour therapy.

6.1 Mechanisms of activation of the post-mitotic checkpoint upon TACC3 depletion and G_1 arrest

The first visible effect of TACC3 depletion was the destabilization of microtubule-chromosome binding at prometaphase. This was demonstrated by confocal laser scanning microscopy, where e.g. TACC3 depleted NIH3T3 cells displayed unattached chromosomes failing to congress at the metaphase midzone (Fig. 15). Due to these errors mitotic progression in TACC3 depleted cells was stalled, as indirectly shown by an increased percentage of mitotic cells (i.e. phospho-Histone H3 positive cells) and also by the delayed degradation of cyclin B1. Apparently though, the lack of TACC3 function was initially not sufficient to induce a permanent spindle assembly checkpoint activation and mitotic arrest. Instead, cells progressed through mitosis and exited with an aneuploid DNA content. Aneuploidy induced by TACC3-*knock down* was observed in all cell lines analyzed in this study, though with varying

degrees of severity as exemplary shown for NIH3T3 cells (Fig. 14). Correspondingly, aneuploidy was also clearly detectable in primary cells derived from TACC3$^{-/-}$ mouse embryos (Piekorz et al., 2002).

A prolonged mitosis leads to stabilization of the tumour suppressor protein p53, which then activates the post-mitotic checkpoint once the cells exit into G_1 (Blagosklonny, 2006; Margolis et al., 2003). Re-entrance into the next phase of the cell cycle, namely the DNA replication (S) phase, is prevented by the transcriptional p53-target and cyclin kinase inhibitor p21^{WAF}. The G_1 arrest function of p21^{WAF} is essential in order to prevent endo-reduplication as previously shown for p21^{WAF} deficient HCT116 cells subjected to paclitaxel-induced mitotic stress (Stewart et al., 1999a). Accordingly, the same cells proved particularly susceptible to TACC3 depletion by becoming polyploid and dying rapidly (Fig. 32). Apparently, p53 also mediates G_1 arrest by increasing the levels of cyclin D1 protein through the function of p21^{WAF} (Chen et al., 1995; Del Sal et al., 1996). Consistent with this, cyclin D1 protein levels were found to be elevated in cell lines subjected to TACC3-siRNA expression. Remarkably, only in HCT116 p21$^{WAF-/-}$ cells no increase in cyclin D1 protein could be detected after TACC3 depletion. Importantly, the subcellular localisation of cyclin D1 should be taken into account to understand the inhibition of cell cycle progression in TACC3 depleted cells despite the high cyclin D1 levels. While nuclear targeting of cyclin D1 and its associated kinase Cdk4 enforces cell cycle progression (i.e. $G_1 \rightarrow S$ transition), cyclin D1 export into the cytosol is associated with its functional inactivation and hence a post-mitotic G_1-arrest (Gladden & Diehl, 2005). Indeed, following TACC3 depletion in NIH3T3 cells, cyclin D1 and Cdk4 were found nearly exclusively in the cytoplasm, in accprdance with the observed inhibition of proliferation.

6.2 Mechanisms associated with transient or permanent G_1 arrest in TACC3 depleted cells

The role of the largely cytosolically localised p21^{WAF} in TACC3 siRNA expressing NIH3T3 cells (Fig. 24) currently represents a complicated issue. The protein levels of p21^{WAF} in TACC3 depleted cells were strongly increased, evidently through the function of p53. Also, the substantial proliferation arrest in TACC3 depleted cells was very likely caused through the cell cycle inhibitory function of p21^{WAF}. Classically,

$p21^{WAF}$ is required in the nucleus in order to inhibit cyclin dependent kinases (Cdks) and hence induce proliferation arrest. In contrast, localization of $p21^{WAF}$ in the cytosol is associated with its role in inhibition of apoptosis and stabilization of cyclin D1/Cdk4 complexes (Blagosklonny, 2002; Coqueret, 2003; Janicke et al., 2007). The stabilization of cyclin D1/Cdk4 through $p21^{WAF}$-binding renders the complex functionally inactive (Olashaw et al., 2004). On the other hand, TACC3 depleted NIH3T3 cells still proliferate, albeit slowly (Fig. 13). Interestingly, in this regard $p21^{WAF}$ was shown to be induced in a p53-dependent manner in nasal squamous carcinoma cell line RPMI-2650 by low doses of paclitaxel and then targeted to the cytoplasm through Akt kinase dependent phosphorylation in order to relieve the proliferation arrest (Heliez et al., 2003). Activation of the Akt pathway, which is dependent on phosphatidylinositol-3-kinase (PI3K) activity, is important for cellular survival, since activation of Akt confers viability in cancer cells, e.g. upon paclitaxel treatment (Torii et al., 2006; West et al., 2002). Indeed, the levels of Akt phosphorylated at Ser-473 (i.e. active Akt kinase) was elevated in paclitaxel treated and/or TACC3 depleted NIH3T3 cells. Also, the higher phospho-Akt levels upon TACC3 depletion were associated with increased amounts of phosphorylated (i.e. inactive) FOXO-3a, a transcription factor and Akt target which induces cells cycle arrest and apoptosis (Greer & Brunet, 2005). Thus, the bypassing of the G_1 arrest by Akt dependent mechanisms likely allows aneuploid TACC3 depleted cells to enter the next cell cycle by progressing into S-phase (Fig. 36).

However, as a back-up, the G_2 checkpoint became activated upon TACC3 depletion, arresting NIH3T3 cells at the G_2/M transition. This was evident through increased levels of inactive Cdk1 (phosphorylated at Tyr-15) and elevated cyclin B1 protein amounts (Fig. 36). Arrest in G_2 can be initiated both through p53-$p21^{WAF}$ activity and via p53-independent effectors, including Chk1 and Chk2 kinases (Taylor & Stark, 2001). Interestingly, induction of G_2 arrest by DNA damaging agents like cisplatin or doxorubicin protects cells from the subsequent paclitaxel effect during mitosis (Blagosklonny et al., 2000; Judson et al., 1999). Nevertheless, this arrest at G_2/M transition is transient and can also be bypassed through adaptation with the consequence of cells entering the next aberrant mitosis (Andreassen et al., 2003). As an overall result, mitotic defects accumulate and leading to increased aneuploidy and inhibition of proliferation, as characterized by elevated protein levels of the cell cycle arrest factors $p21^{WAF}$ (G_1) and Cdk1-pY15 (G_2). Remarkably, this inhibition of cell

cycle progression was not permanent since it could be reversed through the termination of TACC3 siRNA expression by DOX withdrawal (Fig. 18). A model of the effects of TACC3 downregulation on cell cycle progression in G_1 checkpoint proficient cells like NIH3T3 cells and probably also in TACC3$^{-/-}$ embryos is presented in Fig. 36. *In vivo*, the progressive growth inhibition through activation of post-mitotic checkpoints eventually leads to embryonic lethality of TACC3$^{-/-}$ mice and their uteral resorption.

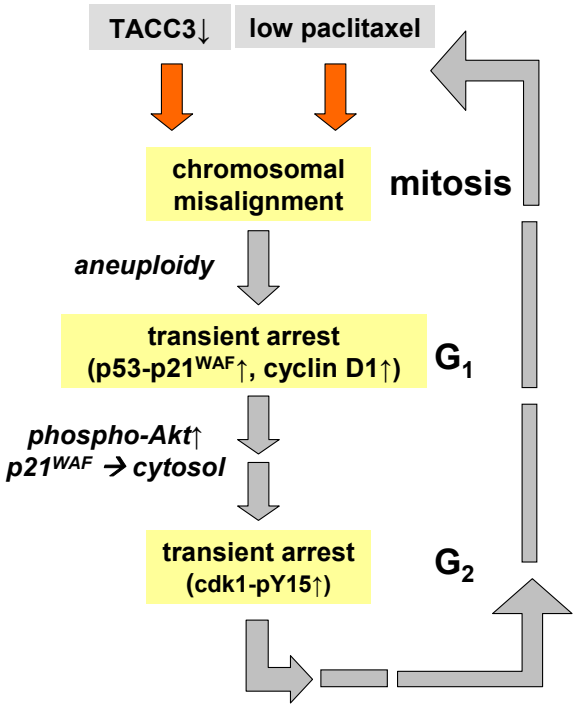

Fig. 36: Model of the effect of TACC3 depletion on cell cycle progression in p53-proficient cells.

Decreased TACC3 levels and low-dose paclitaxel treatment result in chromosomal misalignment and aneuploidy. As a response, p53 is activated and arrests cells in G_1 with increased levels of p21^{WAF} and cytoplasmic cyclin D1. This arrest is partially relieved by translocation of p21WAF into the cytoplasm, where p21^{WAF} in cooperation with Akt plays predominantly an antiapoptotic role. Cells slipping through G_1 then arrest in G_2 through increased Tyr15 phosphorylation of Cdk1. The G_2 arrest is only transient and allows TACC3-depleted cells to enter the next mitotic cycle. With each cycle, the strength of the postmitotic G_1 arrest increases in response to the accumulation of mitotic defects and aneuploidy. Diagram from Schneider et al., 2007b.

In contrast to the phenotype in untransformed NIH3T3 cells, in breast carcinoma MCF7 cells activation of the post-mitotic G_1 checkpoint upon TACC3 depletion was associated with induction of a permanent arrest through cellular senescence. Mechanistically, upon downregulation of TACC3 expression, nuclear accumulation of

p53 was detected in MCF7 cells similarly as in TACC3 depleted NIH3T3 cells. However, MCF7 cells stopped proliferating when TACC3 siRNA was expressed. These cells were unable to overcome the G_1 arrest, as indicated by the reduced levels of the later in the cell cycle expressed cyclins, i.e. cyclin A and B1 (Fig. 21).

MCF7 cells failed to display DNA fragmentation and a significant cell death upon TACC3 depletion. Initiation of apoptosis and DNA fragmentation are largely suppressed in MCF7 cells, since they lack caspase-3 gene expression (Jänicke et al., 1998). Active caspase-3 is required for the initiation of apoptosis (Porter & Jänicke, 1999). Thus, the lack of caspase-3 renders MCF7 cells relatively insensitive towards many chemotherapeutic agents (Simstein et al., 2003). Instead, MCF7 cells can be forced into p53-dependent senescence e.g. by DNA damage through doxorubucine treatment (Elmore et al., 2002) or through γ-irradiation (Essmann et al., 2004). Interestingly, transgenic MCF7 cells stably re-expressing procaspase-3 cDNA still became senescent and did not commit apoptosis when TACC3 was downregulated, indicating that in MCF7 cells caspase-3 expression is not a determinant of an apoptotic response towards mitotic stress.

Why does TACC3 depletion lead to a permanent p53 mediated G_1 arrest in MCF7 cells as opposed to a transient one in NIH3T3 cells? The reason might naturally lie in the transformed nature of the breast carcinoma cell line MCF7 (as opposed to the immortalization status of NIH3T3 cells), which makes MCF7 cells particularly sensitive to mitotic stress through TACC3 depletion. From here, the suppression of apoptotic pathways in MCF7 cells allows induction of p53/$p21^{WAF}$-dependent senescence as the only possible cellular response.

6.3 Co-operative effects of TACC3 depletion and paclitaxel treatment

Different concentrations of the spindle poison paclitaxel execute different effects on cell cycle checkpoint activation. E.g., a high paclitaxel dose (50 nM) caused a strong activation of the SAC followed by sustained mitotic arrest. In contrast, aberrant mitosis, aneuploidy and the activation of the post-mitotic G_1 and G_2 checkpoints have been reported for cells treated with low doses of paclitaxel (≤10 nM; Abal et al., 2003). Here, cells became aneuploid without activating the spindle assembly checkpoint (Chen & Horwitz, 2002). Low doses of paclitaxel (8 nM) failed to overly

impair mitotic progression (Ikui et al., 2005) and arrested the cells post-mitotically in G_1 in a p53-dependent manner (Blagosklonny, 2006). This arrest protects cells from paclitaxel induced polyploidy and cell death (Stewart et al., 1999b). Furthermore, low doses of paclitaxel (≤10 nM) induce senescence in A549 lung carcinoma cells through checkpoint mechanisms (Klein et al., 2005) similar to the ones found in TACC3 depleted MCF7 cells (Fig. 21). Thus, the resemblance of the effects of TACC3 depletion and low paclitaxel treatment and their cooperative action on NIH3T3 (Schneider et al., 2007b) or MCF7 cells is rather striking.

The spectrum of defects in TACC3-depleted cells can be amplified by the addition of paclitaxel at low nanomolar concentrations which leave control siRNA expressing cells largely unaffected. Upon paclitaxel exposure an increased polyploidy and cell death rate became very prominent in TACC3 depleted NIH3T3 cells (Fig. 33). The molecular mechanisms leading to this cell death are unclear at this point. There was no significant evidence for primary apoptosis as analysed by Annexin V labelling or caspase inhibition assays. Similarly, the levels of the p53 target and pro-apoptotic protein Bax and its antagonist Bcl-2 were not significantly altered in TACC3 depleted NIH3T3 cells upon paclitaxel treatment. It is possible that the predominantly cytosol-localized $p21^{WAF}$ still suppresses p53 mediated apoptosis in these cells (Blagosklonny, 2002). However, the elevated levels of the pro-apoptotic Bim-S isoform in TACC3 depleted cells, which is associated with mitotic stress (Mollinedo & Gajate, 2003), indicate a possible involvement of Bim-S in the observed paclitaxel triggered cell death (e.g. by predisposing these cells towards apoptosis upon paclitaxel treatment; Fig. 34). Correspondingly, TACC3 depletion in apoptosis-impaired MCF7 cells led to a profound decline of all Bim isoforms, lack of cell death and development of cellular senescence as the alternative outcome. Additional treatment of MCF7 cells with low nanomolar concentrations of paclitaxel resulted in a significant acceleration of the onset of senescence, while in control siRNA expressing cells the senescence associated β-gal activity was low upon paclitaxel treatment.

Taken together, TACC3 absence and low concentrations of paclitaxel lead through different molecular effector mechanisms to a similar phenotype of impaired microtubule-kinetochore interaction during spindle assembly and resulting misalignment of chromosomes and aneuploidy (Fig. 36). Hence, a decreased TACC3 expression predisposes cells specifically to paclitaxel-induced cell death despite increased protein concentrations of the protective (i.e. anti-apoptotic) cell cycle

inhibitor $p21^{WAF}$. At the same time, apoptosis-impaired cells can be more swiftly forced into senescence, when TACC3 depletion is combined with low paclitaxel treatment. Based on these findings, TACC3 presents itself as a putative target to circumvent $p21^{WAF}$-associated chemotherapeutic protection of cancer cells against paclitaxel-induced cytotoxicity (Schneider et al., 2008).

6.4 Cellular consequences of a suppressed post-mitotic G_1 checkpoint

The activation of the p53-$p21^{WAF}$ pathway and the consequent post-mitotic arrest are apparently the central response mechanisms to TACC3 depletion in cells as determined in this work. Based on the fact that the G_1 checkpoint is compromised in many tumours, it is important to consider the consequences of a defective post-mitotic G_1 checkpoint in the context of TACC3 depletion. This scenario would allow TACC3 depleted cells to progress into the next round of proliferation without a G_1 checkpoint trigerred delay caused by the arising mitotic defects. HeLa cells are known for a suppressed G_1 checkpoint due to the integration of the HPV18 virus, whose constitutively expressed viral proteins E6 and E7 inactivate the p53 protein and the Retinoblastom (Rb) gene, respectively (Hu et al., 1995). As expected, no significant activation of the p53-$p21^{WAF}$ pathway could be detected in this cell line upon TACC3 depletion (Fig. 23). As a main phenotype and unlike in p53-$p21^{WAF}$ proficient NIH3T3 cells, rapid and excessive apoptotic cell death with the failure of TACC3-depleted HeLa cells to assemble a functional mitotic spindle apparatus was observed. In particular, the presented data indicate that prolonged TACC3 depletion in HeLa cells resulted in a progressive accumulation of cells at prometaphase with misaligned and disorganized chromosomes. Clear evidence points towards a strongly impaired microtubule-kinetochore interaction in TACC3-depleted cells. First, the progressive spindle disorganisation was accompanied by a reduction of the scaffold protein Ndc80 at kinetochores. Interestingly, depletion of Ndc80 was reported to result in impaired spindle assembly, activation of the SAC and mitotic cell death (Martin-Lluesma et al., 2002). Second, the mitotic kinase Aurora B and the checkpoint protein BubR1 failed to localize to normal levels at kinetochores of tACC3 depleted HeLa cells (Fig. 27). Mechanistically, Aurora B directs BubR1 and Mad2, essential components of the SAC, to kinetochores during prometaphase (Ditchfield et

al., 2003; Vigneron et al., 2004). Consistently, a damaged kinetochore architecture was shown to culminate in chromosomal misalignment, delocalization of BubR1 and a sustained metaphase arrest (Kline et al., 2006). Thus, a disturbed localization of three kinetochore-associated proteins, i.e. Ndc80, Aurora B and BubR1, from three different and crucial functional complexes (outer kinetochore structure, chromosomal passenger complex resp. spindle assembly checkpoint) hallmarks the deterioration of the kinetochore structure and the resulting impairment of microtubule-kinetochore attachment in TACC3 depleted HeLa cells.

The mechanism(s) through which TACC3 depletion leads to the obvious disturbance of the kinetochore structure is currently unclear. TACC3 might interact with essential kinetochore proteins. Intrinsic kinetochore protein complexes are indeed involved in the regulation of spindle assembly, correct binding of checkpoint proteins to kinetochores and chromosome segregation (McAinsh et al., 2006). Alternatively, the disorganized spindle architecture could result from the fact that depletion of TACC3 (which targets ch-TOG to the centrosome and mitotic spindle; Fig. 2) impairs the localization of ch-TOG at centrosomes and the mitotic spindle, thereby permitting a stronger recruitment of ch-TOG's antagonist and kinesin MCAK toward the centrosome. The essential microtubule-stabilizing function of ch-TOG is required to counteract the microtubule-destabilising activity of MCAK (Holmfeldt et al., 2004). Indeed, preliminary data showed an increased centrosomal MCAK localization and a reduced ch-TOG signal at the mitotic spindle of TACC3 depleted HeLa cells. However, the observation that kinetochore localization of BubR1 was still detectable in ch-TOG depleted HeLa cells (Meraldi et al., 2004) as opposed to TACC3 depleted cells, also argues for critical interactions of TACC3 with additional spindle stabilising proteins which have to be defined in future studies.

Apparently, a prolonged TACC3 depletion exerts a tremendous mitotic stress in G_1 checkpoint deficient cells like HeLa cells. Here from, a particularly enticing model would be that the resulting suppression of Aurora B function represents the major origin of all mitotic defects observed. In fact, the mitotic kinase Aurora B was reported to regulate BubR1 (Ditchfield et al., 2003), Ndc80 (DeLuca et al., 2006), MCAK (Knowlton et al., 2006), and numerous other substrates at the mitotic spindle and kinetochores. Curiously, Aurora B was reported to interact with a different TACC family member, TACC1 (Delaval et al., 2004). Thus, the important questions raised by the offered model are:

1. Does TACC3 directly (or indirectly) interact with Aurora B and how is this interaction regulated?
2. What is the functional role of this interaction?

The observed mitotic defects in TACC3-depleted HeLa cells likely evoked a prolonged activation of the spindle assembly checkpoint (SAC). This checkpoint is crucial in order to arrest cells with spindle defects in prometaphase/metaphase by inhibiting the degradation of cyclin B1 and hence entrance into anaphase (Bharadwaj & Yu, 2004). Apparently and as discussed before, TACC3 depletion per se does not lead to a sustained activation of the SAC in the presence of a functional G_1 checkpoint. In fact, it was shown that during the first round of division following TACC3 depletion (using a transient oligonucleotide-based RNAi approach) HeLa cells display a relatively mild phenotype with partially destabilized spindle microtubules and the occurrence of misaligned chromosomes (Gergely et al., 2003). In contrast, depletion of TACC3's binding partner ch-TOG under the same conditions had much stronger effects and resulted in disorganized spindles, multipolar spindle formation and increased multinucleation (Gergely et al., 2003). Concomitantly, under prolonged TACC3 depletion, defects in the HeLa mitotic spindle architecture accumulate with each aberrant mitosis due to their inability to activate the post-mitotic p53-$p21^{WAF}$ checkpoint. Instead of arresting in G_1, as observed for TACC3 depleted NIH3T3 and MCF7 cells, HeLa cells continue to cycle and enter the next mitosis without the possibility to combat the defects from the previous cycle. Hence, in HeLa cells a prolonged lack of TACC3 is required in order to evoke a sufficiently high degree of spindle disarray.

6.5 Persistent activation of the spindle assembly checkpoint: two different outcomes

Mitotic spindle collapse in G_1 checkpoint deficient HeLa cells caused by prolonged TACC3 depletion also happens in cells treated with high concentrations (>50 nM) of paclitaxel. In this case, paclitaxel treatment arrests cells in mitosis through the activation of the spindle assembly checkpoint (Abal et al., 2003). An increasing amount of evidence indicates a linkage between the SAC activation and induction of cell death from mitosis (Weaver & Cleveland, 2005). It was suggested that the

suspension of transcription during mitosis leads to a decline of anti-apoptotic factors like Bcl2 and consequently to apoptosis, if mitotic arrest is upheld for a longer period of time (Blagosklonny, 2007). Accordingly, mitotic HeLa cells lacking TACC3 expression underwent apoptotic cell death from a cyclin B1 positive state (Fig. 25) with characteristics similar to mitotic catastrophe. This cell death is executed by caspases and does not require the function of p53 (Castedo et al., 2004). In order to prove a possible requirement of the SAC for mitotic cell death in TACC3 depleted cells, TACC3 expression was downregulated in wild-type HCT116 cells and their SAC-impaired counterpart, Mad2 heterozygous HCT116 cells (Michel et al., 2001). Whereas wild-type cells succumbed to death following TACC3 knock down, $Mad2^{+/-}$ cells were significantly protected from apoptosis (Fig. 30). Thus, a functional SAC sensitizes cells to death from mitosis following prolonged TACC3 depletion. On the other hand, the SAC counteracts “mitotic slippage” of cells which display only minor defects and hence tend to escape from mitotic arrest and cell death. Mitotic slippage is based on a slow but continuous degradation of cyclin B1 (Brito & Rieder, 2006). In this respect, during prolonged TACC3 depletion an increased polyploidisation of surviving HeLa cells could be observed. These cells were typically characterized by the occurrence of multiple nuclei and supernumerary centrosomes, likely generated by an aborted cytokinesis and endoduplication. Thus, these findings argue for an adaptation process in order to overcome the SAC-induced arrest and to avoid mitotic cell death upon TACC3 depletion.

In summary, in HeLa cells, prolonged TACC3 depletion leads to an accumulation of mitotic defects, which in turn results in a persistent SAC activation (Schneider et al., 2007a). Here from, only two alternatives remain for the affected cells: 1) mitotic cell death from a pre-anaphase arrest in a cyclin B1 positive state; 2) gradual degradation of cyclin B1 necessary for a subsequent mitotic slippage, which results in polyploidy. The decisive criteria between these outcomes might be the severity of the spindle defects and the dynamics of the continuous degradation of cyclin B1. If a lowering of a certain cyclin B1 threshold is reached in time (Brito & Rieder, 2006), cells can complete mitosis, otherwise mitotic apoptosis is executed.

6.6 Conclusions and Perspectives

Overall, this thesis characterises TACC3 as a crucial factor in mitotic spindle assembly and in the regulation of the binding of chromosomes to spindle microtubules. The crucial role of TACC3 in microtubule dynamics and spindle integrity has been confirmed and further elucidated. Although TACC3 predominantly localises to the spindle poles and minus ends of microtubules, strong evidence points towards a functional interaction of TACC3 with crucial kinetochore proteins, presumably Aurora B. Mitotic defects caused by the absence of TACC3 result in aneuploidy and the consequent activation of the post-mitotic p53-$p21^{WAF}$ mediated checkpoint. The resulting arrest translates into a strong inhibition of proliferation and can even become permanent, i.e. lead to cellular senescence.

The proliferation arrest in G_1 is the likely cellular cause for the growth retardation and embryonic lethality observed in TACC3 deficient mice (Piekorz et al., 2002). It also offers an explanation, why a partial G_1 checkpoint suppression through genetic p53 reduction (p53 heterozygosity) provided a partial rescue of the embryonic lethality caused by TACC3 deficiency (Piekorz et al., 2002). An embryonic growth inhibition, which is caused by cellular checkpoint activation and which most likely leads to resorption of $TACC^{-/-}$ embryos in utero, can be relieved by a partial p53 inactivation. In contrast, in cells with a fully ablated G_1 checkpoint, mitotic defects caused by TACC3 withdrawal exacerbate with each division culminating in sustained SAC activation and mitotic cell death. An extensive overview on the effects of TACC3 depletion on cell cycle progression and checkpoint activation is provided in Fig. 37.

TACC3 could be established as a potential target for cancer treatment. The biological consequences of TACC3 depletion strikingly resemble the effects elicited through treatment of cells with low doses of the microtubule-interfering chemotherapeutic agent paclitaxel (Abal et al., 2003). Consequently, TACC3 depletion combined with paclitaxel treatment had synergistic effects on inhibition of cell proliferation and viability. This was in particular evident in NIH3T3 and MCF7 cells, where paclitaxel treatment potentiated polyploidisation and concomitant cell death (Fig. 33) or the induction of cellular senescence (Fig. 35), respectively.

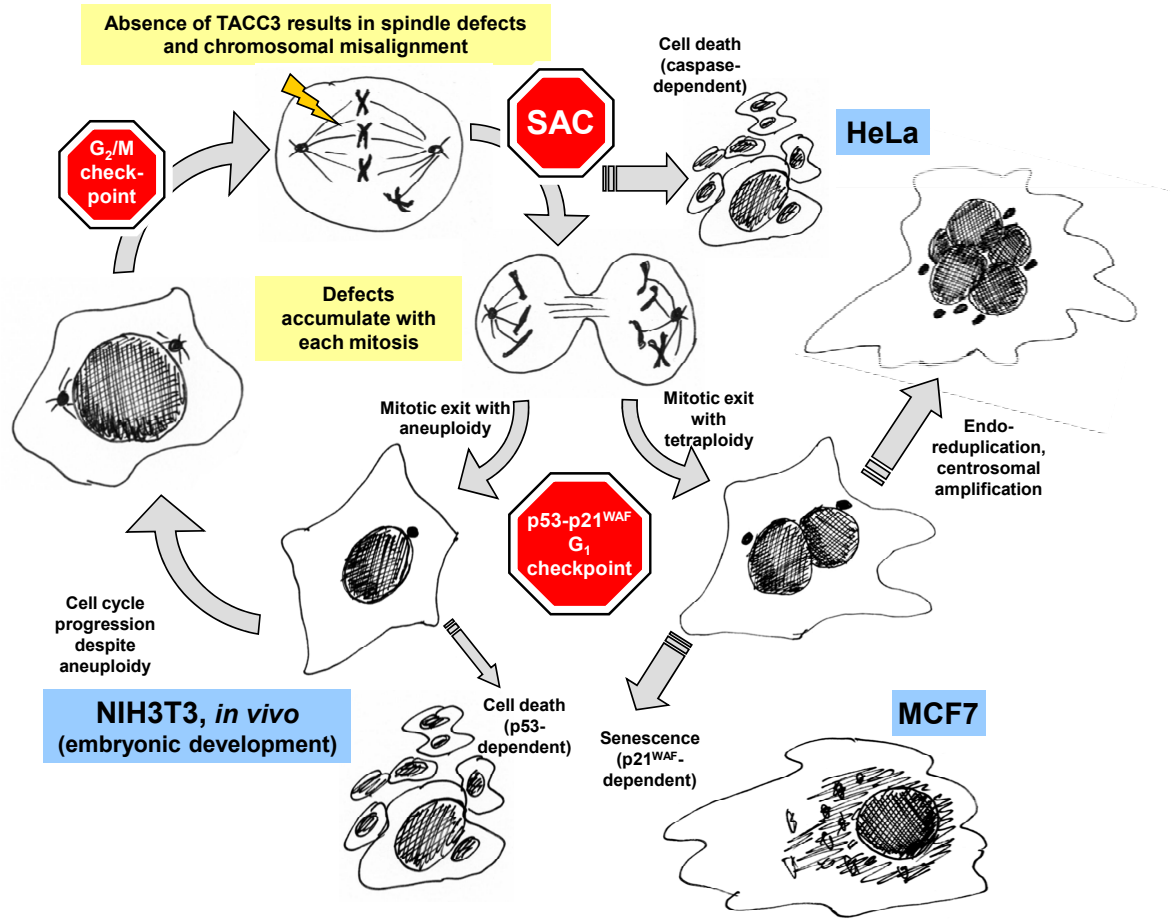

Fig. 37: Cell cycle checkpoint activation in cells lacking TACC3 function.

Similarly to low doses paclitaxel treatment, absence of TACC3 during mitosis results in impaired microtubule-kinetochore interaction and appearance of misaligned chromosomes at metaphase. With each aberrant mitosis, these defects exacerbate and resulting in activation of the spindle assembly checkpoint (SAC). Grave deterioration of the spindle architecture results in a sustained SAC activity and mitotic cell death, which is caspase dependent and p53 independent. Alternatively, a slippage can occur, with cells exiting mitosis in a polyploid state. Cells lacking G_1 checkpoint function continue to endoreduplicate. This process is associated with a recurrent mitotic slippage, polyploidisation and centrosome amplification. G_1 checkpoint proficient cells can preclude error accumulation and sustained SAC activation by arresting post-mitotically in their aneuploid or tetraploid state in a p53-$p21^{WAF}$ dependent manner. This G_1 arrest can either become permanent, leading to senescence, or can be overcome with cells entering the next round of DNA replication. As a backup mechanism, entrance into the next mitotic phase is transiently prohibited by an additional checkpoint activation at the G_2-M transition. All effects of TACC3 depletion can be further potentiated by treatment with already low doses (≤10 nM) of the spindle poison paclitaxel.

Thus, the synergistic effects of TACC3 inhibition and low paclitaxel treatment could be used in order to target even apoptosis-impaired tumour cells through induction of cellular senescence. Indeed, all three members of the TACC family have been linked to certain cancers. TACC proteins map closely to chromosomal translocation breakpoints that are associated with mammary tumors and multiple myeloma (Still *et al.,* 1999a; Still *et al.,* 1999b). Overexpression of TACC1 promotes transformation *in*

vitro (Still *et al.,* 1999a) and *in vivo* (Cully *et al.,* 2005). Interestingly, TACC3 aberrations have been recently described in patients with ovarian, thyroid and non-small cell lung cancer (Jung et al., 2006; Lauffart et al., 2005; Ulisse et al., 2007).

Taken together, this work suggests that TACC3 could be a putative pharmacological target in cancer therapy. Importantly, since various cell cycle checkpoints are naturally inhibited in tumour cells, these may be particularly susceptible to the inhibition of TACC3 function.

7 Summary

TACC (transforming acidic coiled-coil) proteins regulate centrosome-dependent assembly of microtubules during mitosis. The third member of this protein family, TACC3, is highly expressed during the G_2/M phase of the cell cycle where it localises to the centrosome and mitotic spindle apparatus. The critical biological role of TACC3 became evident through constitutive gene inactivation of TACC3 in the mouse which led to an embryonic lethality (Piekorz et al., 2002). Primary cells derived from TACC3 deficient embryos failed to proliferate *ex vivo*. The underlying molecular mechanisms associated with the effects of TACC3 deficiency were unclear. Therefore, in this thesis cell line models were established to characterise the molecular and cellular effects of a conditional, siRNA-mediated TACC3 depletion and hence the role of TACC3 in proliferation and cellular survival. In particular, the following questions were addressed:

(I) Does TACC3 depletion cause aneuploidy and as consequence trigger post-mitotic cell cycle arrest through the activation of a G_1 checkpoint response?

(II) What are the consequences of TACC3 depletion in cells with a compromised G_1 checkpoint response?

(III) Therapeutic interference with the mitotic spindle apparatus using microtubule-interfering agents like paclitaxel is a rationale for the treatment of tumours. Therefore, does depletion of TACC3, which is often expressed at high levels in cancer cells, sensitize cells to paclitaxel-induced growth inhibition or cell death?

Addressing the first point it is shown that depletion of TACC3 in NIH3T3 fibroblasts affected the attachment of spindle microtubules to chromosomes resulting in chromosome misalignment and aneuploidy, but without overtly impairing mitotic progression. Postmitotically, aneuploidy through TACC3 depletion was associated withactivation of the G_1 checkpoint and inhibition of further proliferation. This response was critically dependent on the tumour suppressor protein p53 and its transcriptional target and cell cycle inhibitor $p21^{WAF}$.

In contrast, in p53-$p21^{WAF}$-compromized HeLa cells with a *defective G_1 checkpoint response* and hence *lack of G_1 arrest*, the prolonged absence of TACC3 resulted in a

severe spindle distortion and multipolarity. Moreover, a progressive deterioration of the structure of the kinetochore, where chromosomes are captured by microtubules, occurred as shown by the delocalisation of the kinetochore-associated proteins Ndc80, Aurora B and BubR1. These factors play an essential role in the regulation of microtubule-kinetochore interaction. Consequently, due to severely misaligned chromosomes, TACC3 depleted cells arrested in mitosis prior to anaphase and underwent caspase-dependent apoptosis. Cells that escaped from this arrest by mitotic slippage became highly polyploid and accumulated supernumerary centrosomes. Thus, a functional p53-p21^{WAF} dependent checkpoint in G_1 is indispensable for counteracting genomic instability caused by mitotic stress through TACC3 depletion and further uncontrolled proliferation.

Remarkably, TACC3 *knock down* in NIH3T3 cells elicited similar molecular and cellular effects as reported for cells treated with low, subtoxic concentrations (≤10 nM) of the chemotherapeutically used spindle poison paclitaxel. Interestingly, and unlike in TACC3 expressing cells, paclitaxel co-treatment was able to induce strong polyploidy and subsequent cell death in TACC3 depleted cells. Consistent with this, the induction of cellular senescence as observed in apoptosis-impaired MCF7 cells upon TACC3 depletion was highly accelerated by paclitaxel co-treatment. Thus, TACC3 depletion sensitizes to the growth inhibitory and cell death inducing effects of paclitaxel.

In summary, TACC3 plays an essential role in spindle assembly and proper chromosome segregation and hence in maintenance of genomic stability. TACC3 knock down leads to the activation of a growth inhibitory and p53-p21^{WAF} dependent G_1 checkpoint response. The high susceptibility of transformed and G_1 checkpoint compromised cells to mitotic stress through TACC3 depletion identifies TACC3 as a possible target for cancer treatment, especially in combination with chemotherapeutic spindle poisons like paclitaxel.

8 Zusammenfassung

TACC (transforming acidic coiled-coil) Proteine steuern die Zentrosom-abhängige Mikrotubuli-Dynamik während der Mitose. Das dritte Mitglied dieser Proteinfamilie, TACC3, wird im hohen Maße während der G_2/M-Phase im Zellzyklus exprimiert, wo es an den Zentrosomen und dem mitotischen Spindelapparat lokalisiert. Die essentielle biologische Rolle von TACC3 wurde durch eine konstitutive Geninaktivierung in der Maus deutlich, welche zu einer embryonalen Letalität führte (Piekorz et al., 2002). Primärzellkulturen aus TACC3-defizienten Embryonen konnten *ex vivo* nicht expandiert werden und zeigten einen Proliferationsdefekt. Die zugrundeliegenden molekularen Mechanismen, die die zellulären Defekte nach TACC3-Defizienz zur Folge hatten, waren jedoch unklar. Daher wurden im Rahmen dieser Arbeit Zelllinienmodelle etabliert, um die molekularen und zellulären Auswirkungen einer konditionellen, siRNA-vermittelten TACC3-Depletion und somit die Rolle von TACC3 in Proliferation und Zellüberleben zu charakterisieren. Insbesondere sollten die folgenden Fragen beantwortet werden:

(I) Verursacht TACC3-Depletion Aneuploidie, und wird als Folge ein post-mitotischer Zellzyklusarrest durch die Aktivierung des G_1-Kontrollpunkts ausgelöst?
(II) Was sind die molekularen und zellulären Konsequenzen einer TACC3-Depletion in Zellen mit einer defekten G_1-Kontrollpunkt-Funktion?
(III) Therapeutische Inhibition des mitotischen Spindelapparats mithilfe Mikrotubuli-interferierender Agenzien wie Paclitaxel ist ein Grundprinzip in der Tumorbehandlung. Deshalb sollte geklärt werden, ob eine Depletion von TACC3, das oft in erhöhten Mengen in Krebszellen exprimiert wird, zu einer Sensibilisierung gegenüber Paclitaxel-induzierter Wachstumshemmung oder Zelltod führt.

Bezüglich des ersten Punkts konnte gezeigt werden, dass eine Depletion von TACC3 in NIH3T3-Fibroblasten die Interaktion von Spindel-Mikrotubuli mit Chromosomen beeinträchtigte und somit eine Chromosomenfehlanordnung und Aneuploidie auslöste. Eine deutliche Behinderung der mitotischen Progression trat aber nicht ein. Dagegen war die durch TACC3-Depletion hervorgerufene Aneuploidie postmitotisch mit einer Aktivierung des G_1-Kontrollpunkts und Hemmung der weiteren Zellproliferation assoziert. Diese Antwort war abhängig vom Tumorsuppressor-Protein p53 und seinem transkriptionellen Zielgen und Zellzyklus-Inhibitor $p21^{WAF}$.

Im Gegensatz dazu führte eine Depletion von TACC3 in HeLa-Zellen, die durch einen *defekten G_1-Kontrollpunkt* und folglich durch ein *Fehlen eines G_1-Arrests* gekennzeichnet sind, zu schwerwiegenden Spindeldefekten und Spindel-Multipolarität. Die nach TACC3-Depletion deutlich reduzierte mitotische Lokalisation der normalerweise Kinetochor-assoziierten Proteine Ndc80, Aurora B und BubR1 spricht für strukturelle Defekte am Kinetochor. Diese Faktoren spielen eine essentielle strukturelle und regulatorische Rolle bei der Steuerung der Mikrotubuli-Kinetochor-Interaktion. Entsprechend arretierten TACC3-depletierte Zellen in der Mitose aufgrund einer schwerwiegenden chromosomalen Fehlanordnung, was wiederum zum Zelltod durch Caspase-abhängige Apoptose führte. Zellen, die dem mitotischen Arrest und Zelltod durch ein sog. „mitotic slippage“ entgingen, wurden im hohen Maße polyploid und häuften typischerweise überzählige Zentrosomen an. Zusammenfassend kann also festgestellt werden, dass ein funktioneller p53/$p21^{WAF}$-Kontrollpunkt in G_1 unverzichtbar ist, um einer Genominstabilität entgegenzuwirken, die nach mitotischem Stress durch TACC3-Depletion und unkontrollierter Weiterproliferation verursacht wird.

Ein TACC3-*knock down* in NIH3T3-Zellen löste ähnliche molekulare und zelluläre Effekte aus, wie sie für Zellen berichtet wurden, die mit niedrigen, subtoxischen Konzentrationen des chemotherapeutisch eingesetzten Spindelgiftes Paclitaxel (≤10 nM) behandelt wurden. Interessanterweise führte eine zusätzliche Paclitaxel-Behandlung in TACC3-depletierten Zellen, nicht aber in Kontroll-siRNA exprimierenden Zellen, zu einer starken Polyploidisierung mit nachfolgendem Zelltod. Ebenso wurde die Induktion der zellulären Seneszenz nach TACC3-Depletion in Apoptose-beeinträchtigten MCF7-Zellen durch eine gleichzeitige Paclitaxelbehandlung stark beschleunigt. Demnach kann TACC3-Depletion Zellen gegenüber der wachstumshemmenden und zelltodauslösenden Wirkung von Paclitaxel sensibilisieren.

Zusammenfassend konnte in dieser Arbeit gezeigt werden, dass TACC3 eine essenzielle Rolle in der Spindeldynamik und bei der korrekten Chromosomenverteilung und demzufolge in der Aufrechterhaltung der Genomstabilität spielt. Ein TACC3 *knock down* resultiert in einer Hemmung der Zellproliferation durch Aktivierung der p53/$p21^{WAF}$-abhängigen G_1-Kontrollpunktantwort. Die hohe Anfälligkeit transformierter und oft G_1-Kontrollpunkt-beeinträchtigter Zellen gegenüber mitotischem Stress durch TACC3-Depletion

identifiziert dieses zentrosomale Protein als ein mögliches therapeutisches Target in der Krebsbehandlung, insbesondere in Verbindung mit chemotherapeutisch eingesetzten Spindelgiften wie Paclitaxel.

9 References

Abal, M, JM Andreu, and I Barasoain. (2003) Taxanes: microtubule and centrosome targets, and cell cycle dependent mechanisms of action. *Curr Cancer Drug Targets*, **3,** 193-203.

Andersen, JS, CJ Wilkinson, T Mayor, P Mortensen, EA Nigg, and M Mann. (2003) Proteomic characterization of the human centrosome by protein correlation profiling. *Nature*, **426,** 570-4.

Andreassen, PR, OD Lohez, and RL Margolis. (2003) G2 and spindle assembly checkpoint adaptation, and tetraploidy arrest: implications for intrinsic and chemically induced genomic instability. *Mutat Res*, **532,** 245-53.

Barros, TP, K Kinoshita, AA Hyman, and JW Raff. (2005) Aurora A activates D-TACC-Msps complexes exclusively at centrosomes to stabilize centrosomal microtubules. *J Cell Biol*, **170,** 1039-46.

Basto, R, J Lau, T Vinogradova, A Gardiol, CG Woods, A Khodjakov, and JW Raff. (2006) Flies without centrioles. *Cell*, **125,** 1375-86.

Ben-Porath, I, and RA Weinberg. (2005) The signals and pathways activating cellular senescence. *Int J Biochem Cell Biol*, **37,** 961-76.

Bergemann, AD, F Cole, and K Hirschhorn. (2005) The etiology of Wolf-Hirschhorn syndrome. *Trends Genet*, **21,** 188-95.

Bharadwaj, R, and H Yu. (2004) The spindle checkpoint, aneuploidy, and cancer. *Oncogene*, **23,** 2016-27.

Blagosklonny, MV. (2002) Are p27 and p21 cytoplasmic oncoproteins? *Cell Cycle*, **1,** 391-3.

Blagosklonny, MV. (2003) Cell senescence and hypermitogenic arrest. *EMBO Rep*, **4,** 358-62.

Blagosklonny, MV. (2006) Prolonged mitosis versus tetraploid checkpoint: how p53 measures the duration of mitosis. *Cell Cycle*, **5,** 971-5.

Blagosklonny, MV. (2007) Mitotic arrest and cell fate: why and how mitotic inhibition of transcription drives mutually exclusive events. *Cell Cycle*, **6,** 70-4.

Blagosklonny, MV, Z Darzynkiewicz, HD Halicka, P Pozarowski, ZN Demidenko, JJ Barry, KR Kamath, and RA Herrmann. (2004) Paclitaxel induces primary and postmitotic G1 arrest in human arterial smooth muscle cells. *Cell Cycle*, **3,** 1050-6.

Blagosklonny, MV, R Robey, S Bates, and T Fojo. (2000) Pretreatment with DNA-damaging agents permits selective killing of checkpoint-deficient cells by microtubule-active drugs. *J Clin Invest*, **105,** 533-9.

Boveri, T. (1895) Über das Verhalten der Centrosomen bei der Befruchtung des Seeigel-Eies nebst allgemeinen Bemerkungen über Centrosomen und Verwandtes. *Verh. Phys.-Med. Ges. Würzburg*, **29,** 1-75.

Brito, DA, and CL Rieder. (2006) Mitotic checkpoint slippage in humans occurs via cyclin B destruction in the presence of an active checkpoint. *Curr Biol*, **16,** 1194-200.

Brittle, AL, and H Ohkura. (2005) Centrosome maturation: Aurora lights the way to the poles. *Curr Biol*, **15,** R880-2.

Cassimeris, L, and J Morabito. (2004) TOGp, the human homolog of XMAP215/Dis1, is required for centrosome integrity, spindle pole organization, and bipolar spindle assembly. *Mol Biol Cell*, **15,** 1580-90.

Castedo, M, JL Perfettini, T Roumier, K Andreau, R Medema, and G Kroemer. (2004) Cell death by mitotic catastrophe: a molecular definition. *Oncogene*, **23,** 2825-37.

Chen, JG, and SB Horwitz. (2002) Differential mitotic responses to microtubule-stabilizing and -destabilizing drugs. *Cancer Res*, **62,** 1935-8.

Chen, X, J Bargonetti, and C Prives. (1995) p53, through p21 (WAF1/CIP1), induces cyclin D1 synthesis. *Cancer Res*, **55,** 4257-63.

Ciferri, C, A Musacchio, and A Petrovic. (2007) The Ndc80 complex: Hub of kinetochore activity. *FEBS Lett*, **581,** 2862-9.

Cleveland, DW, Y Mao, and KF Sullivan. (2003) Centromeres and kinetochores: from epigenetics to mitotic checkpoint signaling. *Cell*, **112,** 407-21.

Compton, DA. (2000) Spindle assembly in animal cells. *Annu Rev Biochem*, **69,** 95-114.

Conte, N, E Charafe-Jauffret, B Delaval, J Adelaide, C Ginestier, J Geneix, D Isnardon, J Jacquemier, and D Birnbaum. (2002) Carcinogenesis and translational controls: TACC1 is down-regulated in human cancers and associates with mRNA regulators. *Oncogene*, **21,** 5619-30.

Coqueret, O. (2003) New roles for p21 and p27 cell-cycle inhibitors: a function for each cell compartment? *Trends Cell Biol*, **13,** 65-70.

Crown, J, and M O'Leary. (2000) The taxanes: an update. *Lancet*, **355,** 1176-8.

Cully, M, J Shiu, RP Piekorz, WJ Muller, SJ Done, and TW Mak. (2005) Transforming acidic coiled coil 1 promotes transformation and mammary tumorigenesis. *Cancer Res*, **65,** 10363-70.

Del Sal, G, M Murphy, E Ruaro, D Lazarevic, AJ Levine, and C Schneider. (1996) Cyclin D1 and p21/waf1 are both involved in p53 growth suppression. *Oncogene*, **12,** 177-85.

Delaval, B, A Ferrand, N Conte, C Larroque, D Hernandez-Verdun, C Prigent, and D Birnbaum. (2004) Aurora B -TACC1 protein complex in cytokinesis. *Oncogene*, **23,** 4516-22.

DeLuca, JG, WE Gall, C Ciferri, D Cimini, A Musacchio, and ED Salmon. (2006) Kinetochore microtubule dynamics and attachment stability are regulated by Hec1. *Cell*, **127,** 969-82.

Dimri, GP, X Lee, G Basile, M Acosta, G Scott, C Roskelley, EE Medrano, M Linskens, I Rubelj, O Pereira-Smith, M Peacocke, and J Campisi. 1995. A Biomarker that Identifies Senescent Human Cells in Culture and in Aging Skin in vivo. Vol. 92. 9363-9367.

Ditchfield, C, VL Johnson, A Tighe, R Ellston, C Haworth, T Johnson, A Mortlock, N Keen, and SS Taylor. (2003) Aurora B couples chromosome alignment with

anaphase by targeting BubR1, Mad2, and Cenp-E to kinetochores. *J Cell Biol*, **161,** 267-80.

Doxsey, S. (2002) Duplicating dangerously: linking centrosome duplication and aneuploidy. *Mol Cell*, **10,** 439-40.

Doxsey, S, W Zimmerman, and K Mikule. (2005) Centrosome control of the cell cycle. *Trends Cell Biol*, **15,** 303-11.

Elmore, LW, CW Rehder, X Di, PA McChesney, CK Jackson-Cook, DA Gewirtz, and SE Holt. (2002) Adriamycin-induced senescence in breast tumor cells involves functional p53 and telomere dysfunction. *J Biol Chem*, **277,** 35509-15.

Essmann, F, IH Engels, G Totzke, K Schulze-Osthoff, and RU Jänicke. (2004) Apoptosis resistance of MCF-7 breast carcinoma cells to ionizing radiation is independent of p53 and cell cycle control but caused by the lack of caspase-3 and a caffeine-inhibitable event. *Cancer Res*, **64,** 7065-72.

Gergely, F, VM Draviam, and JW Raff. (2003) The ch-TOG/XMAP215 protein is essential for spindle pole organization in human somatic cells. *Genes Dev*, **17,** 336-41.

Gergely, F, C Karlsson, I Still, J Cowell, J Kilmartin, and JW Raff. (2000) The TACC domain identifies a family of centrosomal proteins that can interact with microtubules. *Proc Natl Acad Sci U S A*, **97,** 14352-7.

Giannakakou, P, R Robey, T Fojo, and MV Blagosklonny. (2001) Low concentrations of paclitaxel induce cell type-dependent p53, p21 and G1/G2 arrest instead of mitotic arrest: molecular determinants of paclitaxel-induced cytotoxicity. *Oncogene*, **20,** 3806-13.

Giet, R, D McLean, S Descamps, MJ Lee, JW Raff, C Prigent, and DM Glover. (2002) Drosophila Aurora A kinase is required to localize D-TACC to centrosomes and to regulate astral microtubules. *J Cell Biol*, **156,** 437-51.

Gladden, AB, and JA Diehl. (2005) Location, location, location: the role of cyclin D1 nuclear localization in cancer. *J Cell Biochem*, **96,** 906-13.

Gould, KL, and P Nurse. (1989) Tyrosine phosphorylation of the fission yeast cdc2+ protein kinase regulates entry into mitosis. *Nature*, **342,** 39-45.

Greer, EL, and A Brunet. (2005) FOXO transcription factors at the interface between longevity and tumor suppression. *Oncogene*, **24,** 7410-25.

Groisman, I, YS Huang, R Mendez, Q Cao, W Theurkauf, and JD Richter. (2000) CPEB, maskin, and cyclin B1 mRNA at the mitotic apparatus: implications for local translational control of cell division. *Cell*, **103,** 435-47.

Han, EK, SC Ng, N Arber, M Begemann, and IB Weinstein. (1999) Roles of cyclin D1 and related genes in growth inhibition, senescence and apoptosis. *Apoptosis*, **4,** 213-9.

Heliez, C, L Baricault, N Barboule, and A Valette. (2003) Paclitaxel increases p21 synthesis and accumulation of its AKT-phosphorylated form in the cytoplasm of cancer cells. *Oncogene*, **22,** 3260-8.

Holmfeldt, P, S Stenmark, and M Gullberg. (2004) Differential functional interplay of TOGp/XMAP215 and the KinI kinesin MCAK during interphase and mitosis. *Embo J*, **23,** 627-37.

Hu, G, W Liu, EG Hanania, S Fu, T Wang, and AB Deisseroth. (1995) Suppression of tumorigenesis by transcription units expressing the antisense E6 and E7 messenger RNA (mRNA) for the transforming proteins of the human papilloma virus and the sense mRNA for the retinoblastoma gene in cervical carcinoma cells. *Cancer Gene Ther*, **2,** 19-32.

Hung, DT, TF Jamison, and SL Schreiber. (1996) Understanding and controlling the cell cycle with natural products. *Chem Biol*, **3,** 623-39.

Ikui, AE, CP Yang, T Matsumoto, and SB Horwitz. (2005) Low concentrations of taxol cause mitotic delay followed by premature dissociation of p55CDC from Mad2 and BubR1 and abrogation of the spindle checkpoint, leading to aneuploidy. *Cell Cycle*, **4,** 1385-8.

Jablonski, SA, ST Liu, and TJ Yen. (2003) Targeting the kinetochore for mitosis-specific inhibitors. *Cancer Biol Ther*, **2,** 236-41.

Janicke, RU, D Sohn, F Essmann, and K Schulze-Osthoff. (2007) The Multiple Battles Fought by Anti-Apoptotic p21. *Cell Cycle*, **6**.

Jänicke, RU, ML Sprengart, MR Wati, and AG Porter. (1998) Caspase-3 is required for DNA fragmentation and morphological changes associated with apoptosis. *J Biol Chem*, **273,** 9357-60.

Jordan, MA, and L Wilson. (2004) Microtubules as a target for anticancer drugs. *Nat Rev Cancer*, **4,** 253-65.

Judson, PL, JM Watson, PA Gehrig, WC Fowler, Jr., and JS Haskill. (1999) Cisplatin inhibits paclitaxel-induced apoptosis in cisplatin-resistant ovarian cancer cell lines: possible explanation for failure of combination therapy. *Cancer Res*, **59,** 2425-32.

Jung, CK, JH Jung, GS Park, A Lee, CS Kang, and KY Lee. (2006) Expression of transforming acidic coiled-coil containing protein 3 is a novel independent prognostic marker in non-small cell lung cancer. *Pathol Int*, **56,** 503-9.

Kadura, S, and S Sazer. (2005) SAC-ing mitotic errors: how the spindle assembly checkpoint (SAC) plays defense against chromosome mis-segregation. *Cell Motil Cytoskeleton*, **61,** 145-60.

Kinoshita, K, B Habermann, and AA Hyman. (2002) XMAP215: a key component of the dynamic microtubule cytoskeleton. *Trends Cell Biol*, **12,** 267-73.

Kinoshita, K, TL Noetzel, L Pelletier, K Mechtler, DN Drechsel, A Schwager, M Lee, JW Raff, and AA Hyman. (2005) Aurora A phosphorylation of TACC3/maskin is required for centrosome-dependent microtubule assembly in mitosis. *J Cell Biol*, **170,** 1047-55.

Klein, LE, BS Freeze, AB Smith, 3rd, and SB Horwitz. (2005) The microtubule stabilizing agent discodermolide is a potent inducer of accelerated cell senescence. *Cell Cycle*, **4,** 501-7.

Kline, SL, IM Cheeseman, T Hori, T Fukagawa, and A Desai. (2006) The human Mis12 complex is required for kinetochore assembly and proper chromosome segregation. *J Cell Biol*, **173,** 9-17.

Knowlton, AL, W Lan, and PT Stukenberg. (2006) Aurora B Is Enriched at Merotelic Attachment Sites, Where It Regulates MCAK. *Current Biology*, **16,** 1705-1710.

Lauffart, B, MM Vaughan, R Eddy, D Chervinsky, RA DiCioccio, JD Black, and IH Still. (2005) Aberrations of TACC1 and TACC3 are associated with ovarian cancer. *BMC Womens Health*, **5,** 8.

Leung, RK, and PA Whittaker. (2005) RNA interference: from gene silencing to gene-specific therapeutics. *Pharmacol Ther*, **107,** 222-39.

Ley, R, KE Ewings, K Hadfield, and SJ Cook. (2005) Regulatory phosphorylation of Bim: sorting out the ERK from the JNK. *Cell Death Differ*, **12,** 1008-14.

Li, JJ, and SA Li. (2006) Mitotic kinases: the key to duplication, segregation, and cytokinesis errors, chromosomal instability, and oncogenesis. *Pharmacol Ther*, **111,** 974-84.

Lodish, H, A Berk, SL Zipursky, P Matsudaira, D Baltimore, and J Darnell. 1999. Molecular Cell Biology. W. H. Freeman and Company, New York.

Luders, J, and T Stearns. (2007) Microtubule-organizing centres: a re-evaluation. *Nat Rev Mol Cell Biol*, **8,** 161-7.

Mansilla, S, M Bataller, and J Portugal. (2006) Mitotic catastrophe as a consequence of chemotherapy. *Anticancer Agents Med Chem*, **6,** 589-602.

Marchler-Bauer, A, and SH Bryant. (2004) CD-Search: protein domain annotations on the fly. *Nucleic Acids Res*, **32,** W327-31.

Margolis, RL, OD Lohez, and PR Andreassen. (2003) G1 tetraploidy checkpoint and the suppression of tumorigenesis. *J Cell Biochem*, **88,** 673-83.

Martin-Lluesma, S, VM Stucke, and EA Nigg. (2002) Role of Hec1 in spindle checkpoint signaling and kinetochore recruitment of Mad1/Mad2. *Science*, **297,** 2267-70.

McAinsh, AD, P Meraldi, VM Draviam, A Toso, and PK Sorger. (2006) The human kinetochore proteins Nnf1R and Mcm21R are required for accurate chromosome segregation. *Embo J*, **25,** 4033-49.

McKeveney, PJ, VM Hodges, RN Mullan, P Maxwell, D Simpson, A Thompson, PC Winter, TR Lappin, and AP Maxwell. (2001) Characterization and localization of expression of an erythropoietin-induced gene, ERIC-1/TACC3, identified in erythroid precursor cells. *Br J Haematol*, **112,** 1016-24.

Meijer, HA, HE Radford, LS Wilson, S Lissenden, and CH de Moor. (2007) Translational control of maskin mRNA by its 3' untranslated region. *Biol Cell*.

Meraldi, P, VM Draviam, and PK Sorger. (2004) Timing and checkpoints in the regulation of mitotic progression. *Dev Cell*, **7,** 45-60.

Michel, LS, V Liberal, A Chatterjee, R Kirchwegger, B Pasche, W Gerald, M Dobles, PK Sorger, VV Murty, and R Benezra. (2001) MAD2 haplo-insufficiency causes premature anaphase and chromosome instability in mammalian cells. *Nature*, **409,** 355-9.

Mikule, K, B Delaval, P Kaldis, A Jurcyzk, P Hergert, and S Doxsey. (2007) Loss of centrosome integrity induces p38-p53-p21-dependent G1-S arrest. *Nat Cell Biol*, **9,** 160-70.

Millband, DN, L Campbell, and KG Hardwick. (2002) The awesome power of multiple model systems: interpreting the complex nature of spindle checkpoint signaling. *Trends Cell Biol*, **12,** 205-9.

Mollinedo, F, and C Gajate. (2003) Microtubules, microtubule-interfering agents and apoptosis. *Apoptosis*, **8,** 413-50.

Motoyama, N, and K Naka. (2004) DNA damage tumor suppressor genes and genomic instability. *Curr Opin Genet Dev*, **14,** 11-6.

Nasmyth, K. (2002) Segregating sister genomes: the molecular biology of chromosome separation. *Science*, **297,** 559-65.

Nigg, EA. (2002) Centrosome aberrations: cause or consequence of cancer progression? *Nat Rev Cancer*, **2,** 815-25.

Nigg, EA. (2006) Origins and consequences of centrosome aberrations in human cancers. *Int J Cancer*, **119,** 2717-23.

Nurse, P. (1990) Universal control mechanism regulating onset of M-phase. *Nature*, **344,** 503-8.

O'Brien, LL, AJ Albee, L Liu, W Tao, P Dobrzyn, SB Lizarraga, and C Wiese. (2005) The Xenopus TACC homologue, maskin, functions in mitotic spindle assembly. *Mol Biol Cell*, **16,** 2836-47.

O'Connor, L, A Strasser, LA O'Reilly, G Hausmann, JM Adams, S Cory, and DC Huang. (1998) Bim: a novel member of the Bcl-2 family that promotes apoptosis. *Embo J*, **17,** 384-95.

Olashaw, N, TK Bagui, and WJ Pledger. (2004) Cell cycle control: a complex issue. *Cell Cycle*, **3,** 263-4.

Persons, DA, MG Mehaffey, M Kaleko, AW Nienhuis, and EF Vanin. (1998) An improved method for generating retroviral producer clones for vectors lacking a selectable marker gene. *Blood Cells Mol Dis*, **24,** 167-82.

Peset, I, J Seiler, T Sardon, LA Bejarano, S Rybina, and I Vernos. (2005) Function and regulation of Maskin, a TACC family protein, in microtubule growth during mitosis. *J Cell Biol*, **170,** 1057-66.

Peters, DG, DM Kudla, JA Deloia, TJ Chu, L Fairfull, RP Edwards, and RE Ferrell. (2005) Comparative gene expression analysis of ovarian carcinoma and normal ovarian epithelium by serial analysis of gene expression. *Cancer Epidemiol Biomarkers Prev*, **14,** 1717-23.

Piekorz, RP, A Hoffmeyer, CD Duntsch, C McKay, H Nakajima, V Sexl, L Snyder, J Rehg, and JN Ihle. (2002) The centrosomal protein TACC3 is essential for hematopoietic stem cell function and genetically interfaces with p53-regulated apoptosis. *Embo J*, **21,** 653-64.

Pietenpol, JA, and ZA Stewart. (2002) Cell cycle checkpoint signaling: cell cycle arrest versus apoptosis. *Toxicology*, **181-182,** 475-81.

Pines, J. (2006) Mitosis: a matter of getting rid of the right protein at the right time. *Trends Cell Biol*, **16,** 55-63.

Porter, AG, and RU Jänicke. (1999) Emerging roles of caspase-3 in apoptosis. *Cell Death Differ*, **6,** 99-104.

Pu, JJ, C Li, M Rodriguez, and D Banerjee. (2001) Cloning and structural characterization of ECTACC, a new member of the transforming acidic coiled coil (TACC) gene family: cDNA sequence and expression analysis in human microvascular endothelial cells. *Cytokine*, **13,** 129-37.

Pushkarev, VM, DV Starenki, VA Saenko, H Namba, J Kurebayashi, MD Tronko, and S Yamashita. (2004) Molecular mechanisms of the effects of low concentrations of taxol in anaplastic thyroid cancer cells. *Endocrinology*, **145,** 3143-52.

Rancati, G, V Crispo, G Lucchini, and S Piatti. (2005) Mad3/BubR1 phosphorylation during spindle checkpoint activation depends on both Polo and Aurora kinases in budding yeast. *Cell Cycle*, **4,** 972-80.

Rieder, CL, S Faruki, and A Khodjakov. (2001) The centrosome in vertebrates: more than a microtubule-organizing center. *Trends Cell Biol*, **11,** 413-9.

Rieder, CL, and H Maiato. (2004) Stuck in division or passing through: what happens when cells cannot satisfy the spindle assembly checkpoint. *Dev Cell*, **7,** 637-51.

Roninson, IB, EV Broude, and BD Chang. (2001) If not apoptosis, then what? Treatment-induced senescence and mitotic catastrophe in tumor cells. *Drug Resist Updat*, **4,** 303-13.

Sadek, CM, M Pelto-Huikko, M Tujague, KR Steffensen, M Wennerholm, and JA Gustafsson. (2003) TACC3 expression is tightly regulated during early differentiation. *Gene Expr Patterns*, **3,** 203-11.

Salisbury, JL, KM Suino, R Busby, and M Springett. (2002) Centrin-2 is required for centriole duplication in mammalian cells. *Curr Biol*, **12,** 1287-92.

Sanchez, I, and BD Dynlacht. (2005) New insights into cyclins, CDKs, and cell cycle control. *Semin Cell Dev Biol*, **16,** 311-21.

Sato, M, N Koonrugsa, T Toda, L Vardy, S Tournier, and JB Millar. (2003) Deletion of Mia1/Alp7 activates Mad2-dependent spindle assembly checkpoint in fission yeast. *Nat Cell Biol*, **5,** 764-6; author reply 766.

Schmit, TL, and N Ahmad. (2007) Regulation of mitosis via mitotic kinases: new opportunities for cancer management. *Mol Cancer Ther*, **6,** 1920-31.

Schneider, L, F Essman, A Kletke, P Rio, H Hanenberg, W Wetzel, K Schulze-Osthoff, B Nürnberg, and RP Piekorz. (2007a) The transforming acidic coiled coil 3 protein is essential for spindle-dependent chromosome alignment and mitotic survival. *J Biol Chem*, **282,** 29273-83.

Schneider, L, F Essmann, A Kletke, P Rio, H Hanenberg, K Schulze-Osthoff, B Nürnberg, and RP Piekorz. (2007b) TACC3 depletion sensitizes to paclitaxel-induced cell death and overrides p21(WAF)-mediated cell cycle arrest. *Oncogene***,** doi: 10.1038/sj.onc.1210628.

Schneider, L, F Essmann, A Kletke, P Rio, H Hanenberg, K Schulze-Osthoff, B Nürnberg, and RP Piekorz. (2008) TACC3 depletion sensitizes to paclitaxel-induced cell death and overrides p21(WAF)-mediated cell cycle arrest. *Oncogene*, **27,** 116-125.

Schuendeln, MM, RP Piekorz, C Wichmann, Y Lee, PJ McKinnon, K Boyd, Y Takahashi, and JN Ihle. (2004) The centrosomal, putative tumor suppressor protein TACC2 is dispensable for normal development, and deficiency does not lead to cancer. *Mol Cell Biol*, **24,** 6403-9.

Simstein, R, M Burow, A Parker, C Weldon, and B Beckman. (2003) Apoptosis, chemoresistance, and breast cancer: insights from the MCF-7 cell model system. *Exp Biol Med (Maywood)*, **228,** 995-1003.

Sluder, G. (2005) Two-way traffic: centrosomes and the cell cycle. *Nat Rev Mol Cell Biol*, **6,** 743-8.

Stewart, JP, A Thompson, M Santra, B Barlogie, TR Lappin, and J Shaughnessy, Jr. (2004) Correlation of TACC3, FGFR3, MMSET and p21 expression with the t(4;14)(p16.3;q32) in multiple myeloma. *Br J Haematol*, **126,** 72-6.

Stewart, ZA, SD Leach, and JA Pietenpol. (1999a) p21(Waf1/Cip1) inhibition of cyclin E/Cdk2 activity prevents endoreduplication after mitotic spindle disruption. *Mol Cell Biol*, **19,** 205-15.

Stewart, ZA, D Mays, and JA Pietenpol. (1999b) Defective G1-S cell cycle checkpoint function sensitizes cells to microtubule inhibitor-induced apoptosis. *Cancer Res*, **59,** 3831-7.

Still, IH, M Hamilton, P Vince, A Wolfman, and JK Cowell. (1999a) Cloning of TACC1, an embryonically expressed, potentially transforming coiled coil containing gene, from the 8p11 breast cancer amplicon. *Oncogene*, **18,** 4032-8.

Still, IH, AK Vettaikkorumakankauv, A DiMatteo, and P Liang. (2004) Structure-function evolution of the transforming acidic coiled coil genes revealed by analysis of phylogenetically diverse organisms. *BMC Evol Biol*, **4,** 16.

Still, IH, P Vince, and JK Cowell. (1999b) The third member of the transforming acidic coiled coil-containing gene family, TACC3, maps in 4p16, close to translocation breakpoints in multiple myeloma, and is upregulated in various cancer cell lines. *Genomics*, **58,** 165-70.

Taylor, WR, and GR Stark. (2001) Regulation of the G2/M transition by p53. *Oncogene*, **20,** 1803-15.

Torii, S, T Yamamoto, Y Tsuchiya, and E Nishida. (2006) ERK MAP kinase in G cell cycle progression and cancer. *Cancer Sci*, **97,** 697-702.

Tuschl, T, and A Borkhardt. (2002) Small interfering RNAs: a revolutionary tool for the analysis of gene function and gene therapy. *Mol Interv*, **2,** 158-67.

Ulisse, S, E Baldini, M Toller, JG Delcros, A Gueho, F Curcio, E De Antoni, L Giacomelli, FS Ambesi-Impiombato, S Bocchini, M D'Armiento, and Y Arlot-Bonnemains. (2007) Transforming acidic coiled-coil 3 and Aurora-A interact in human thyrocytes and their expression is deregulated in thyroid cancer tissues. *Endocr Relat Cancer*, **14,** 827-37.

Vigneron, S, S Prieto, C Bernis, JC Labbe, A Castro, and T Lorca. (2004) Kinetochore localization of spindle checkpoint proteins: who controls whom? *Mol Biol Cell*, **15,** 4584-96.

Vogel, C, A Kienitz, I Hofmann, R Muller, and H Bastians. (2004) Crosstalk of the mitotic spindle assembly checkpoint with p53 to prevent polyploidy. *Oncogene*, **23,** 6845-53.

Weaver, BA, and DW Cleveland. (2005) Decoding the links between mitosis, cancer, and chemotherapy: The mitotic checkpoint, adaptation, and cell death. *Cancer Cell*, **8,** 7-12.

West, KA, SS Castillo, and PA Dennis. (2002) Activation of the PI3K/Akt pathway and chemotherapeutic resistance. *Drug Resist Updat*, **5,** 234-48.

Willis, SN, and JM Adams. (2005) Life in the balance: how BH3-only proteins induce apoptosis. *Current Opinion in Cell Biology*, **17,** 617-625.

Wiznerowicz, M, and D Trono. (2003) Conditional suppression of cellular genes: lentivirus vector-mediated drug-inducible RNA interference. *J Virol*, **77,** 8957-61.

Yao, R, Y Natsume, and T Noda. (2007) TACC3 is required for the proper mitosis of sclerotome mesenchymal cells during formation of the axial skeleton. *Cancer Sci*.

Yu, J, and L Zhang. (2005) The transcriptional targets of p53 in apoptosis control. *Biochem Biophys Res Commun*, **331,** 851-8.

11 Acknowledgments

This thesis was preceded by four years of laboratory work and over one year of writing. During that time I learned a lot, especially about conducting research, group leading and responsibility. I learned all this from my two mentors, Dr. Roland Piekorz and Prof. Dr. Dr. Bernd Nürnberg.

First of all I would like to thank my advisor, Dr. Roland Piekorz. I am very grateful for his motivating support, for interesting and valuable discussions and precious advices and guidance at all stages of this thesis. His insightful ideas and his thoughtful and constructive criticism helped considerably in the completion of this study. I am also mostly appreciative to Dr. Piekorz for sharing his excellent scientific expertise and his extraordinary skills of scientific writing and English language, from which I humbly hope to have learnt while watching my manuscripts being improved. Last but not least I deeply acknowledge all his time and the extraordinary work he put forth at the completion phase of my thesis.

Furthermore I am indebted to Prof. Dr. Dr. Bernd Nürnberg, Chairman of the Institute for Biochemistry und Molecular Biology II and Dean of the Medical Faculty for offering me the opportunity to conduct this PhD thesis at his research facilities. Without his intensive mentoring and his excellent scientific and organisational guidance and support, my career in scientific research could never be possible. His singular understanding of science, his outstanding research and institutional career and his remarkable leadership qualities shall always be my most desirable beacon in all my future work in science.

I would like to thank Prof. Dr. Peter Westhoff, Chairman of the Institute of Plant Molecular and Developmental Biology and Dean of the Mathematical and Natural Sciences Faculty, for his interest and his kind willingness to represent this work at the Mathematical and Natural Science Faculty of the Heinrich-Heine-University.

I also would like to thank:

- Prof. Dr. Klaus Schulze-Osthoff, Chairman of the Institute for Molecular Medicine, for his extraordinary support of my research and career
- Dr. Frank Essmann and Ms. BTA Anja Kletke for their considerable input and especially their assistance in cLSM data acquisition

- PD Dr. Reza Ahmadian for his helpful comments to this thesis
- Ms. Dr. Wiebke Wetzel for teaching me the method of flow cytometry and her assistance with RNA analysis

I also thank all other present and former members of the institute for providing a very amicable working environment and for their help and collegiality.

My special thanks go to my most wonderful friend PD Dr. Christoph V. Suschek for all his invaluable moral support and advice and also to Dr. Elisabeth M. Jeanclos and Dr. Antje Gohla for their friendship and backing in difficult times.

Die hier vorgelegte Dissertation habe ich eigenständig und ohne unerlaubte Hilfe angefertigt. Die Dissertation wurde in der vorgelegten oder in ähnlicher Form noch bei keiner anderen Institution eingereicht. Ich habe bisher keine erfolglosen Promotionsversuche unternommen.

Mailand, den 05.06.2008

(Leonid Schneider)